NAVAL POSTGRADUATE SCHOOL
Monterey, California

THESIS

RESONANT BLADE RESPONSE IN TURBINE ROTOR SPIN TESTS USING A LASER-LIGHT PROBE NON-INTRUSIVE MEASUREMENT SYSTEM

by

Michael R. Mansisidor

March 2002

Thesis Advisor:	Raymond P. Shreeve
Second Reader:	Garth V. Hobson

Approved for public release; distribution is unlimited.

THIS PAGE INTENTIONALLY LEFT BLANK

REPORT DOCUMENTATION PAGE			Form Approved OMB No. 0704-0188
Public reporting burden for this collection of information is estimated to average 1 hour per response, including the time for reviewing instruction, searching existing data sources, gathering and maintaining the data needed, and completing and reviewing the collection of information. Send comments regarding this burden estimate or any other aspect of this collection of information, including suggestions for reducing this burden, to Washington headquarters Services, Directorate for Information Operations and Reports, 1215 Jefferson Davis Highway, Suite 1204, Arlington, VA 22202-4302, and to the Office of Management and Budget, Paperwork Reduction Project (0704-0188) Washington DC 20503.			
1. AGENCY USE ONLY *(Leave blank)*	**2. REPORT DATE** March 2002	**3. REPORT TYPE AND DATES COVERED** Master's Thesis	
4. TITLE AND SUBTITLE: Resonant Blade Response in Turbine Rotor Spin Tests Using A Laser-light Probe Non-Intrusive Measurement System.			**5. FUNDING NUMBERS**
6. AUTHOR(S): Mansisidor, Michael R.			
7. PERFORMING ORGANIZATION NAME(S) AND ADDRESS(ES) Naval Postgraduate School Monterey, CA 93943-5000			**8. PERFORMING ORGANIZATION REPORT NUMBER**
9. SPONSORING /MONITORING AGENCY NAME(S) AND ADDRESS(ES) N/A			**10. SPONSORING/MONITORING AGENCY REPORT NUMBER**
11. SUPPLEMENTARY NOTES The views expressed in this thesis are those of the author and do not reflect the official policy or position of the Department of Defense or the U.S. Government.			
12a. DISTRIBUTION / AVAILABILITY STATEMENT Distribution Statement (mix case letters)			**12b. DISTRIBUTION CODE**

13. ABSTRACT ***(maximum 200 words)***

Procedures to qualify turbo-machinery components for a designed lifetime free of high cycle fatigue (HCF) failures have not yet evolved. As part of an initiative to address this issue, in the present study, laser-light probes were used in a Non-Intrusive Measurement System (NSMS) to measure the unsteady deflections created in the blades of a second-stage turbine rotor in an evacuated spin pit. Air-jet and eddy-current excitation (ECE) methods were used to stimulate blade resonance. The NSMS was calibrated directly to gauge measurements of strain, and testing was conducted toward three additional goals; assessing the effectiveness of an advanced internal damping system; attaining higher excitation amplitudes with ECE by silver plating blades, and improving the repeatability of resonance data by adding plastic inserts between the fir-tree blade roots and the disk. It was concluded that the ability of NSMS to record the response of all blades is key to understanding the rotor system behavior and quantifying the statistical variability between blades.

14. SUBJECT TERMS: Non-Intrusive Stress Measurement System, NSMS, Laser-light Probes, Hood Technology, spin-pit, magnet excitation, air-jet excitation, XTE-66, resonance.			**15. NUMBER OF PAGES** 132
			16. PRICE CODE
17. SECURITY CLASSIFICATION OF REPORT Unclassified	**18. SECURITY CLASSIFICATION OF THIS PAGE** Unclassified	**19. SECURITY CLASSIFICATION OF ABSTRACT** Unclassified	**20. LIMITATION OF ABSTRACT** UL

NSN 7540-01-280-5500 Standard Form 298 (Rev. 2-89)
Prescribed by ANSI Std. 239-18

THIS PAGE INTENTIONALLY LEFT BLANK

Approved for public release; distribution is unlimited.

RESONANT BLADE RESPONSE IN TURBINE ROTOR SPIN TESTS USING A LASER-LIGHT PROBE NON-INTRUSIVE MEASUREMENT SYSTEM

Michael R. Mansisidor
Lieutenant, United States Navy
B.S., University of Idaho, 1993

Submitted in partial fulfillment of the
requirements for the degree of

MASTER OF SCIENCE IN AERONAUTICAL ENGINEERING

from the

NAVAL POSTGRADUATE SCHOOL
March 2002

Author: Michael R. Mansisidor

Approved by: Raymond P. Shreeve
Thesis Advisor

Garth V. Hobson
Second Reader

Maximilian F. Platzer
Chairman
Department of Aeronautics and Astronautics

THIS PAGE INTENTIONALLY LEFT BLANK

ABSTRACT

Procedures to qualify turbomachinery components for a designed lifetime free of high cycle fatigue (HCF) failures have not yet evolved. As part of an initiative to address this issue, in the present study, laser-light probes were used in a Non-Intrusive Measurement System (NSMS) to measure the unsteady deflections created in the blades of a second-stage turbine rotor in an evacuated spin pit. Air-jet and eddy-current excitation (ECE) methods were used to stimulate blade resonance. The NSMS was calibrated directly to gauge measurements of strain, and testing was conducted toward three additional goals; assessing the effectiveness of an advanced internal damping system; attaining higher excitation amplitudes with ECE by silver plating blades, and improving the repeatability of resonance data by adding plastic inserts between the fir-tree blade roots and the disk. It was concluded that the ability of NSMS to record the response of all blades is key to understanding the rotor system behavior and quantifying the statistical variability between blades.

THIS PAGE INTENTIONALLY LEFT BLANK

TABLE OF CONTENTS

I. INTRODUCTION....1
A. BACKGROUND....1
B. PROGRAM GOALS....3

II. FACILITY DESCRIPTION AND TEST PROCEDURE....5
A. FACILITY....5
B. TEST ARTICLE....5
C. BLADE EXCITATION & TEST PROCEDURE....7

III. BLADE VIBRATION MEASUREMENT SYSTEM....9
A. OVERVIEW....9
A. INTEGRATED FIBER OPTIC LASER PROBE (IFOLP)....9
B. LASER TRASMITTER, RECEIVER, AND FIBER-OPTIC CABLE....9
C. BLADE VIBRATION SENSOR INTERFACE (BVSI)....10
D. OSCILLOSCOPE....12
E. PC COMPUTER....12

IV. SOFTWARE AND DATA MANIPULATION....13
A. OVERVIEW....13
B. NSMS DATA ACQUISITION (VERSION 3.0)....13
C. NSMS DATA VIEWER (VERSION 1.3)....16
D. MICROSOFT EXCEL....19

V. TEST PROGRAM AND RESULTS....23
A. OVERVIEW....23
B. EXPERIMENT 1 – AIR-JET EXCITATION AND EFFECT OF DAMPERS....25
C. EXPERIMENT 2 – EDDY-CURRENT EXCITATION AND CALIBRATION OF THE NSMS TO STRAIN MEASUREMENTS....28
D. EXPERIMENT 3 – EFFECT OF SILVER PLATING....38
E. EXPERIMENT 4 – EFFECT OF PLASTIC INSERTS....47

VI. CONCLUSIONS AND RECOMMENDATIONS....51
A. CONCLUSIONS....51
B. RECOMMENDATIONS....52

APPENDIX A : THEORY OF MEASUREMENT....53
A. BLADE MODES, FREQUENCIES, AND ENGINE ORDERS....53
B. CLASSIFICATION AND SENSORS....54
C. DEFLECTION MEASUREMENT USING TOA INFORMATION....55
D. GEOMETRIC CONSIDERATIONS FOR AMPLITUDE ESTIMATES....61
E. THE CURVE FIT AND SINGLE DEGREE OF FREEDOM....63
F. DETRENDING....66

APPENDIX B : NSMS OPERATIONAL PROCEDURE....69

APPENDIX C : PROCESSED DATA....81

A. EXPERIMENT 1: AJE AND EFFECT OF DAMPERS 81
B. EXPERIMENT 2: ECE AND NSMS CALIBRATION TO STRAIN GAUGES 82
C. EXPERIMENT 3: EFFECT OF SILVER PLATING 83
D. EXPERIMENT 4: EFFECT OF PLASTIC INSERTS 83

APPENDIX D : AJE DATA AT 8EO, 10EO, AND 12EO 85
A. AIR JET TEST RESULTS FOR EVERY BLADE AT 8EO AND 10EO. ...85
B. AIR JET TEST RESULTS FOR EVERY BLADE AT 12EO. 88

APPENDIX E : STRAIN GAUGE VS. NSMS CORRELATION 93
A. STRAIN 11 = PROBE 1 BLADE25 = PROBE 2 BLADE 20 93
B. STRAIN 13 = PROBE 1 BLADE 28 = PROBE 2 BLADE 23.....94
C. STRAIN 14 = PROBE 1 BLADE 15 = PROBE 2 BLADE 10 95

APPENDIX F : CORRELATION DATA OF STRAIN GAUGES TO PROBES.....97
A. STRAIN GAUGE 11 TO NSMS.....97
B. STRAIN GAUGE 13 TO NSMS.....98
C. STRAIN GAUGE 14 TO NSMS.....99
D. FINAL PLOTS RELATING STRAIN GAUGES TO PROBES 1 AND 2. 100

APPENDIX G : EXPERIMENT 3 DATA 101
A. NON-PLATED: PROBE 1(WHITE), PROBE 2 (GRAY).....101
B. PLATED: PROBE 1 (WHITE), PROBE 2 (GRAY) 101

APPENDIX H : EXPERIMENT 4 DATA 103

APPENDIX I PROBE AND BLADE NUMBER IDENTIFICATIONS.....107

LIST OF REFERENCES.....111

INITIAL DISTRIBUTION LIST 113

LIST OF FIGURES

Figure 1 NPS Spin Pit 5
Figure 2 XTE-66 Second Stage Turbine Rotor 6
Figure 3 Identities of XTE-66 blades 7
Figure 4 Air Jet Excitation Setup 8
Figure 5 ECE Excitation Setup 8
Figure 6 Laser Transmitters (top) and Receivers (bottom) 10
Figure 7 Blade Vibration Sensor Interface Board 11
Figure 8 Infinium Oscilloscope 12
Figure 9 Main Display of Data Acquisition Software 14
Figure 10 Data Acquisition Hardware Setup 15
Figure 11 Operating Acquisition NSMS Software 16
Figure 12 Data Viewer Main Page 17
Figure 13 Slider Bars Encompassing the Resonance 18
Figure 14 Good Curve Fit 19
Figure 15 Excel Workbook Example 21
Figure 16 Sample Excel Data Page 22
Figure 17 Magnet Pair at the Blade Tips [Right-Side Magnet (Unmarked) is a South Pole] 24
Figure 18 Air Jet Tests With and Without Dampers at 8EO and Without at 10EO 27
Figure 19 Air Jet Tests With and Without Dampers at 12EO Before Modifications (Sep) and After Modifications (Oct) 28
Figure 20 ECE with Two Sets of Magnets 29
Figure 21 Strain Gauges on the XTE-66 Turbine Blade 31
Figure 22 Average Deflections vs. Magnet Offset for Probe 1 32
Figure 23 Average Deflections vs. Magnet Offset for Probe 2 32
Figure 24 Average Deflections vs. Magnet Offset for Probe 1 33
Figure 25 Average Deflections vs. Magnet Offset for Probe 2 33
Figure 26 Effect of Magnet Offset on Deflections from Probe 1 35
Figure 27 Effect of Magnet Offset on Deflections from Probe 2 35
Figure 28 One Standard Deviation Error Bars 36
Figure 29 Probe 1 NSMS Correlation to Strain Gauges 37
Figure 30 Probe 2 NSMS Correlation to Strain Gauges 37
Figure 31 Effect of Plating from Probe 1 43
Figure 32 Effect of Plating from Probe 2 44
Figure 33 Effect of Plating – Average of Probe 1 and 2 44
Figure 34 Typical Non-Plated Blade: No 5100 RPM Resonance 45
Figure 35 Typical Plated Blade: With 5100 RPM Resonance 46
Figure 36 5100 RPM Resonant Deflections 46
Figure 37 Blade Microstrain with Inserts (5 Tests) 49
Figure 38 Blade Microstrain with Inserts (Last 3 Tests) 49
Figure 39 Campbell Diagram Example 53
Figure 40 Illustration of Blade Time-of Arrival 55

Figure 41 Synchronous Blade Resonance as Seen by Two Detectors 58
Figure 42 Asynchronous Blade Resonance as Seen by a Detector 60
Figure 43 Geometric Consideration: Mode Shape, Point Sensor, Line Sensor 62
Figure 44 Geometry for Specific Detectors 63
Figure 45 Different Values of Q for Normalized RPM....65
Figure 46 Sensor Output as a Function of Shaft Rate and Sensor Location to Node 66
Figure 47 Laser Transmitter/Receiver Case....69
Figure 48 HP Infinium Display Set up....70
Figure 49 Infinium Display with 1/Rev Trigger Level Shown 71
Figure 50 HP Infinium Final Display....71
Figure 51 Digitizer Set up 72
Figure 52 BVSI Arm/Trigger Manipulation 73
Figure 53 Arm Level to Probe Output....73
Figure 54 Arm and Trigger Levels....74
Figure 55 BVSI 1/rev Correct Placement for Inverse Switch....75
Figure 56 Data Acquisition Main....75
Figure 57 Data Acquisition Hardware Setup 76
Figure 58 Operating Acquisition NSMS Software....77
Figure 59 Data Viewer Main Page....77
Figure 60 Processed Data Using 1/rev as TOA Reference 78
Figure 61 Processed Data Using Transformation of Inter-Blade Angle 78
Figure 62 Strain 11 Compared to Probes 1 and 2: 93
Figure 63 Strain 13 Compared to Probes 1 and 2: 94
Figure 64 Strain 14 Compared to Probes 1 and 2: 95
Figure 65 Average of 3 Sweeps in Test 1 103
Figure 66 Average of 3 Sweeps in Test 2 104
Figure 67 Average of 3 Sweeps in Test 3 104
Figure 68 Average of 3 Sweeps in Test 4 105
Figure 69 Average of 3 Sweeps in Test 5 105
Figure 70 “Start/Stop” Standard Deviations for No Plastic inserts....106
Figure 71 Continuous Standard Deviations for No Plastic Inserts....106
Figure 72 Names of Blades and Actual Position on Rotor....107
Figure 73 Probe 1 Assignments, November....108
Figure 74 Probe 2 Assignment, November 108
Figure 75 Probes 1 and 2 Blade Assignments, December 109

LIST OF TABLES

Table 1. Air Jet Experiment 26
Table 2. Runs at Different Magnet Positions 29
Table 3. NSMS Blade Number for Strain-Gauged Blades 30
Table 4. Average Blade System Deflections for the Magnet Runs 34
Table 5. Plated and Unplated Runs 38
Table 6. Identification of Probes with Blade Numbers 39
Table 7. Excitation Increase After Plating 41
Table 8. Average Effect of Plating 42
Table 9. Experiment 4 Data File Names 48
Table 10. Standard Deviation (Average of All Blades and 3 Sweeps) 50
Table 11. Results of Reference Tests (No Inserts) 50

THIS PAGE INTENTIONALLY LEFT BLANK

LIST OF ABBREVIATIONS, ACRONYMS, AND SYMBOLS

AJE	Air-jet excitation
AEDC	Arnold Engineering Development Center, Tullahoma, TN
ECE	Eddy-current excitation
EO	Engine order…See explanation in Appendix A, Figure 39.
GUI	Graphic user interface
HCF	High cycle fatigue
IFOLP	Integrated Fiber-Optic Laser Probe
NAVAIR	Naval Aviation Systems TEAM
NSMS	Non-Intrusive Stress Measurement System
P&W	Pratt & Whitney
RPM	Revolutions per minute
SDOF	Single degree of freedom

THIS PAGE INTENTIONALLY LEFT BLANK

ACKNOWLEDGMENTS

I want to thank Professor Raymond Shreeve for all his support and guidance during my time here at the Naval Postgraduate School, and especially for his friendship and inspiration during our testing at the Turbopropulsion Lab. Special thanks goes out to John Gibson for all his technical expertise in placement of the laser probes and Rick Still for always having the spin pit ready for operation. I would also like to thank Professor Garth Hobson and Doug Seivwright for their ingenious advice and answering my continuous questions. Finally, I would like to thank my wife, Judy, for all her love and support during my quest for completion of this report.

THIS PAGE INTENTIONALLY LEFT BLANK

I. INTRODUCTION

A. BACKGROUND

Knowing the fatigue life of jet engine compressor and turbine blades is required in order to properly schedule cost saving maintenance procedures and to ensure the safe and reliable operation of military aircraft engines. Changing out an engine from an aircraft because of blade failure is an expensive and time-consuming procedure. Blade failure can sometimes lead to the loss of an engine and, as a result, loss of the aircraft. Thus a thorough understanding of the potential high-cycle fatigue (HCF) life of engine parts is required to ensure higher operational readiness and lower failure rates. However, the determination of the potential fatigue life of engine blades is difficult. Engine tests are expensive, and measuring and understanding the unsteady response of blades operating within the engine, is difficult. Hence the engineering process used to qualify engine parts involves a combination of bench testing, spin testing (in a vacuum spin pit, to reduce the required drive power), engine testing, and analysis. Whether testing is in an engine or in a spin-pit, measurements of the vibrational behavior of blades, as they are excited through resonance, are required.

Non-Intrusive Stress Measurement System (NSMS) technology allows measurements to be made of blade vibrations in a turbomachine without contacting the blades themselves. NSMS, using laser-light probes to measure time-of-arrival of each blade from the light reflected (either from the tip, leading edge, etc), determines the blade deflections, which are related to the stresses in the blades. In principle, the stresses can be derived from the deflections using finite-element structural analysis. In practice, the stresses measured by strain gauges on specific blades can be used to calibrate deflections to stresses in all the blades. The stresses can thus be determined from a time history of blade resonance. Such information is required to develop techniques to design and subsequently qualify parts that are not susceptible to failure due to high cycle fatigue (HCF).

Pratt & Whitney (P&W) began using NSMS techniques in the 1980's, beginning with flutter monitoring, and measuring deflection only [Ref. 1]. The need to develop

NSMS techniques was recognized at Air Force's Arnold Engineering Development Center (AEDC), and work was subsequently sponsored by the Air Force [Ref. 2, p. 2]. In 1999, P&W began using 'Generation 4' software and 'Generation 3+' hardware, resulting in on-line monitoring of multi-mode integral orders of the blade response [Ref. 1]. Measurement thresholds as low as 2 to 3 mils, peak to peak, can now be obtained inside an operating engine at up to 800 degrees Fahrenheit. The NSMS systems employed at P&W included optical (light probes) and non-optical probe types, including capacitance and eddy current sensors. NSMS was also used successfully by P&W in spin tests [Ref. 1]; however, no specific hardware and software package was developed for application to spin testing.

Beginning in 1998, the engine-scale spin pit at Naval Postgraduate School (NPS) was refurbished under NAVAIR sponsorship to serve as the Navy Rotor-Spin Research Facility [Ref. 3]. The goals were to develop blade excitation and measurement techniques for HCF-related spin testing, and transition that expertise to the Navy's Rotor Spin Facility at the Naval Air Warfare Center at Patuxent River, MD. The Air Force loaned four Integrated Fiber-Optic Laser Probes (IFOLP), with associated transmitters and receivers, to NPS, to enable NSMS experiments. In June of 2000, Nicholas Osburn completed his NPS Master's thesis, "Implementation of a Two-Probe Tip-Timing Technique to Determine Compressor Blade Vibrations", wherein he demonstrated and verified the capability of the probes to obtain blade tip timing, time of arrival (TOA), and vibration data on a low-speed compressor. [Ref. 4] The probes were subsequently installed in the spin pit and used in the current project.

The methodology for measuring and analyzing turbine blade vibrations, using the newly installed laser-light probe NSMS, was developed in the present study. The data collected were used to estimate stress in all the rotating blades during an RPM sweep, by correlating NSMS to strain gauge data from specific blades. A fir-tree root, bladed-disk rotor (XTE-66 turbine), with strain gauges attached, was the test specimen. The strains were recorded using a multi-channel acquisition system. NSMS data acquisition used a blade vibration sensor interface (BVSI) board to a PC with LABVIEW software from

Hood Technology, for data collection and data reduction. [Ref. 5] EXCEL was used for post processing and presentation.

B. PROGRAM GOALS

The main goal of the program was to set up and calibrate the laser probe NSMS in the spin pit. Initially, the software was exercised and consistent procedures were developed to analyze the results of the data collection. The goal then was to develop a relationship between strain gauge measurements of (inferred) stress, and NSMS measurements of deflection, for the XTE-66 turbine rotor, and then use this relationship in all follow-on experiments. Finally, the procedures to be followed in future HCF-related spin testing were to be determined and documented.

THIS PAGE INTENTIONALLY LEFT BLANK

II. FACILITY DESCRIPTION AND TEST PROCEDURE

A. FACILITY

The Naval Postgraduate School spin pit test chamber is 63 inches in diameter and approximately three feet deep. The pit can be evacuated to a vacuum of 100 to 300 millitorr. The turbine drive system is powered by compressed air and can be run continuously. A view of the facility is shown in Figure 1. Details of the construction and capability of the facility are given in Ref. 3.

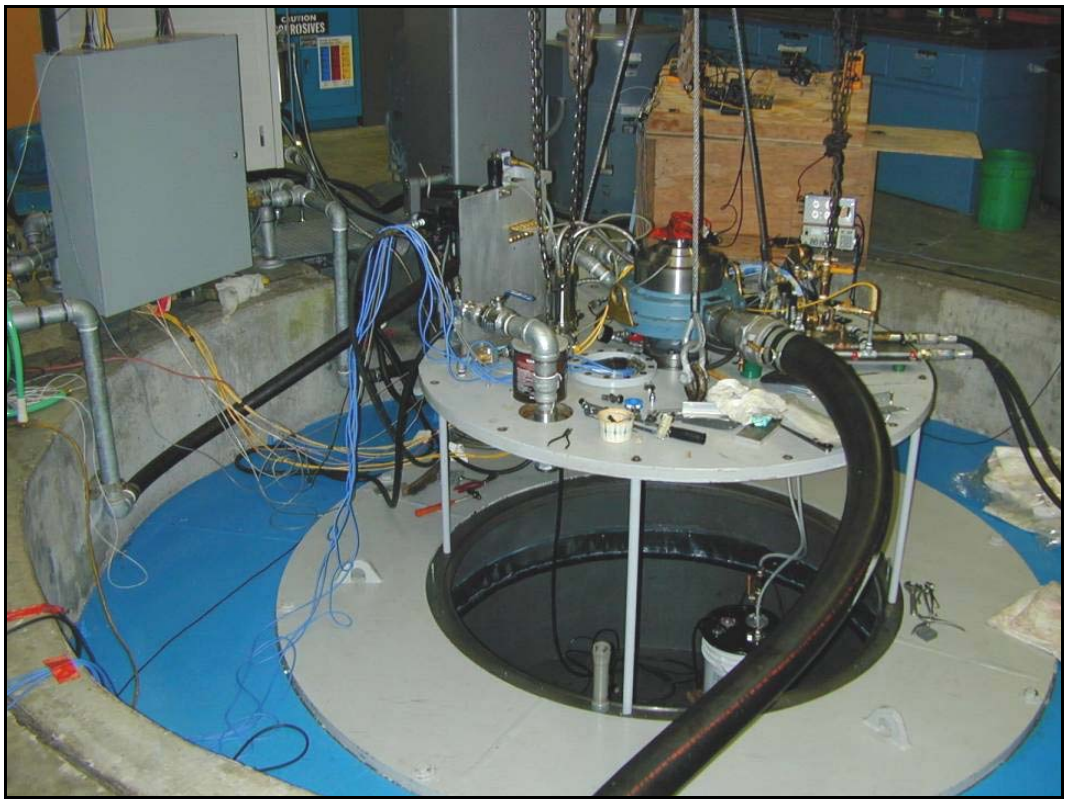

Figure 1 NPS Spin Pit

B. TEST ARTICLE

The rotor used in the present program was the Pratt & Whitney XTE-66 second stage turbine rotor. The 22.5-inch diameter, 58-blade rotor was partially bladed using 28 XTE-66 turbine blades in two sections (14 blades in each section on opposite sides of the rotor), and 30 dummy blades in two sections of 15, filling in the remaining gaps. A view of the rotor is shown in Figure 2. The layout of the blades, showing blade numbers inherited from previous P&W test programs is shown in Figure 3. The rotor was

balanced before installation. An allowance of 0.050 inches for runout due to imbalance during start up and shut down was made in positioning light probes outboard of the tips. The largest runout measured was 0.020 to 0.025 inches.

Figure 2 XTE-66 Second Stage Turbine Rotor

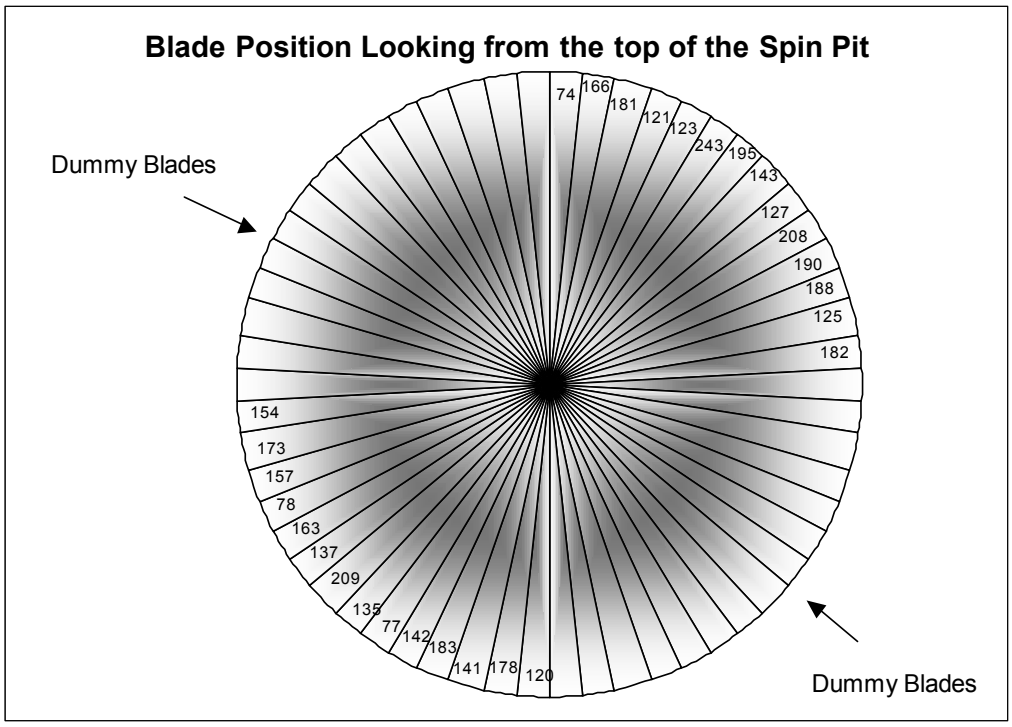

Figure 3 Identities of XTE-66 blades

The strain gauge wires running along the base of the bladed section can also be seen in Figure 2. The test rotor was fitted with 32 strain gauges to measure the strain on the blades at the root and mid-span on either the pressure or suction side of the blades. At the time of the present experiment, only six strain gauges were functioning and three of those were root gauges. The root gauges were used to correlate the laser probe displacement measurements to the strains.

C. BLADE EXCITATION & TEST PROCEDURE

In the work reported here either air-jet excitation (AJE) or eddy-current excitation (ECE) was used to excite resonance. One geometry of AJE is shown in Figure 4. The test procedure with AJE was to stabilize the rotational speed above the RPM required for resonance, open a solenoid valve to supply pressure to the jets, and record data during the resulting natural deceleration caused by air-drag. One geometry of ECE is shown in Figure 5. The test procedure with ECE was to stabilize the RPM above the RPM required for resonance, raise the ring holding the arrangement of permanent magnets to a

preset gap, and record data during the natural deceleration caused by magnetic drag forces.

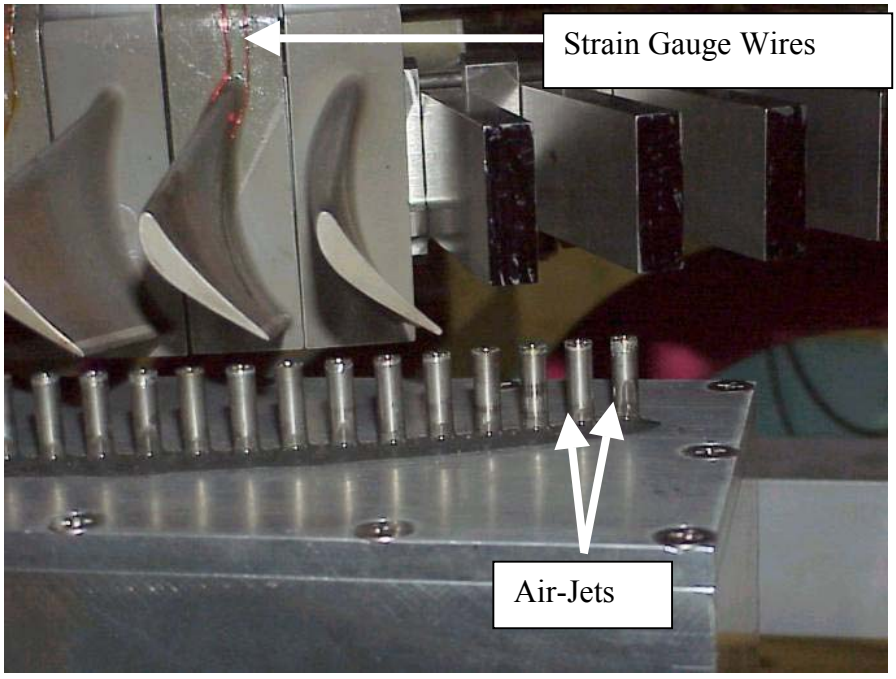

Figure 4 Air Jet Excitation Setup

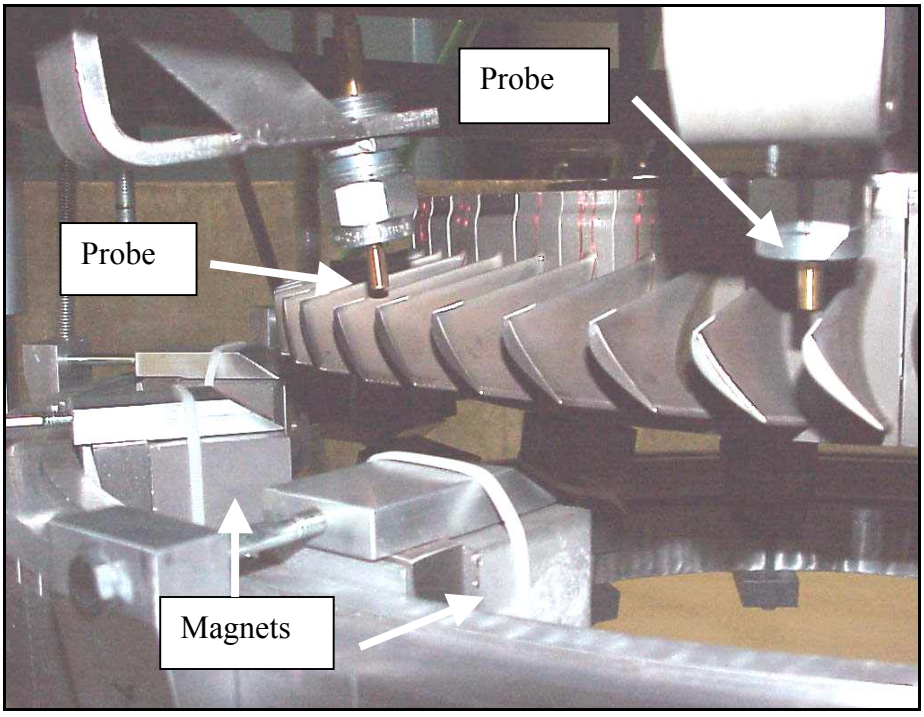

Figure 5 ECE Excitation Setup

III. BLADE VIBRATION MEASUREMENT SYSTEM

A. OVERVIEW

Two laser-light probes were positioned to emit and receive light reflected from each passing blade. The time-of-arrival (TOA) of the reflected light, after a one-per-rev (1/rev) signal, was then a measurement of the deflected position of the blade. A synopsis of the underlying concepts and data analysis is given in Appendix A. The two probes provided two independent measurements. For each channel a laser transmitter sent its signal through the fiber optic cable to the laser probe. The reflected light was then transmitted back to a receiver where it was output as a TTL pulse or an analog waveform. Typically, the analog pulse was processed through a Blade Vibration Sensor Interface (BVSI), sent to a National Instruments PCI-6602 counter board, and then LabVIEW software recorded and displayed the acquired data. The signals into and out of the BVSI could then be selected for display on an HP Infinium four-channel PC oscilloscope.

A. INTEGRATED FIBER OPTIC LASER PROBE (IFOLP)

The integrated fiber optic laser probe was a cylindrical probe, designed for mounting into the casing of an engine, or in this case, to a bracket inside the spin pit. Figure 5 shows the two probes mounted to look at the leading edges of the rotor. The probes used integrated fiber optics technology to deliver a spatially coherent laser spot to the blade tip [Ref.6, p. 10]. Low-pressure air could be used to protect the tip of the probe from contamination, but was not used in the present experiment. A tissue soaked in isopropanol alcohol was used to clean the lens, after each run. A more extensive discussion of the probes is given in Ref 7.

B. LASER TRASMITTER, RECEIVER, AND FIBER-OPTIC CABLE

The transmitter module (IFO-TX1) provided continuous laser output at a wavelength of 780 nm at a power level of 6mW. The fiber optic cable for the transmitter contained a single mode optical fiber (green cable), terminated with an FC/PC (physical contact, end face polished) diamond optical connector. The fiber optic cable for the

receiver contained a low loss, high numerical aperture, multimode optical fiber (orange cable), terminated with an SMA (threaded) connector. The receiver module (IFO-RX2) used a reverse biased avalanche photodiode (APD) to detect the optical signal as a series of photoelectron pulses. The pulses were then amplified and converted to voltage pulses through a JFET transimpedance amplifier. The output (OUT2) gave a voltage waveform, which maintained the shape and height of the optical pulse as the blade tip passed the laser point (gold cable). The receiver also generated a TTL pulse (OUT1), which was not used in the present experiment. [Ref 6, p. 8, 10]

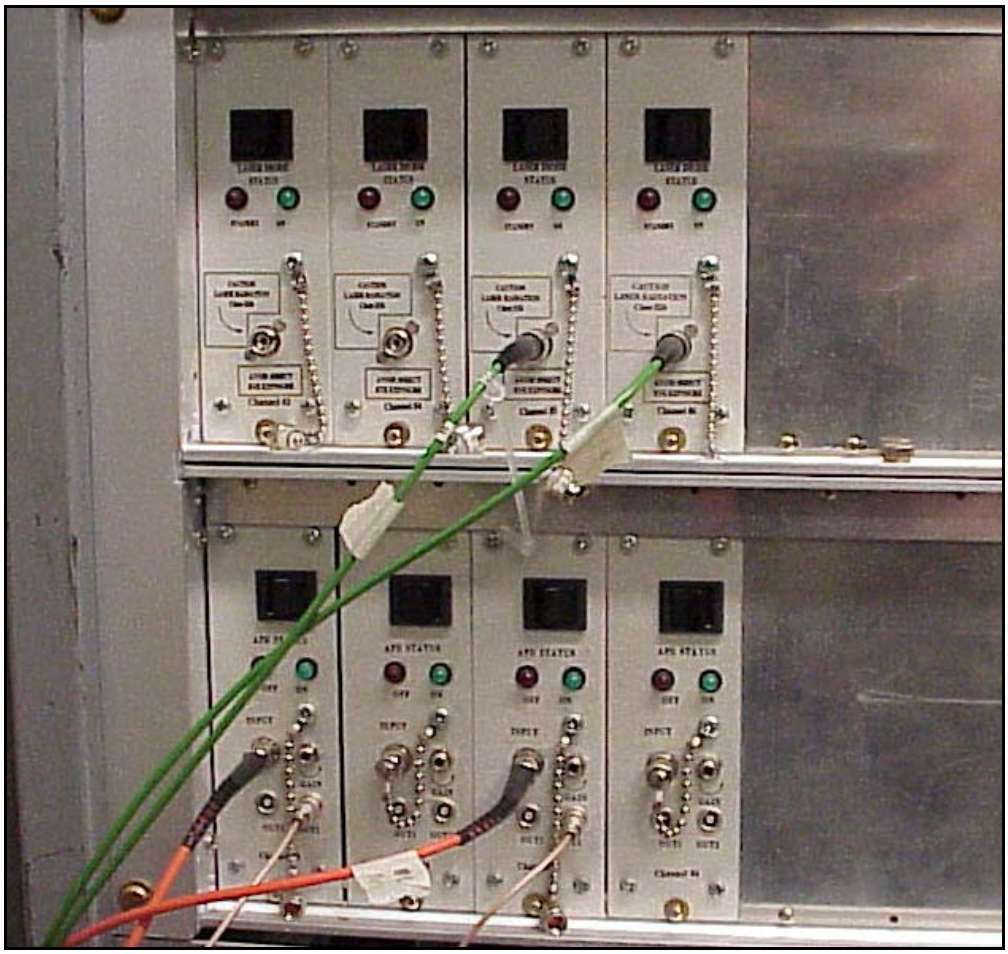

Figure 6 Laser Transmitters (top) and Receivers (bottom)

C. BLADE VIBRATION SENSOR INTERFACE (BVSI)

The purpose of the BVSI, a product of Hood Technology Corporation shown in Figure 7, was to convert the voltage waveform output of the receiver into a TTL pulse to

be used as an input to the PCI counter board. The LabVIEW software programmed the counter to output the number of PCI board clock pulses before blade arrival, and to convert this number to displacement using the concurrently determined clock pulses per rotation, and rotor circumference. The BVSI also allowed a selection of signals to be displayed on each of two oscilloscope channels.

For inputs (from the left side of Figure 7), probe 1 output was taken from laser receiver 1, probe 2 output was taken from laser receiver 2, and a one-per-revolution (1/rev) signal was taken from a laser diode and detector system viewing through a hole in a disk on the drive turbine shaft. The first toggle switch selected what signal type was input, BNC or Sub-D. It was left in the "up" position for BNC. The next switch grounded the signal and was not used.

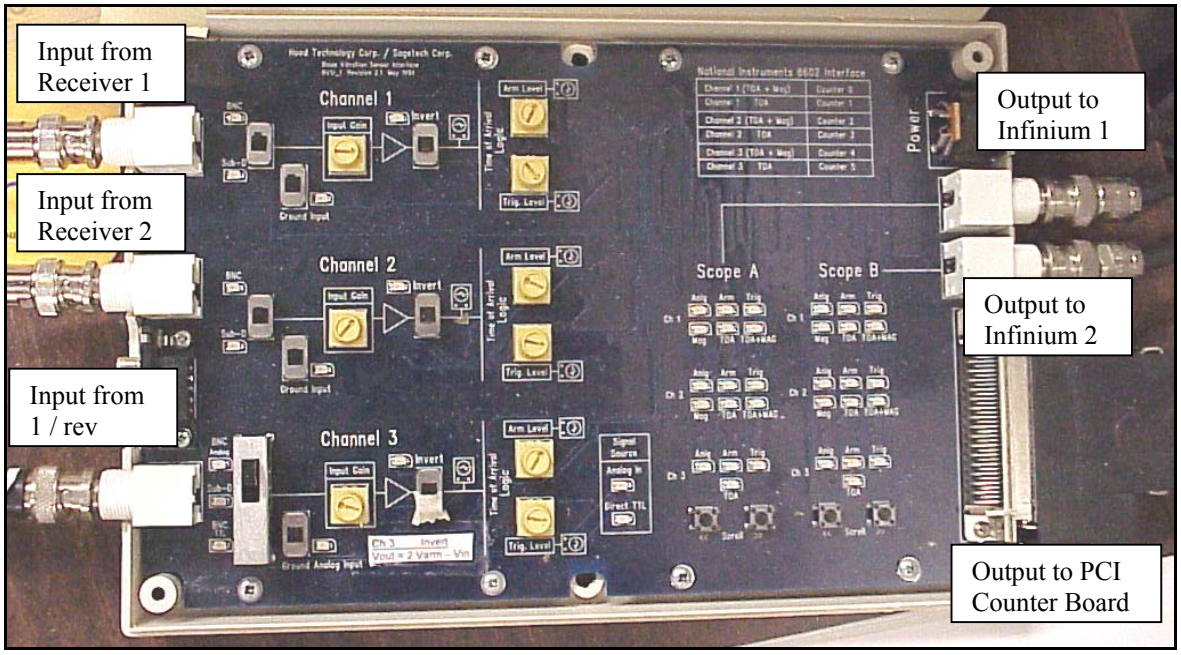

Figure 7 Blade Vibration Sensor Interface Board

The first screw adjustment was the signal gain, followed by a switch to invert the signal. The inverted signal switch was only used for the 1/rev, and allowed the pulse to be generated by the steep rising edge of the signal. The following two screw adjustments (one above of the other) were for the arm (top screw) and trigger settings for the arrival pulse of each channel. The display of lights on the right half of the BVSI board allowed the user to select a signal to display on the Infinium oscilloscope. The two push buttons at the bottom of each set of lights enabled the user to scroll between sixteen signals and

display one on “Scope A” and one on “Scope B.” For example, “Scope A” could display the arming signal level of probe 1 while “Scope B” could display the trigger level of probe 1, while the trigger level was being adjusted. The right side of the board shows the two output BNC’s and the interface connection to the PCI counter board in the computer.

D. OSCILLOSCOPE

An HP Infinium Oscilloscope, shown in Figure 8, was used to display on channels 1 and 2, the signals connected to “Scope A” and “Scope B,” respectively. Channel 4 was used to display the 1/rev signal. Setup and usage are described in Appendix B.

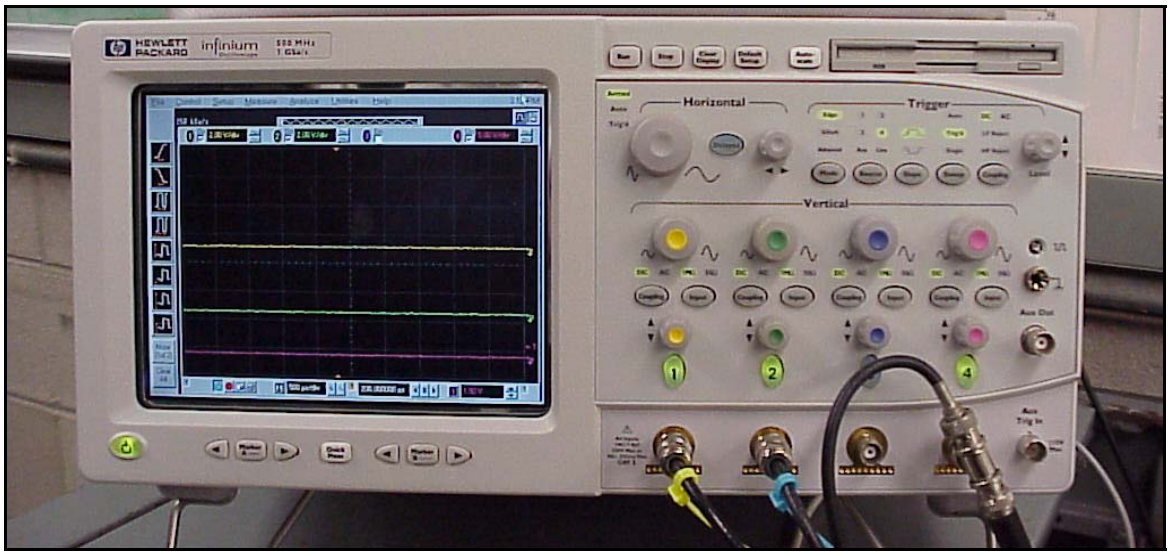

Figure 8 Infinium Oscilloscope

E. PC COMPUTER

A Micron Pentium III, 500MHz PC with 256k of RAM and two 20 Gig hard drives was used with the Windows 2000 operating system, Microsoft Office 97 and LABVIEW 5.1. Two National Instruments PCI-6602 counter boards and associated software drivers were installed, as described by Osburn [Ref. 4].

IV. SOFTWARE AND DATA MANIPULATION

A. OVERVIEW

The acquisition and processing software used in the present experiment was developed by Hood Technology Corporation. A detailed description of the theory of measurement is given in Appendix A. A basic description of the software and its usage follows. The three programs used to acquire, process and display the NSMS data, and post-process the results were the Data Acquisition Program (version 3.0), the Data Viewer Program (version 1.3) and Microsoft Excel, respectively.

The acquisition and viewer software both ran as executable files in the LabVIEW 5.1 program. The acquisition software recognized the PCI counter board, which was set up to read the signals from the BVSI board, and recorded and displayed RPM and TOA from laser probe reflections. The viewer software processed the acquisition program's four output files into Blade Lag Deflection vs. RPM. A single degree of freedom (SDOF) curve fit was then applied manually to determine the resonance frequency, quality (Q), deflection and phase angle. The resonance data were manually written to a text file (through a software interface) and then imported into an Excel spreadsheet. The spreadsheet allowed the user to apply averaging, calculate standard deviations and to create figures that illustrated how the blades reacted during resonance. [Ref 8]

B. NSMS DATA ACQUISITION (VERSION 3.0)

The data acquisition software was easy to install and simple to use. The user's manual was provided [Ref 8]. A description follows of the process used to acquire and reduce data. [Detailed steps in the procedure are given in Appendix B]

After connecting the PCI counter board (one of two in the computer) to the BVSI, the data acquisition software required the user to input specific data about the rotor and counter board clock set up. The GUI screen is shown in Figure 9. The main page displayed the following components: a) RPM History Graph, b) Operation Buttons, c) Data Writing Criteria, d) Data Acquisition Notes, e) Analog Signal Amplitude Graph, f) Analog Signal Selection, g) Sensor Status Table.

The first step was to set up the hardware configuration, as shown in Figure 10. The two counter boards in the computer allowed several clock settings; 20 Mhz was selected. The rotor dimensions were entered. Each counter board was referred to as a device. The device was capable of receiving three inputs from the three-channel BVSI. The first device was used for TOA pulses from the two probes and RPM from the one-per-rev. Device two was not used, and therefore was disabled. The RETURN bar brought the main page back into view. The Data Writing Criteria was set at "Manually Dump Data to Disk" in order to facilitate the start/stop in coordination with strain gauge recording during an RPM sweep. The Range and Notes options were not used.

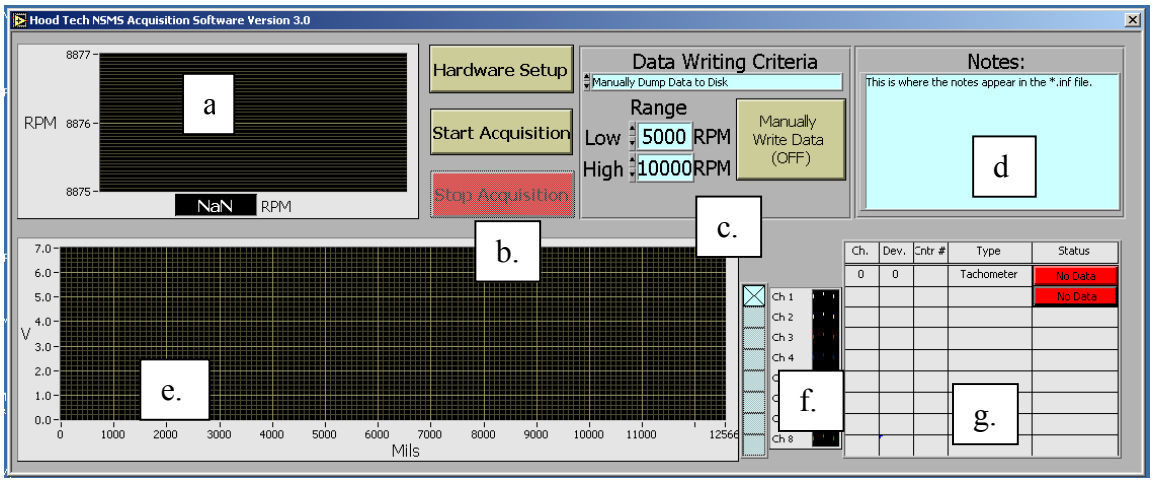

Figure 9 Main Display of Data Acquisition Software

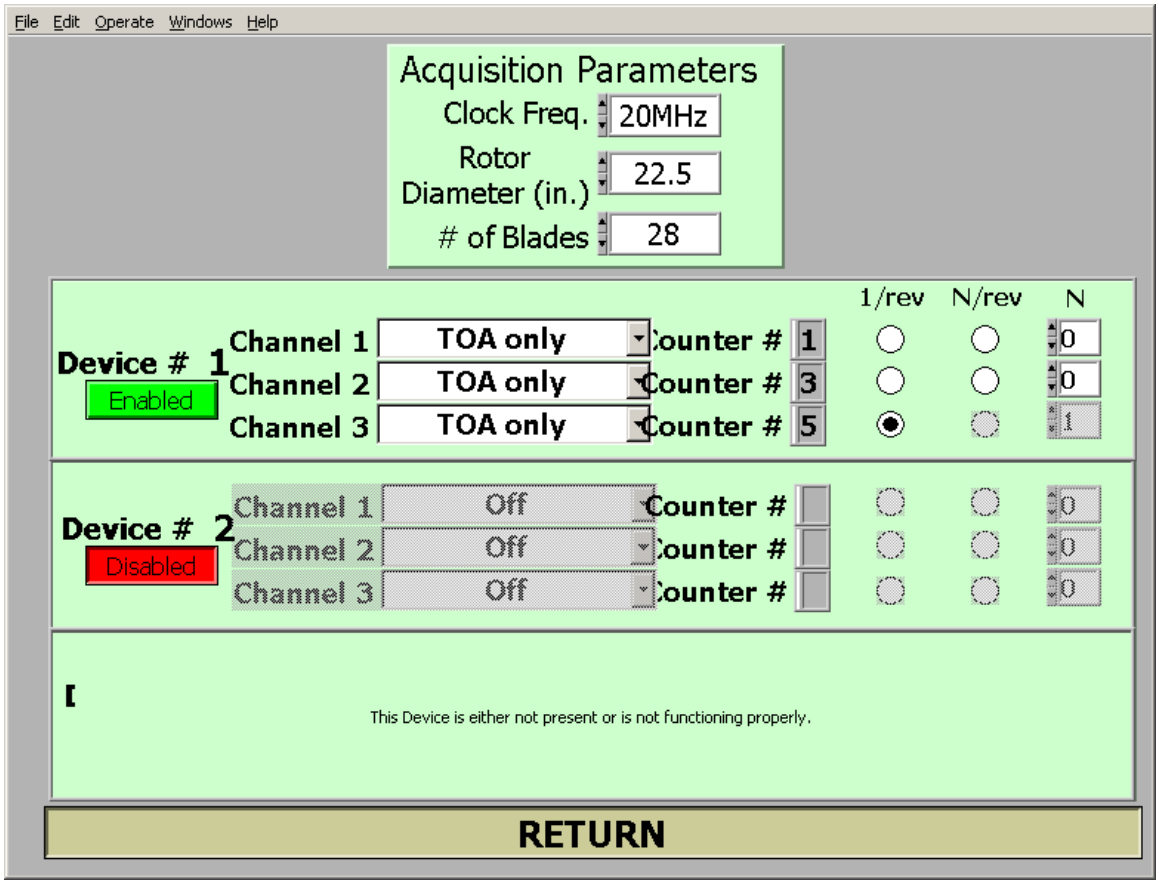

Figure 10 Data Acquisition Hardware Setup

Once the spin pit was set up and the turbine was running, the Start Acquisition button was selected to start receiving data flow from the counter board. The Manually Write Data button was selected, and deselected, at the desired start and stop RPM levels. The display appeared similar to Figure 11 during the recording of data. Notice the RPM History as the rotor was brought up to speed, stabilized, and then run through the resonance while decelerating. The Analog Signal Amplitude Graph showed (as vertical 5-volt bars) all 28 blades for both probe 1 and probe 2 with their respective positions around the circumference of the rotor (the x-axis on the graph). The x-axis corresponded to the 22.5-inch diameter rotor (22.5/2*π*2=70.686 inches), displayed in mils or thousandths of an inch (0.001 inch = 1 mil). Individual probe blade placements could be viewed by deselecting the "X" in either CH.1 or CH. 2. The Status display was an essential feature in setting up the arm and trigger of the system for each channel. If the arm and trigger were set too low, "Extra Pulses" was displayed, and the levels had to be

raised using the BVSI screw adjustments. Conversely, "Missing Pulses" was displayed if the arm and trigger levels were adjusted too high. Through the Infinium oscilloscope, the arm and trigger levels could be adjusted so that "Good Data" appeared, and was taken, throughout the experiment.

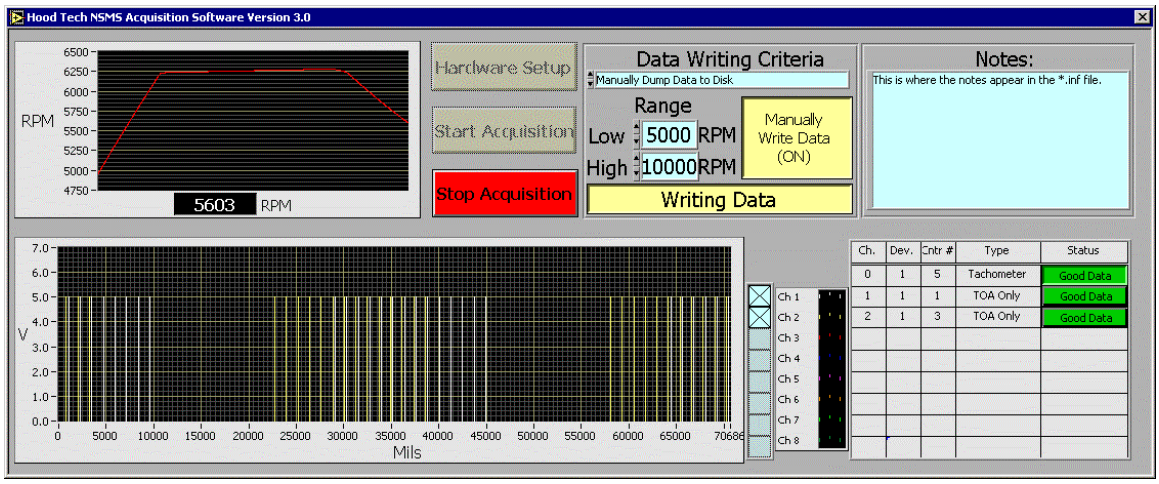

Figure 11 Operating Acquisition NSMS Software

The output of the data acquisition software consisted of four files. The first file contained the hardware setup information. The other three files were the 1/rev RPM, the probe 1 TOA, and the probe 2 TOA, respectively. The data viewer used the files to calculate and display the computed behavior through the RPM sweep.

One selection on the BVSI, which was found to be critical, was to invert the 1/rev on channel 3. The BVSI TTL output was set to arm on the up slope and trigger on the down slope of the incoming voltage. The incoming 1/rev is shown in Figure 53. Since the width and slanted downslope of the 1/rev signal varied with RPM, triggering on the downslope would move the trigger point around the rotor. By inverting the 1/rev, the arm was set on the moving edge of the signal and the trigger occurred on the fixed leading edge, as shown in Figure 55.

C. NSMS DATA VIEWER (VERSION 1.3)

The data viewer was the essential tool used to process the TOA data and derive characteristics of the resonant behavior. The screen of the data viewer is shown in Figure

12. Results were designated by ‘run,’ ‘test’ and ‘sweep’ numbers. The ‘run’ characterized a fixed configuration of the spin pit on a specific day. A ‘test’ consisted of one start up to shut down of the rotor. The ‘sweep’ consisted of one acceleration or deceleration of the rotor through resonance. [After a sweep was recorded, the rotor could be spun back up (or down) to the initial RPM for another sweep, or stopped, thus ending the test.] The data viewer was used to process the results of each sweep. The operator assigned file names that would identify the sweep to be within the appropriate test and run numbers.

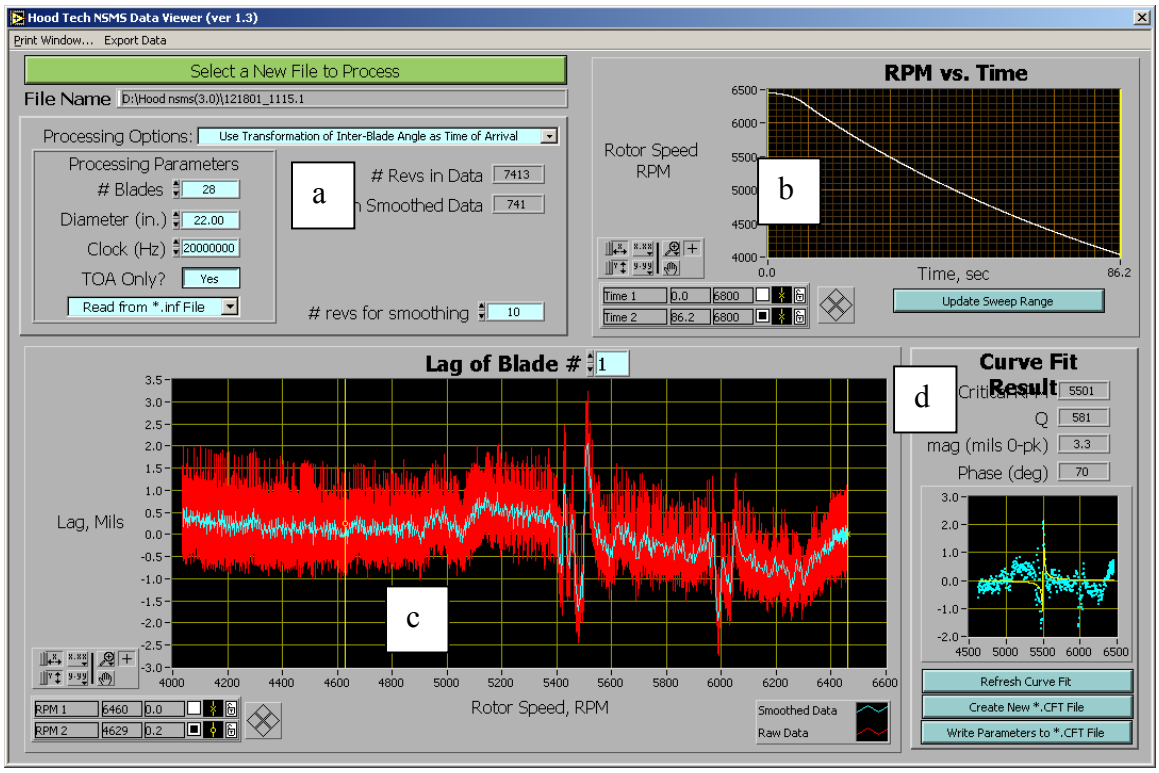

Figure 12 Data Viewer Main Page

The data viewer main page had four main areas: a) The data viewer Processing Options and Parameters, which allowed the user to load files in, view the acquisition parameters and select between two processing options; b) The RPM vs. Time Graph, which showed a plot of RPM as a function of time over the course of the sweep. The user could define a specific range of time (using the slider bars) to be displayed in the Lag of Blade vs. RPM graph; c) The Lag of Blade vs. RPM window showed individual blade lag as a function of RPM. The scroll window, to the right of “Lag of Blade #,”

allowed the user to select the desired blade number; d) The Curve Fit Results window showed the results of a single degree of freedom curve fit (SDOF) to the data within the adjustable slider bars in the Lag of Blade window. The results were displayed in both graphical and parametric form.

To process the results of a sweep, the desired data file was selected and processed using the "Inter-Blade Angle for Time of Arrival" option. Then, each blade was selected in the Lag of Blade # scroll window. For each blade selected, the slider bars were positioned around the resonance as shown in Figure 13. The curve fit window was "refreshed" in order to calculate the results. The placement of the slider bars was very important in order for the curve fit to work.

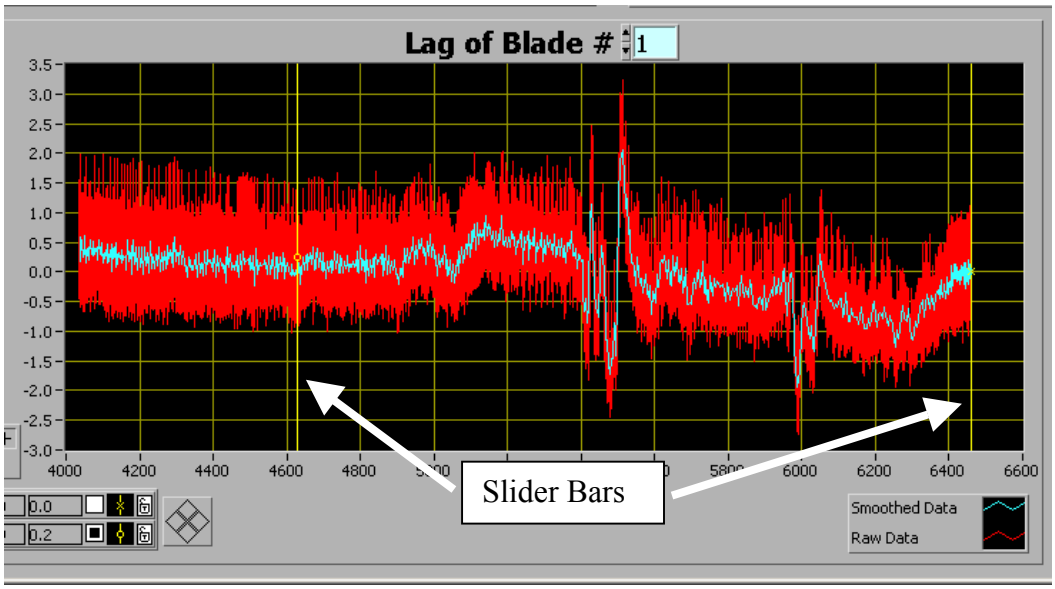

Figure 13 Slider Bars Encompassing the Resonance

Figure 14 shows a good curve fit, in that both ends of the fit are along the zero lag line. This was achieved by adjusting the positions of the slider bars and refreshing the curve fit. Notice that the magnitude is given in mils, 0 to peak.

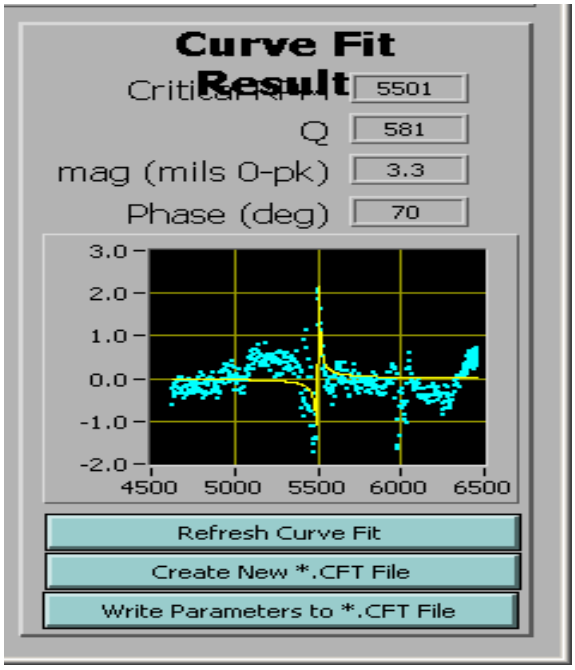

Figure 14 Good Curve Fit

The results were written to a file of the users choice. The author used 'date_time' stamps in order to keep track of when each set of data was taken. The output file (*.cft) was created by selecting "Create New *.CFT File." Then "Write Parameters to *.CFT File" was selected for every blade, once a good curve fit was achieved. Data were appended to the file every time the button was pressed. The file ultimately contained the blade number, resonant RPM, Q, deflection, and phase angle for all 28 blades. The file could then be viewed as a notepad or wordpad file to ensure all data were stored correctly. A new *.cft file was created for each sweep. Appendix C shows a listing of the processed data files (*.cft) for the experiments reported here.

D. MICROSOFT EXCEL

Excel was chosen to post-process the data. Data from each *.cft file were cut and pasted into one data sheet in Excel. An example is shown in Figure 15. Notice at the bottom of the Excel workbook, the *.cft data filename was used to identify the worksheet. This ensured that the correct probes, sweeps, tests, and runs were used to average data and plot the results. Figure 16 is a sample of how the data were collected and correlated in Excel. This particular example shows the strain gauge data, from strain

14, with the deflections for the same blade obtained with probes 1 and 2, in the process of deriving the correlation of strain gauges to NSMS.

Excel spreadsheets were linked, blade-to-blade, frequency-to-frequency, deflection-to-deflection, etc. This approach simplified the process of analyzing data, for example, to obtain a comparison of all blades in one entire sweep to another sweep, or a comparison of one blade to the same blade in different sweeps. Also, standard deviations were computed by linking the averages through the 'stdev' function. The software allowed trend-fitting graphs and multiple run analysis to be carried out. Notice in Figure 16 how the spreadsheet was used to add identifying information, such as run number, run date and times, and magnet placement. Excel was easy to use and allowed a 'big picture' view of the data.

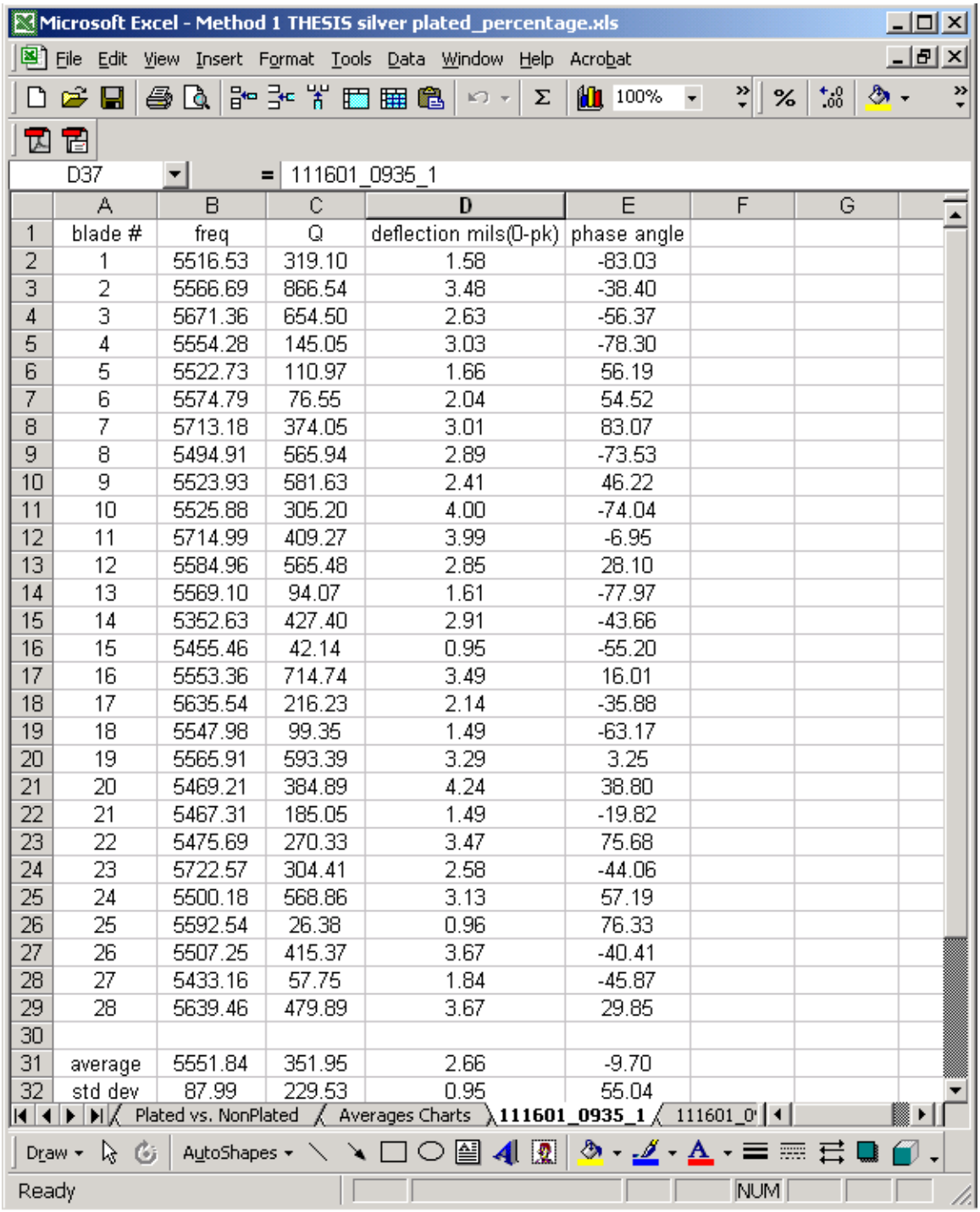

	A	B	C	D	E	F	G
1	blade #	freq	Q	deflection mils(0-pk)	phase angle		
2	1	5516.53	319.10	1.58	-83.03		
3	2	5566.69	866.54	3.48	-38.40		
4	3	5671.36	654.50	2.63	-56.37		
5	4	5554.28	145.05	3.03	-78.30		
6	5	5522.73	110.97	1.66	56.19		
7	6	5574.79	76.55	2.04	54.52		
8	7	5713.18	374.05	3.01	83.07		
9	8	5494.91	565.94	2.89	-73.53		
10	9	5523.93	581.63	2.41	46.22		
11	10	5525.88	305.20	4.00	-74.04		
12	11	5714.99	409.27	3.99	-6.95		
13	12	5584.96	565.48	2.85	28.10		
14	13	5569.10	94.07	1.61	-77.97		
15	14	5352.63	427.40	2.91	-43.66		
16	15	5455.46	42.14	0.95	-55.20		
17	16	5553.36	714.74	3.49	16.01		
18	17	5635.54	216.23	2.14	-35.88		
19	18	5547.98	99.35	1.49	-63.17		
20	19	5565.91	593.39	3.29	3.25		
21	20	5469.21	384.89	4.24	38.80		
22	21	5467.31	185.05	1.49	-19.82		
23	22	5475.69	270.33	3.47	75.68		
24	23	5722.57	304.41	2.58	-44.06		
25	24	5500.18	568.86	3.13	57.19		
26	25	5592.54	26.38	0.96	76.33		
27	26	5507.25	415.37	3.67	-40.41		
28	27	5433.16	57.75	1.84	-45.87		
29	28	5639.46	479.89	3.67	29.85		
30							
31	average	5551.84	351.95	2.66	-9.70		
32	std dev	87.99	229.53	0.95	55.04		

Figure 15 Excel Workbook Example

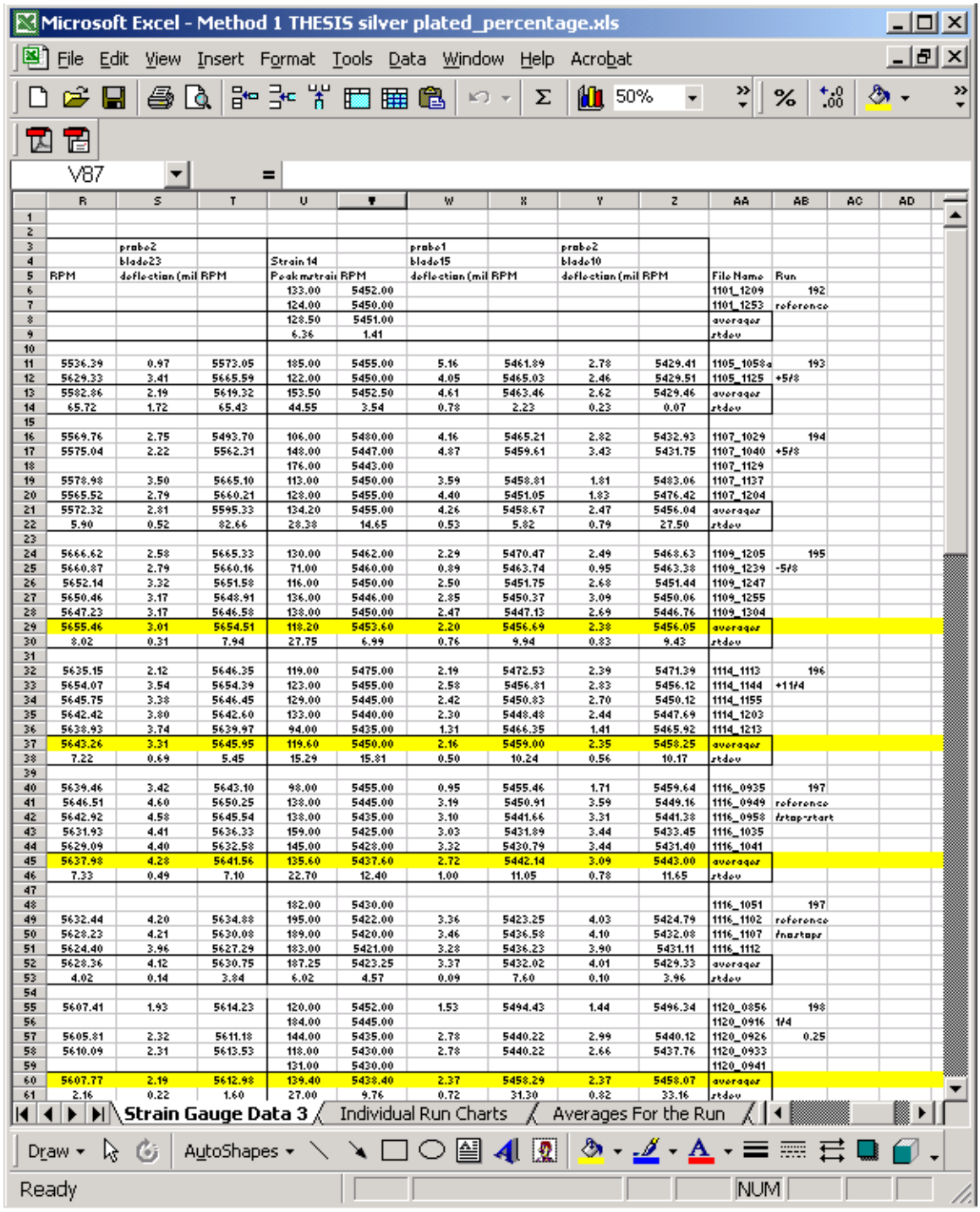

Figure 16 Sample Excel Data Page

V. TEST PROGRAM AND RESULTS

A. OVERVIEW

Following a preliminary test program in which only strain measurements were taken, four series of tests were conducted using the NSMS system with the XTE-66 rotor. For the purposes of reporting, the four series of tests will be referred to as experiments 1 through 4. The first experiment involved AJE and served to obtain a preliminary comparison between strain and NSMS measurements. The second experiment involved ECE (magnet) excitation, and determined the correlation of NSMS to strain measurements, and hence to stresses in the blades. The last two experiments applied the (now calibrated) NSMS system to obtain useful information in the study of the rotor system. This overview will present a brief chronology of the experiments before the results are discussed.

From 11 May to 12 June 2001, experiments were conducted to determine the best magnet arrangement for twelve engine order (12EO) and then 9EO excitation of the XTE-66 turbine blades. Twelve pairs of magnets were arranged around the rotor with the intention of producing the highest magnitude of unsteady strain. The NSMS system was not yet available. The best configuration of magnets (raised and lowered by a stepping motor to vary the distance between the magnets and blade trailing edges) was a set of north-south/south-north arrangements at 0.5 inches of gap. Since the unsteady stress levels produced were too low, an additional ring of magnet pairs was designed and built. It was raised over the tips of the blades as shown in Figure 17. The double ring was first used in the second experiment.

Figure 17 Magnet Pair at the Blade Tips [Right-Side Magnet (Unmarked) is a South Pole]

The first experiment with NSMS involved the use of air jets to excite resonance in the blades to establish the effectiveness of a proposed resonance damper system. Again several air-jet configurations were tried in order to obtain the highest strain values. From 19 June to 11 October 2001, four engine orders were studied with different jet configurations at different air pressures. The NSMS system was set up and procedures were developed to relate strain to deflection in the course of these experiments. The NSMS data supported that obtained from the strain gauges, for three of the four engine orders studied.

The second NSMS experiment took place from 1 November to 20 November 2001. ECE was set up with two sets of magnet pairs, one along the trailing edge and one at the blade tips (after the two ring combination was raised). Tests were then conducted to find the relative magnet position (one ring with respect to the other), which gave the maximum strain. During these tests, a correlation of strain to NSMS deflection was developed. The success of the correlation allowed further tests to be conducted when all the strain gauges had failed.

The third experiment followed the plating of six blades with 0.010 inches of silver. NASA had reported doubling the strain produced after plating similar blades. NASA's system consisted of only two blades, rotating on a single rotor with no dummy

blades. Test runs on the silver-plated blades were conducted on 17 and 18 December 2001. During these tests, the NSMS was stand alone, without concurrent strain gauge data.

The fourth experiment was conducted on 17 January 2002. This experiment established the effect of plastic inserts, placed between the root of the blade and rotor, on the repeatability of the measurements taken between rotor stops and starts. It had been noted that there was a wider variation of data from tests in which the rotor was started after a complete stop, as compared to sweeps between which the rotor was not stopped completely. The NSMS measurements successfully quantified the effect of supporting the blades in their seats using plastic inserts.

B. EXPERIMENT 1 – AIR-JET EXCITATION AND EFFECT OF DAMPERS

Air-jet excitation tests were made to examine blade resonant response at 200EO, 12EO, 8EO and then 10EO. Pratt & Whitney was developing an advanced internal damper system and sought verification and extension of their results from the NPS tests. The damping system was designed to reduce the amplitude of the unsteady strain at resonance. In order to excite the blades initially at 200EO, four blocks of 15 air-jets were installed under the rotor. The jets were directed vertically upwards at the trailing, approximately 0.25 inches from the blade tips, as shown in Figure 4. Very low strain amplitudes were found at 200EO, but high amplitudes were found at 8EO in the first bending mode. Masking jets inside the 4 boxes, and leaving 12 active jets, the 8EO magnitudes were maximized, (i.e. injection over an arc length equivalent to one sixteenth of the circumference, in four places). Tests were subsequently conducted using six boxes with 8 jets active to provide 12EO, and five boxes with 10 jets active to provide 10EO. The runs are summarized in Table 1.

Table 1. Air Jet Experiment

Run #	Date /Name	EO	Dampers	# of tests (continuous)	# of Sweeps, With a Different Air Pressure for each Sweep	
184	0913	8	No	1	4	25-95 psia
185	0918	8	Yes	1	7	12-103 psia
186	0919	8	No	1	7	11-104 psia
187	0925	12	No	1	7	14-98 psia
188	0927	12	Yes	1	8	13-102 psia
189	1004	12	Yes	1	6	20-104 psia
190	1005	12	No	1	5	20-105 psia
191	1012	10	No	1	3	38-101 psia

Detailed results are given in Appendix D. Figure 18 shows the average deflection amplitude for all 28 blades as a function of air injection pressure for the 8EO and 10EO test runs. The damped blade system at 8EO showed slightly lower amplitudes. Additional pressure above 90 psia did not increase the deflection, for two possible reasons. First, at the higher pressure, air was pumped into the spin pit at a faster rate, thereby causing a faster deceleration rate through the resonance. Second, the higher pressure gave progressively more 'blooming' of the jets after they exited the straight tubes at sonic conditions.

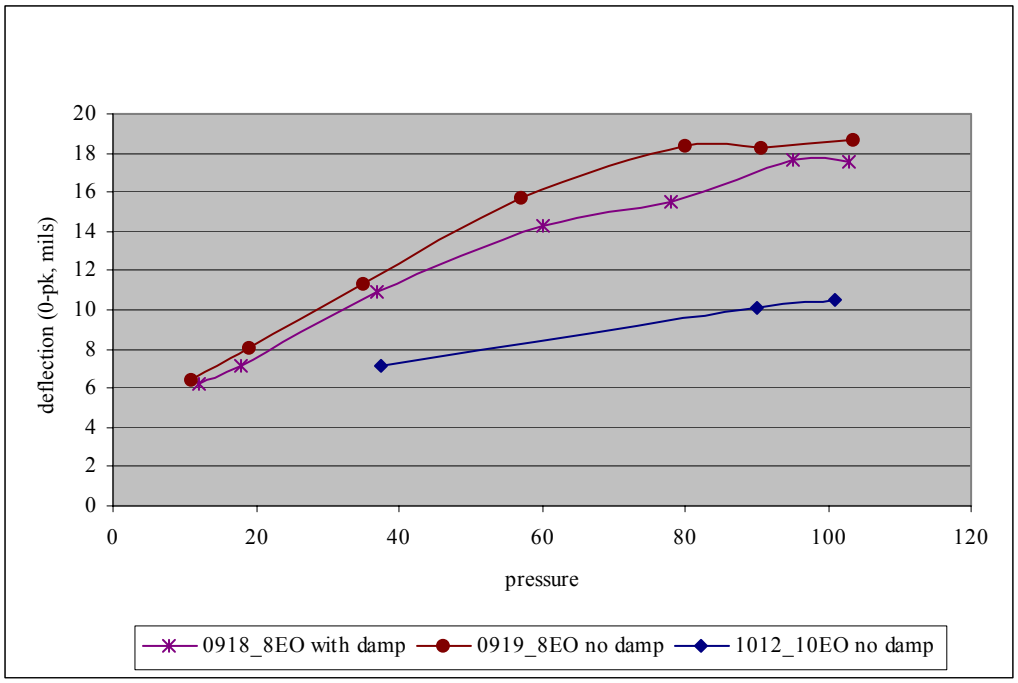

Figure 18 Air Jet Tests With and Without Dampers at 8EO and Without at 10EO

Results of 12EO tests are shown in Figure 19. Lower deflections were attained at 12EO than at 10EO. The 8EO deflections were higher than the 10EO at corresponding injection pressures. It was noted that excitation at 8EO (48 jets total) used 4 blocks with 12 air jets open, while the 12EO used 6 blocks with 8 air jets open (48 jets total). But it must be noted that the RPM for resonance in first bending at each engine order was different. Resonance at 8EO was approximately 8400 RPM, or 140 revolutions per second, so that each blade encountered 6720 jets per second. Resonance at 12EO was at approximately 5600 RPM, or 93 revolutions per second, so that each blade encountered 4480 jets per second. In both cases, the blade resonated at 1120 cycles per second, and therefore, the reduced excitation energy input per oscillation cycle explains the reduced amplitudes of response at the higher engine orders.

After run 188, a modification was made to the air-jet blocks in an attempt to reduce the blooming involved when the air entered the vacuum of the spin pit. In fact, the modification, which was in place for runs 189-191 (1004, 1005, and 1012), was unsuccessful and produced lower strains and deflections. The 12EO tests before the

modification showed a negligible effect of dampers on the blade response, whereas the tests after the modification showed a small effect at higher air pressures.

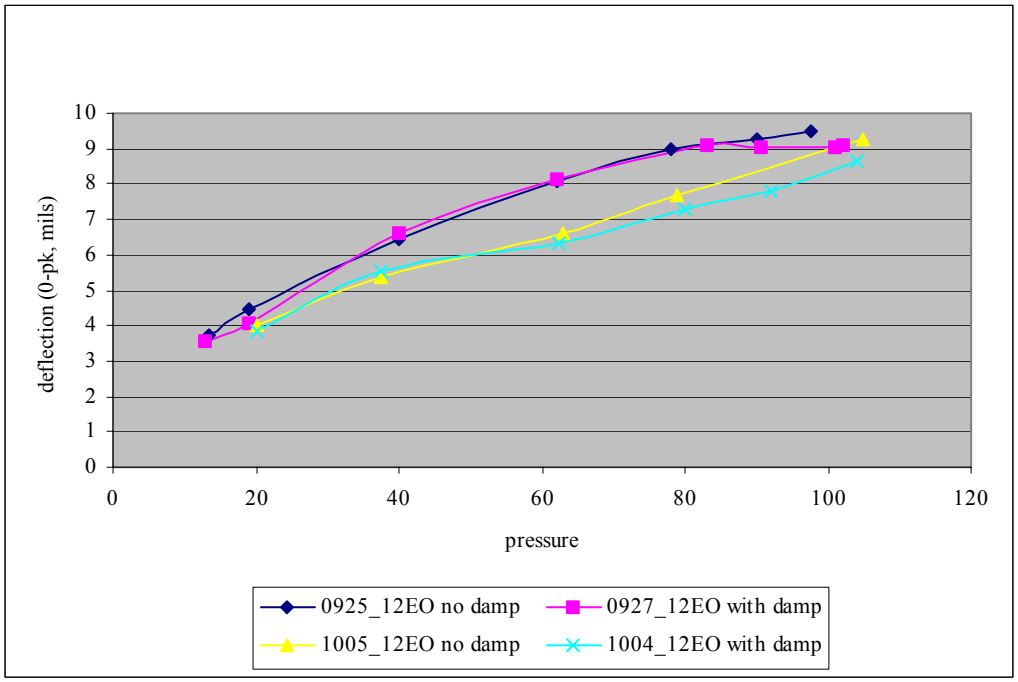

Figure 19 Air Jet Tests With and Without Dampers at 12EO Before Modifications (Sep) and After Modifications (Oct)

C. EXPERIMENT 2 – EDDY-CURRENT EXCITATION AND CALIBRATION OF THE NSMS TO STRAIN MEASUREMENTS

Eddy-current excitation was used in this and subsequent experiments. There were two rings of 12 magnet pairs positioned around the rotor to excite the blades. One ring placed magnets at the tips of the blades while the other ring placed magnets under the blades along the trailing edges, near the tips. A view of the arrangement is shown in Figure 20. The entire 2-ring system was raised and lowered while the rotor was spinning. The offset, referred to as the 'ECE position offset' in Table 2, was the peripheral displacement of the magnets at the tips of the blades from the magnets at the trailing edges of the blades, where the zero-reference position was of one magnet directly above the other. The 5/8-inch displacement was chosen because each magnet was 5/8 inches wide. Therefore one and two magnet widths, either side of centerline, were set in an attempt to produce a higher resonant strain than the reference (N-S/S-N) arrangement

initially in place. Table 2 shows the series of runs in which both NSMS and strain data were successfully recorded. Appendix F contains the complete list of data.

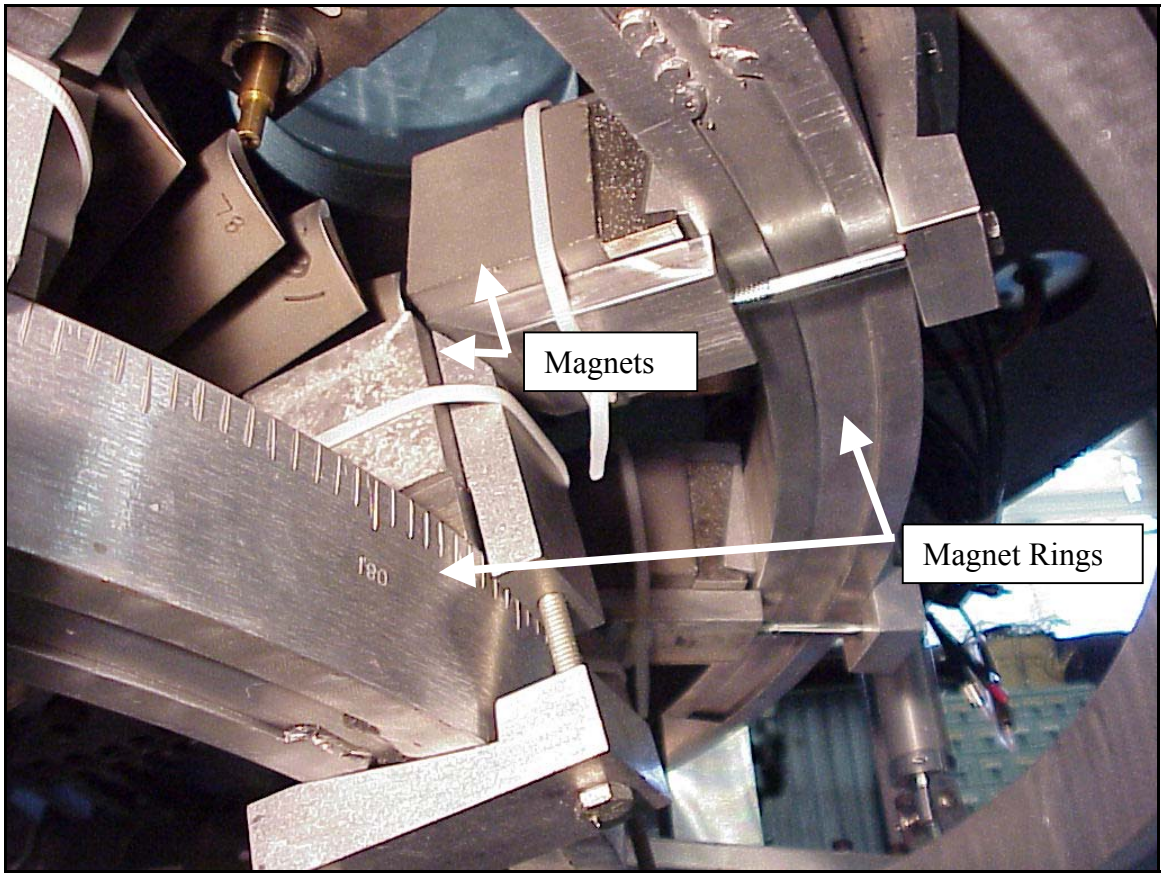

Figure 20 ECE with Two Sets of Magnets

Table 2. Runs at Different Magnet Positions

Run	Date	ECE Position Offset	# of Tests in the Run	# of Sweeps per Test
195	1109	-5/8	1	5
196	1114	+1 ¼	1	5
197	1116	0 ref	1	5
198	1120	+ ¼	1	3

Thirty-six strain gauges were active at the start of the XTE-66 experiments but only three blades were left with operational strain gauges at the roots of the blades (strains 11, 13, and 14), during experiment 2. The position of the gauges on the blade can

be seen in Figure 21. The three root gauges were used to correlate the deflection measured by the probes to the strains measured by the gauges.

Young's modulus (E) for the XTE-66 material was 18.6*10^ 6 psia. Through the relationship of stress (σ) and strain (ε), $E = \sigma / \varepsilon$, the stresses in the blades at the roots were correlated to deflections recorded by the NSMS. The software used in both the NSMS system and the strain gauge measurement system recorded the zero-to-peak value of the deflection and the strain, respectively. While it is not uncommon for industry to talk in terms of peak-to-peak stress levels, all deflections and strains reported here are zero-to-peak values. It should also be noted that 5 blades separated probes 1 and 2, as can be seen in Figure 5. Since the 1/rev pulse on the drive turbine occurred when the probes were over blades rather than over dummy blades, the blade numbers corresponding to the strain-gauged blades were different for the two probes. The strain-gauged blade numbers for probe 1 and probe 2 are listed in Table 3. . Figure 62, Figure 63, and Figure 64 in Appendix E show a comparison of the results of an order analysis of the strain gauge signals with the NSMS resonant behavior derived from probes 1 and 2, for the blades respectively. It can be seen that there was excellent agreement in the qualitative behavior of strain and NSMS results.

Table 3. NSMS Blade Number for Strain-Gauged Blades

Strain Gauge Number	Probe 1 Blade Number	Probe 2 Blade Number	P&W Blade Number
11	#25	#20	157
13	#28	#23	137
14	#15	#10	143

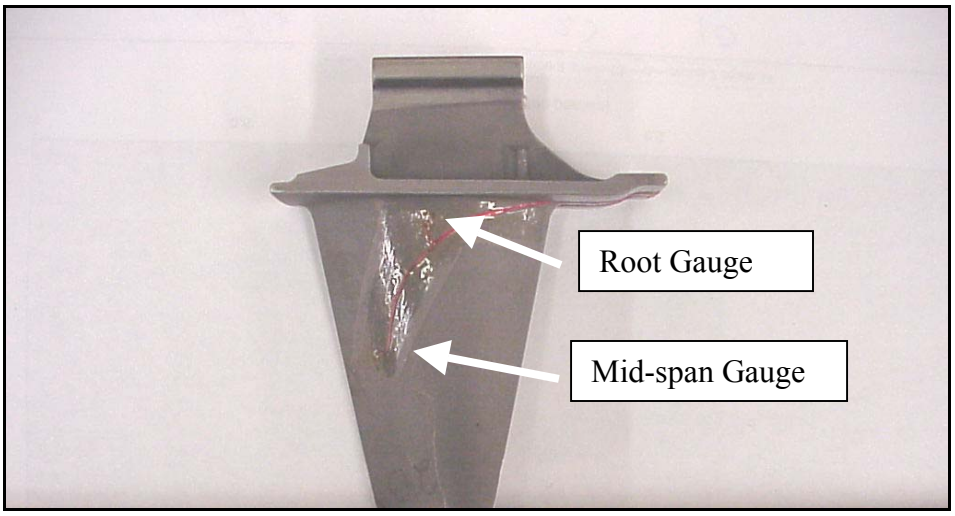

Figure 21 Strain Gauges on the XTE-66 Turbine Blade

The results for runs 195, 196, and 197 are shown in Figure 22 for probe 1, and Figure 23 for probe 2. The reference position showed the highest deflection, and the highest strain. Strain measurements taken at +5/8 inch offset (NSMS was unavailable) showed magnitudes that were above the trends in Figure 22 and Figure 23, therefore, an additional run was conducted at ¼-inches (Run 198). The results are shown in Figure 24 and Figure 25.

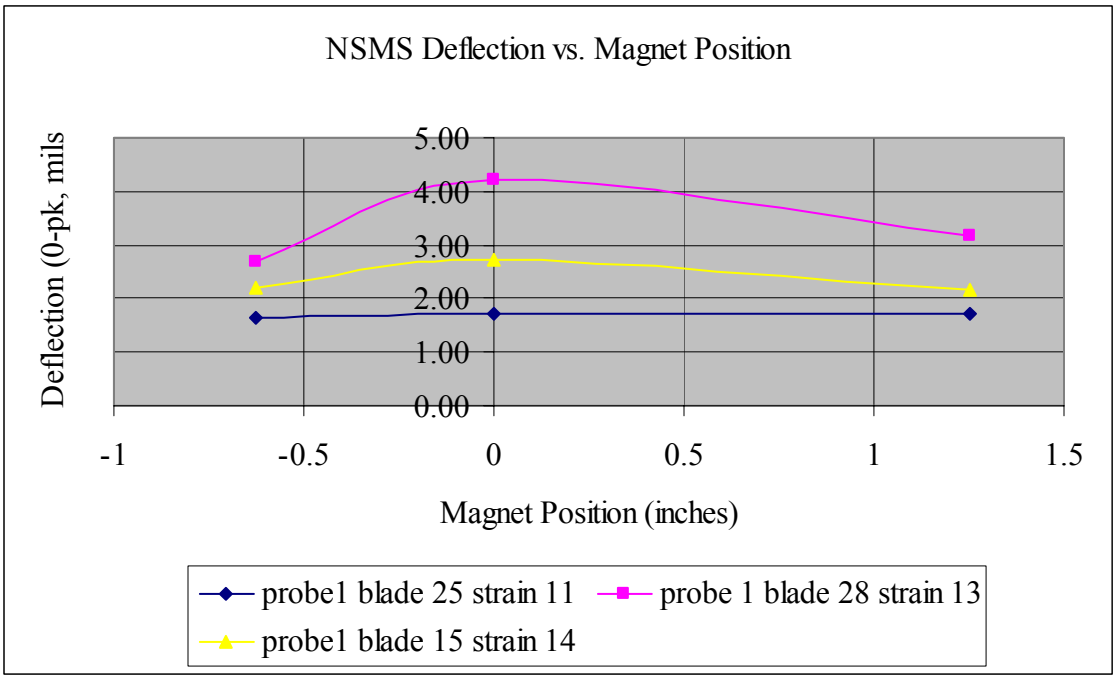

Figure 22 Average Deflections vs. Magnet Offset for Probe 1

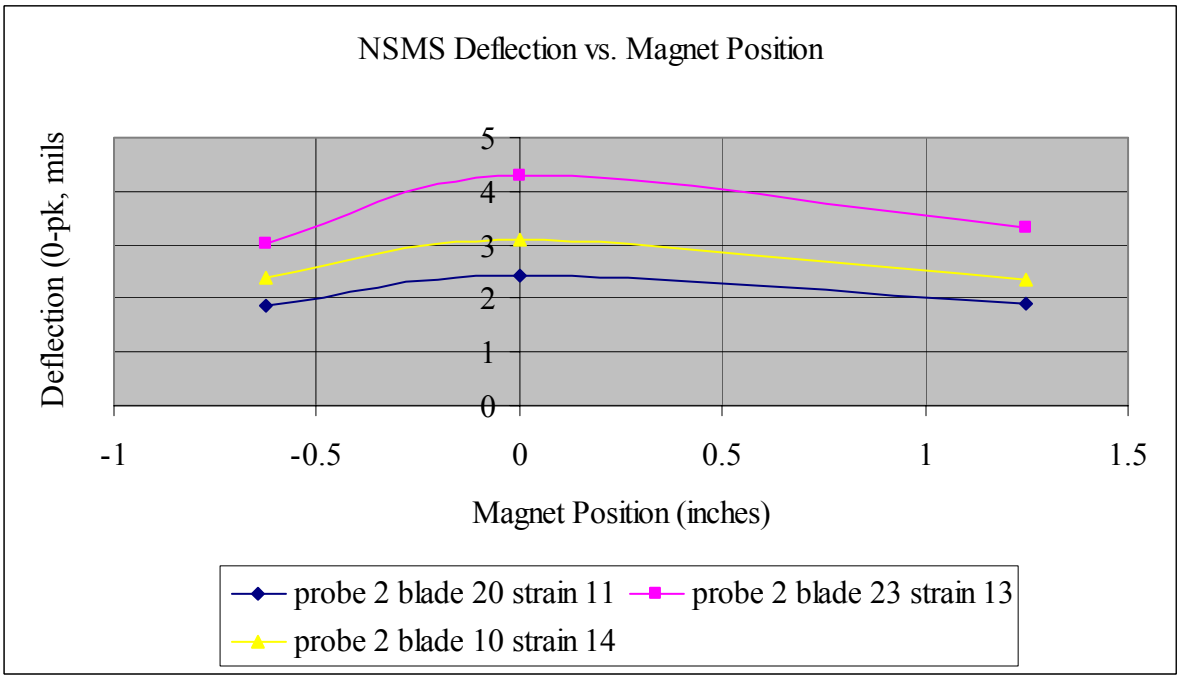

Figure 23 Average Deflections vs. Magnet Offset for Probe 2

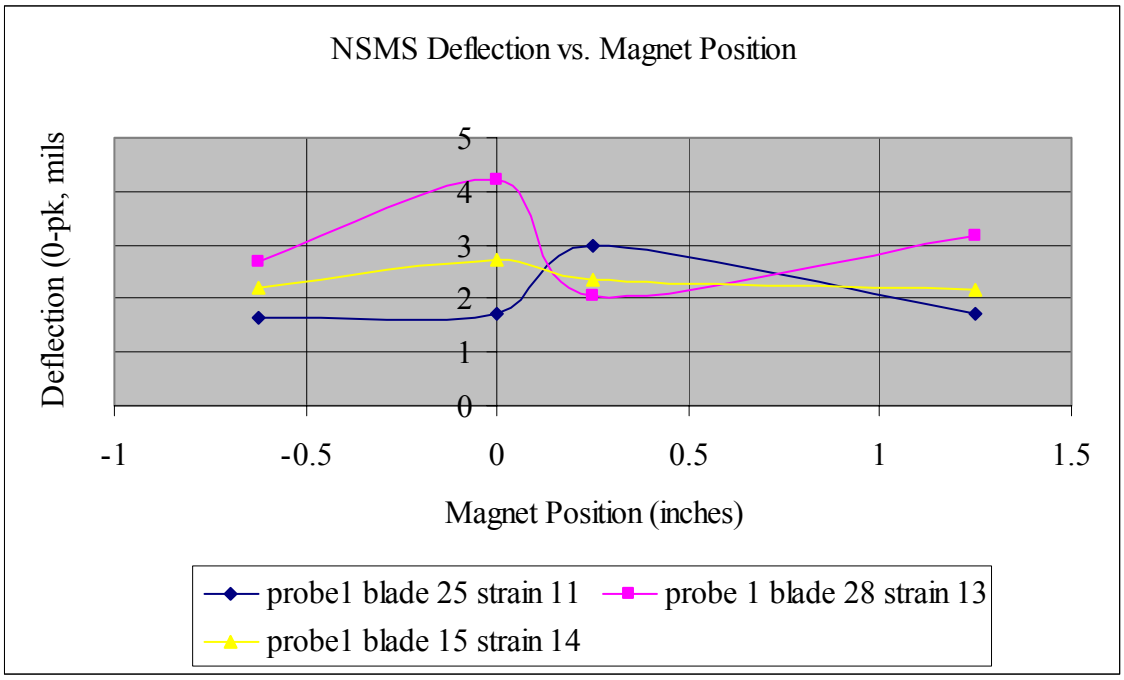

Figure 24 Average Deflections vs. Magnet Offset for Probe 1

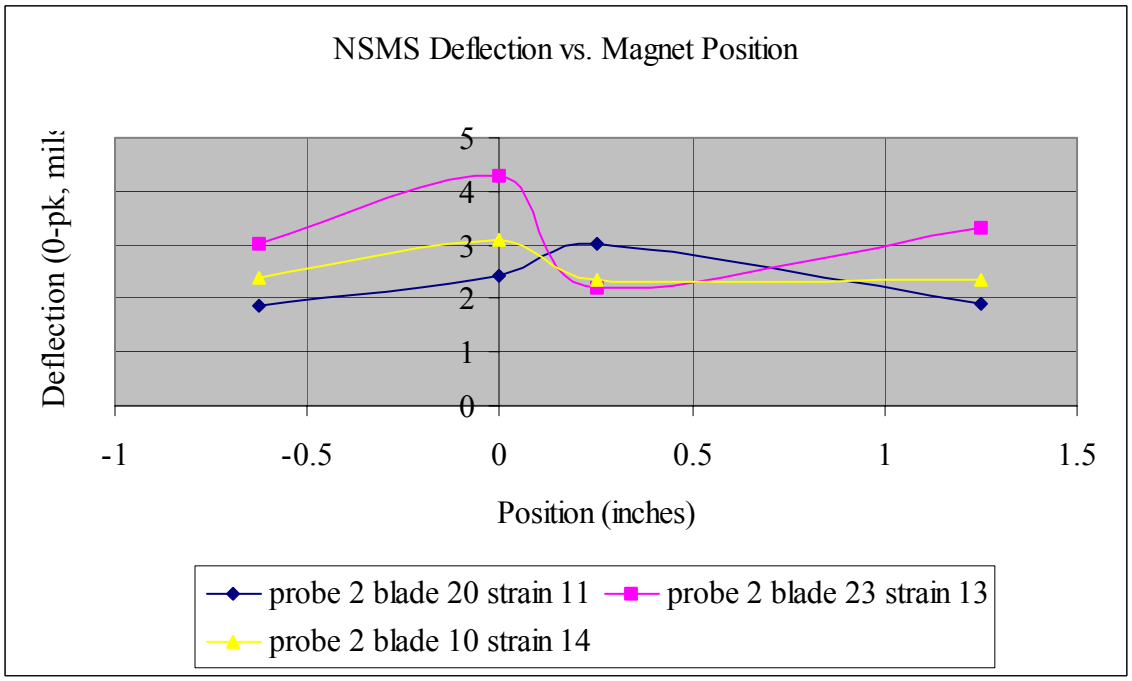

Figure 25 Average Deflections vs. Magnet Offset for Probe 2

It can be seen that strain 11 did increase in magnitude, as was expected. However, the deflection magnitudes for strains 13 and 14 were lower, which was not expected. If only the three strain gauges were available, it would have been difficult to understand these results. However, when the deflections of all the blades were examined, Run 198 was seen as having the highest average deflections. The deflections of all blades for the four runs are shown in Figure 26 (probe 1) and Figure 27 (probe 2), and the ensemble averages for all blades for each run are given in Table 4. Notice that run 198 gave higher overall average deflection levels, hence higher excitation, as expected. The reason for the drop in strain 13 (probe 1: blade 28, probe 2: blade 23) and strain 14 (probe 1: blade 15, probe 2: blade10) was unexplained. However, it was evident that the rotor/blade system dynamics was complex. There was clearly a pattern to the response of the blades depending on location in the rotor, and the amplitude of the blade deflection could vary around the rotor by as much as a factor of 2.7.

The results in Figure 27 clearly show that an expected increase over the runs 195, 196 and 197 should have occurred for blade 23, probe 2 in run 198; however, this did not happen. The reason could be that it is a system effect, and that the increase in amplitude of the adjacent blades causes a decrease in amplitude in specific blades, or 'counter-resonance.' The identification of blade numbers for the probe 1 data in Figure 26 is shown in Figure 73 and a for the probe 2 data in Figure 27 is shown in Figure 74.

Table 4. Average Blade System Deflections for the Magnet Runs

Probe 1	
Run #	Deflection (mils, 0-pk)
195	1.96
196	2.26
197	2.77
198	3.04

Probe 2	
Run #	Deflection (mils, 0-pk)
195	2.09
196	2.42
197	2.92
198	3.13

The data in Table 4 is shown plotted in Figure 28 with one standard deviation of variability for the sweeps is indicated. This accounts for about 65% of the data [Ref. 11, p. 45]. Notice that as the deflections became larger, the deviation between samples increased also.

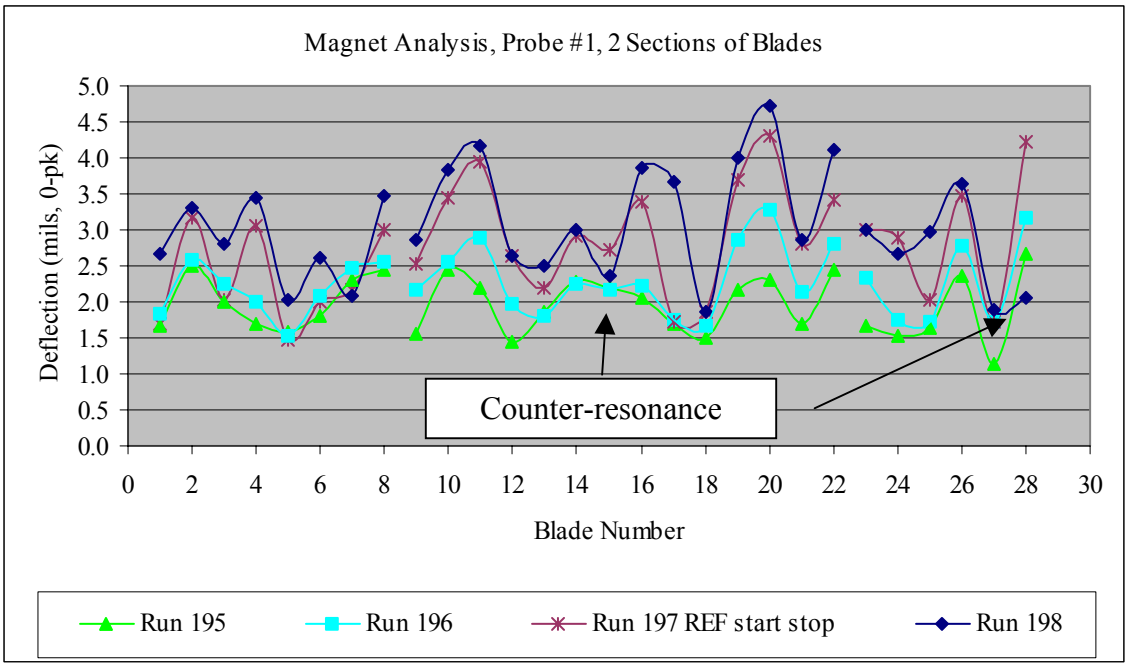

Figure 26 Effect of Magnet Offset on Deflections from Probe 1

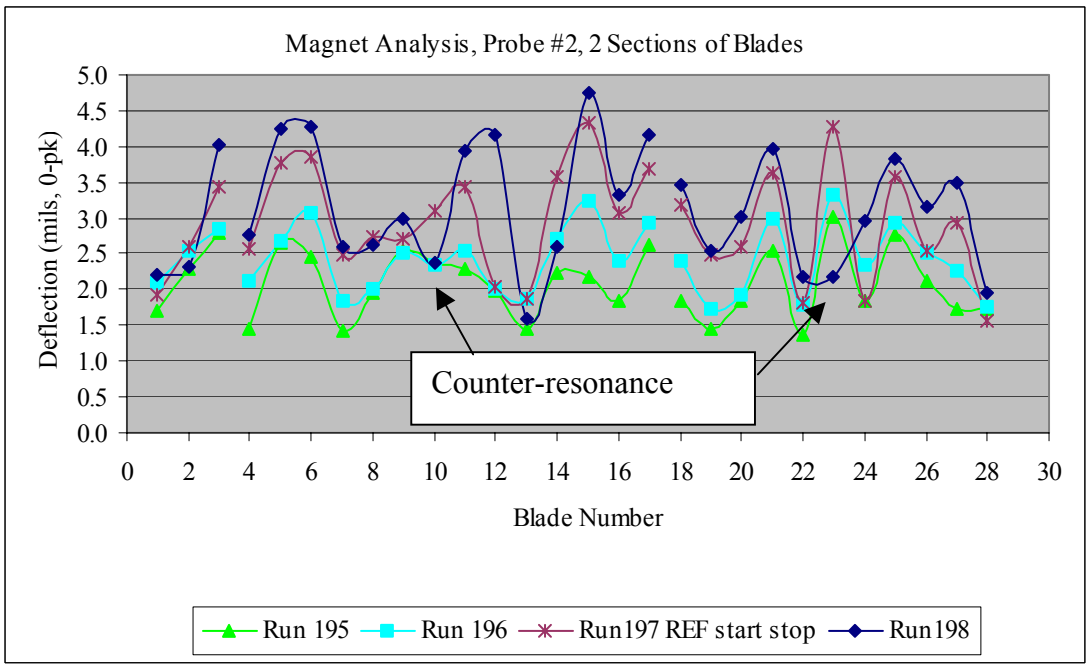

Figure 27 Effect of Magnet Offset on Deflections from Probe 2

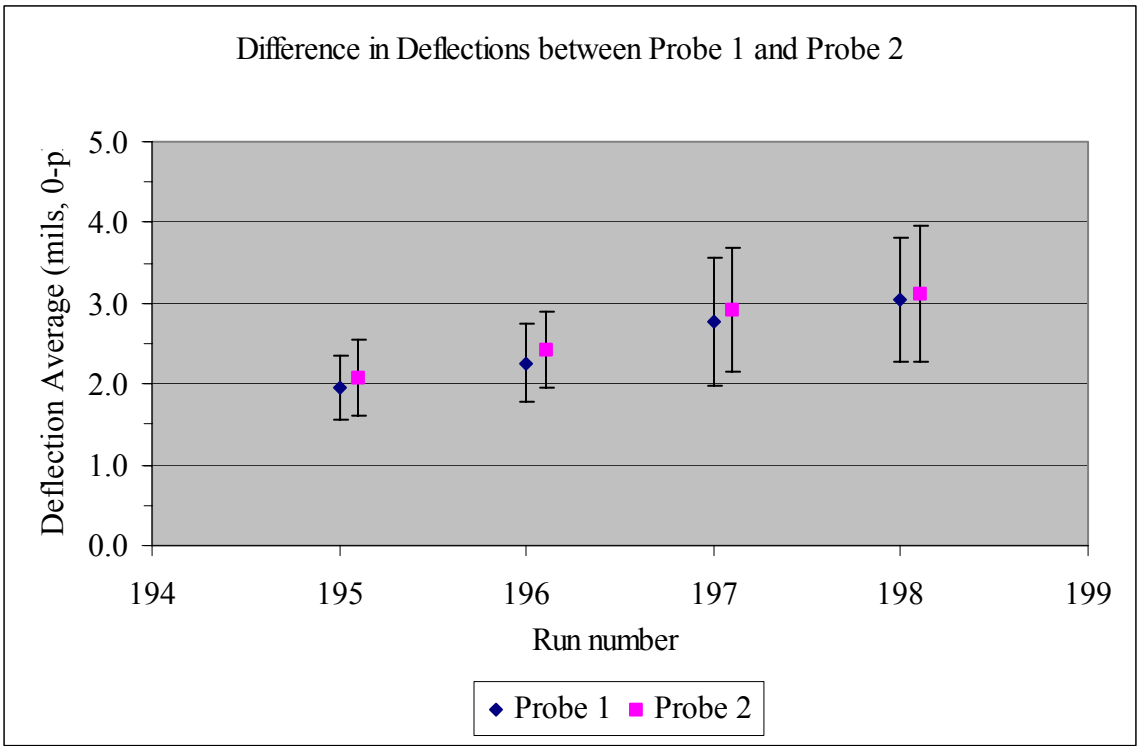

Figure 28 One Standard Deviation Error Bars

The micro-strain levels recorded by the strain gauge acquisition system were incorporated into the spreadsheet for the NSMS deflection measurements at resonance. The data are given in Appendix F. The calibration of the strain gauges to the NSMS for probe 1 is shown in Figure 29, with a linear curve fit to the data. The calibration for probe 2 is shown in Figure 30, with a linear curve fit to the data.

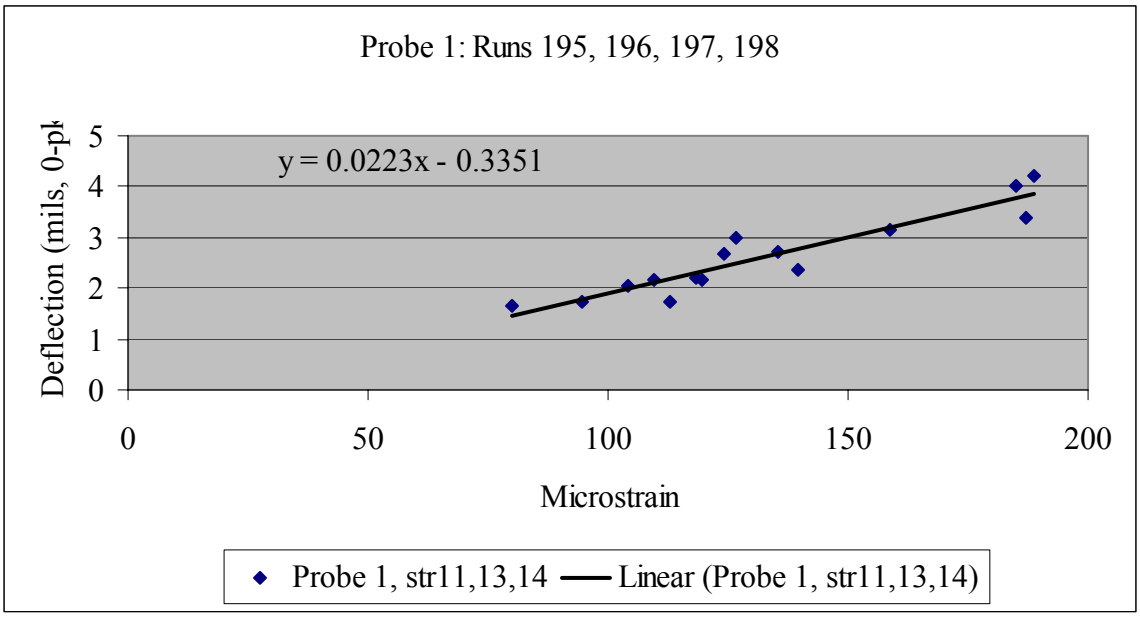

Figure 29 Probe 1 NSMS Correlation to Strain Gauges

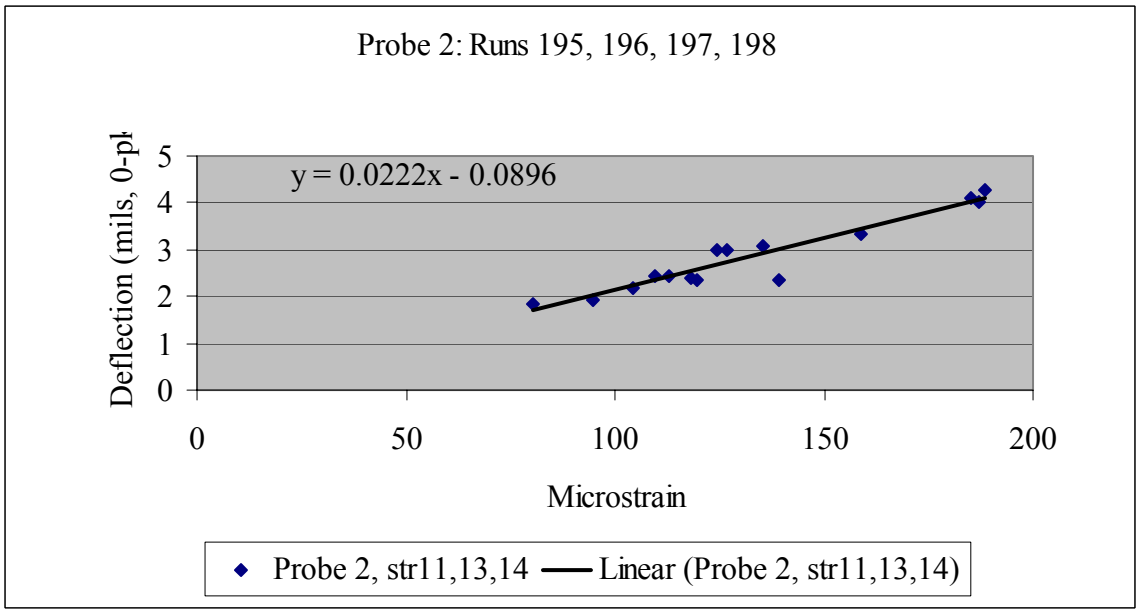

Figure 30 Probe 2 NSMS Correlation to Strain Gauges

Notice that the slopes for the curve fits are very similar, which suggests that the manual curve fitting analysis using the data viewer was carried out consistently. The difference in the constant values could be due to differences between the probe aim point locations on the blades. Probe 1 was slightly closer to the tip edge of the blade than

probe 2 due to the hardware in the pit, hence giving a larger deflection. The success of the NSMS to strain calibration allowed further experiments to be conducted without the availability of strain gauge measurements.

D. EXPERIMENT 3 – EFFECT OF SILVER PLATING

Six XTE-66 blades were removed from the rotor and plated with 0.010 inches of silver plating. NASA had reported that coating the blades with a conductive material (silver), during ECE tests, could raise the excitation levels between two to three times that previously recorded [Ref. 12]. Since no strain gauges remained on the coated blades, the NSMS system was essential in relating the old strain levels to the new ones. Data were collected in four runs. Each run involved 3 to 5 sweeps. For each run, data were averaged over the multiple sweeps for each blade. The runs were all at 12EO and are summarized in Table 5.

Table 5. Plated and Unplated Runs

Run #	Date	# of tests recorded	Magnet Position	Plated vs. Unplated
197	16 Nov 01	5	0.0” ref	Unplated
198	20 Nov 01	3	0.25“	Unplated
201	18 Dec 01	4	0.25”	Plated
202	18 Dec 01	4	0.0” ref	Plated

The probe blade numbering changed from the November runs (197, 198) to the December runs (201, 202). Table 6 summarizes the blade identification data. The data are also given graphically in Appendix I.

Table 6. Identification of Probes with Blade Numbers

P&W Blade Number		November non plated		December Plated	
		probe1	probe2	Probe 1&2	
182		9	4	1	
125		10	5	2	
188		11	6	3	
190		12	7	4	
208		13	8	5	
127		14	9	6	
143	strain 14	**15**	**10**	**7**	**Plated**
195		**16**	**11**	**8**	**Plated**
243		17	12	9	
123		18	13	10	
121		19	14	11	
181		20	15	12	
166		**21**	**16**	**13**	**Plated**
74		22	17	14	
154		23	18	15	
173		24	19	16	
157	strain 11	25	20	17	
78		26	21	18	
163		27	22	19	
137	strain 13	28	23	20	
209		**1**	**24**	**21**	**Plated**
135		**2**	**25**	**22**	**Plated**
77		3	26	23	
142		4	27	24	
183		5	28	25	
141		6	1	26	
178		**7**	**2**	**27**	**Plated**
120		8	3	28	

The results of a comparison of the computed strains at resonance after the six blades were plated, to before they were plated, at two settings of the magnet offset, are shown in Table 7. All percentages are the increase or decrease from the reference unplated value of microstrain. The reference (unplated) data were from run 197 (Table 5). The plated blades are shown in bold font. The average of probe 1 and 2 data at the

0.25 magnet position are shown in Table 8. There was an overall average of 27% increase (1.27 times the old value) in resonant strain for the 6 plated blades. The maximum increase was seen in blade 7 with a 99% increase (about double) in microstrain. Blade 8 showed that the plated blade microstrain was decreased from the unplated results with a –22% change. Looking at the data from the six blades, the picture is unclear. It was reasonable to assume that all plated blades would show a dramatic increase in microstrain, but this was not the case.

Table 7. Excitation Increase After Plating

Percent of increase (non-plated to plated)				
	Magnet Offset = 0.0		Magnet Offset = 0.25	
blade #	probe 1	probe 2	probe 1	probe 2
1	13%	20%	16%	18%
2	7%	11%	9%	9%
3	7%	12%	19%	29%
4	-5%	7%	-16%	-8%
5	28%	19%	5%	28%
6	-23%	-20%	-17%	-21%
7	**49%**	**33%**	**81%**	**118%**
8	**-9%**	**-6%**	**-26%**	**-18%**
9	45%	13%	-13%	-31%
10	-3%	-3%	7%	13%
11	-40%	-44%	-39%	-18%
12	-15%	-18%	-16%	-14%
13	**19%**	**23%**	**6%**	**10%**
14	5%	-2%	15%	9%
15	3%	-3%	11%	-1%
16	-20%	-7%	-16%	-16%
17	-5%	-8%	-9%	-6%
18	14%	21%	16%	20%
19	73%	70%	72%	55%
20	-41%	-53%	11%	-41%
21	**46%**	**28%**	**-11%**	**-1%**
22	**6%**	**-4%**	**10%**	**-1%**
23	-8%	-15%	-32%	-32%
24	-38%	-31%	-27%	-19%
25	72%	107%	39%	76%
26	23%	40%	-3%	31%
27	**46%**	**35%**	**65%**	**85%**
28	-40%	-45%	-44%	-48%
Average	7%	6%	4%	8%

Table 8. Average Effect of Plating

Probe 1 and Probe 2 Averaged Together (Non-plated vs. Plated) for the 0.25 Magnet Excitation Only				
	Average for the changes		Calibrated Microstrain	
Blade #	Probe 1 and 2 at magnet position 0.25		Unplated Average	Plated Average
1	17%		136	159
2	9%		191	208
3	24%		199	246
4	-12%		127	112
5	16%		125	145
6	-19%		145	118
7	99%	**99%**	116	230
8	-22%	**-22%**	185	144
9	-22%		185	143
10	10%		87	95
11	-28%		158	109
12	-15%		222	189
13	8%	**8%**	148	161
14	12%		195	219
15	5%		155	163
16	-16%		127	107
17	-7%		144	133
18	18%		180	213
19	64%		100	164
20	-15%		105	90
21	-6%	**-6%**	136	127
22	5%	**5%**	170	178
23	-32%		143	98
24	-23%		165	127
25	58%		99	155
26	14%		118	131
27	75%	**75%**	109	190
28	-46%		178	96
Ave	all blades	6 plated blades	Unplated Overall Average	Plated Overall Average
	6%	27%	148	152

However, an examination of all 28 blades in Table 8 raises questions. Blade 3 was non-plated and yet it had a higher microstrain (246) than the plated blade 7 (230). Why was the microstrain so high (increased by 24%) for the unplated blade 3? Could it be that the system dynamics were changed as a result of the plated blades, and this affected blade #3. It is also possible that blade 3 was more susceptible to resonance at 12EO. Each blade, although nominally similar in geometry, was subject to tolerances in internal structure, and therefore some blades might react more to excitation than others. Consequently, the statistical average of all the blades in the system is meaningful. The measurement of one or two blades in the present rotor is clearly not enough to draw accurate conclusions about the average behavior of the blades while in the engine. The ability of NSMS to measure every blade is a major asset in analyzing the response of turbo-machinery blading.

The data in Table 7 are shown plotted in Figure 31 (probe 1) and Figure 32 (probe 2). The data in Table 8 are shown plotted in Figure 33. It is seen that the plated blades did not follow a consistent trend. A better experiment would result from plating all the blades in the rotor and then measuring how the entire system behaves. Plating only six blades gave somewhat inconclusive results as to the effect of silver plating on excitation levels using ECE.

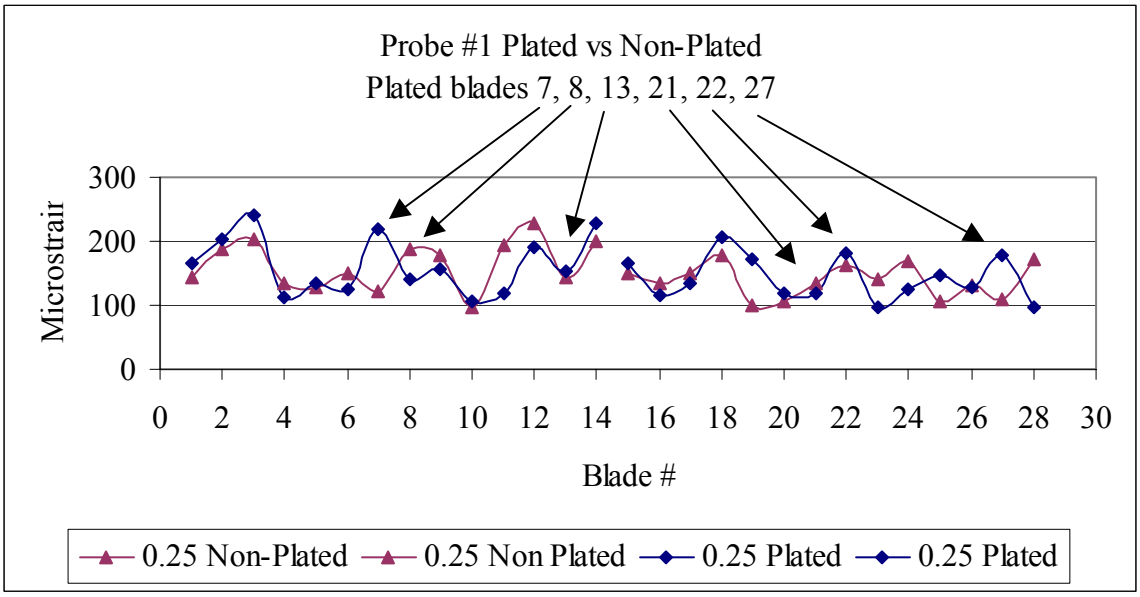

Figure 31 Effect of Plating from Probe 1

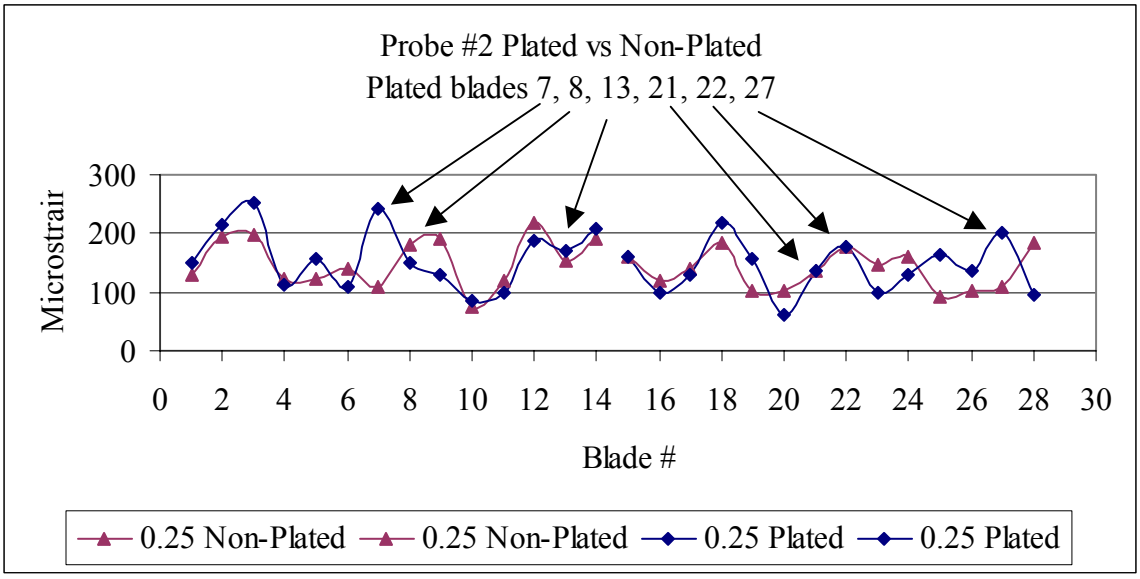

Figure 32 Effect of Plating from Probe 2

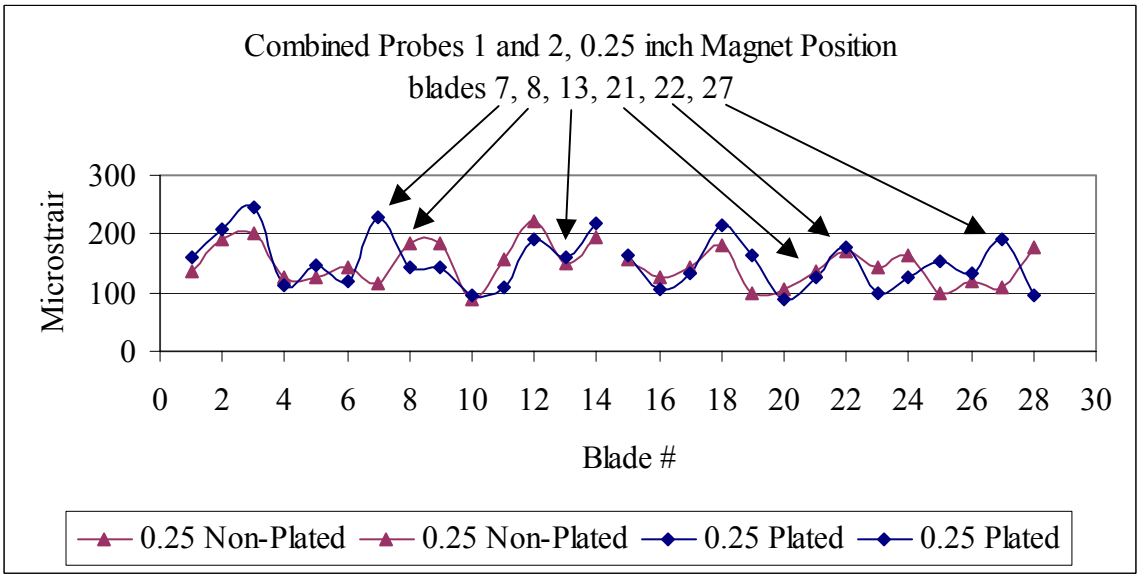

Figure 33 Effect of Plating – Average of Probe 1 and 2

Another unusual feature that was noticed was an increase in a resonance for the plated blades at about 5100 RPM for the plated blades during run 202 (file 121801_1115). This was the only test recorded that went low enough in rpm to identify this peculiarity. The following displays (Figure 34 and Figure 35) show the 5100 RPM resonance, which was greater than the resonance at 12EO at about 5600 RPM. All the plated blades showed a similar pronounced resonance, but none of the non-plated blades

showed any significant magnitude. The results of curve-fitting the 5100 RPM resonance for all blades is shown in Figure 36. The resonance clearly gave very high displacements.

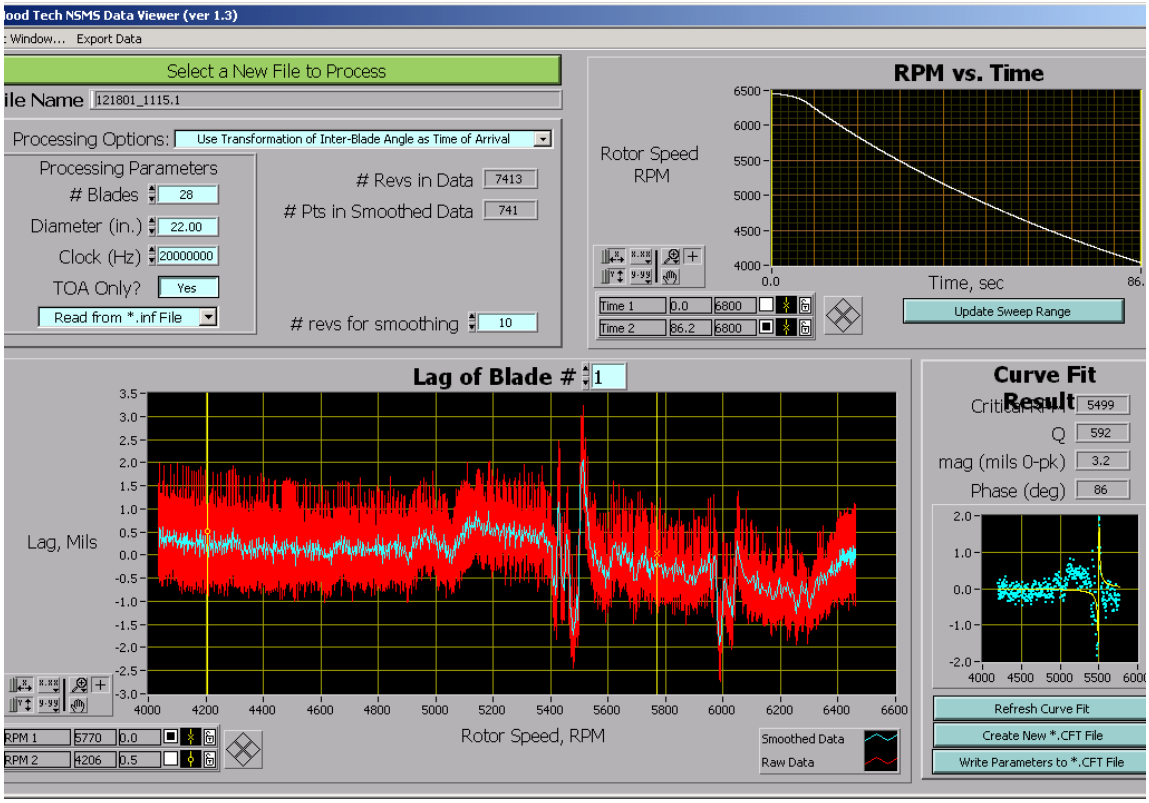

Figure 34 Typical Non-Plated Blade: No 5100 RPM Resonance

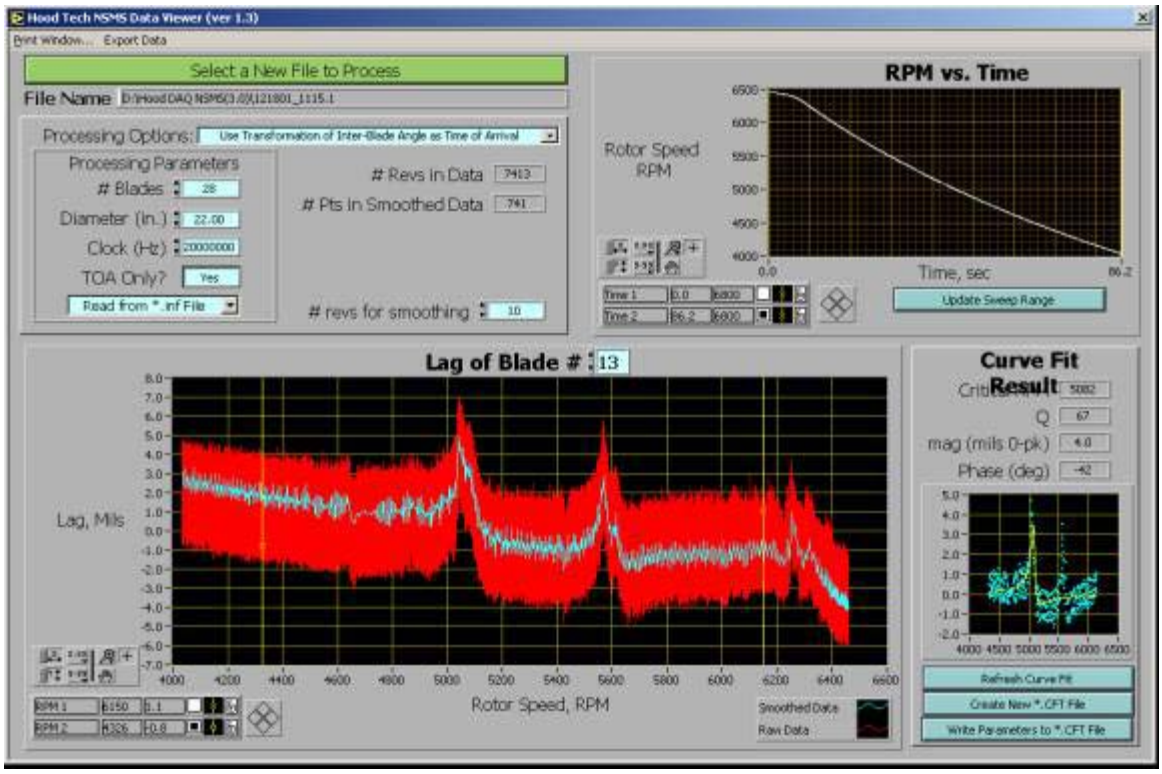

Figure 35 Typical Plated Blade: With 5100 RPM Resonance

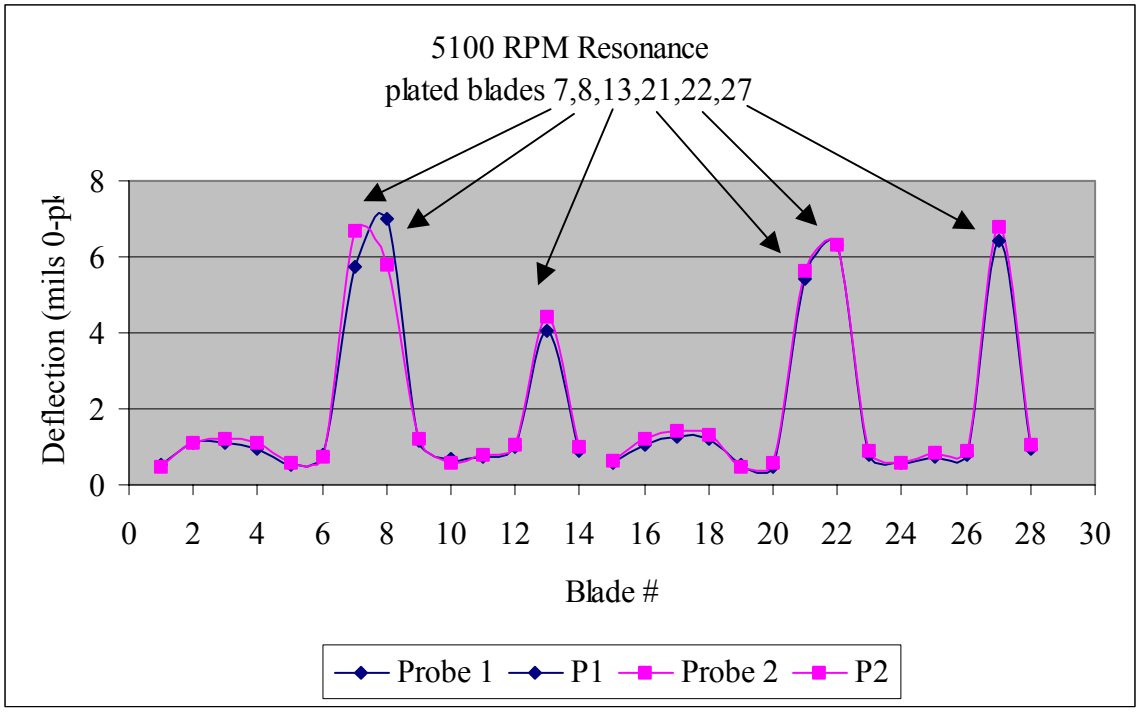

Figure 36 5100 RPM Resonant Deflections

There was almost 7 times more displacement in the plated blades over the non-plated blades at this RPM. However, since the resonance occurred at a different RPM than the one where the microstrain data was calibrated during experiment 2, and may not be the same mode, conversion from displacement to microstrain is not strictly applicable. The XTE-66 Campbell diagram (P&W proprietary) was examined at multiples of the 12 engine order excitation. The 5100 RPM resonance was close to either the 1st span-wise bending at 36EO or 1st torsion at 48EO. But it is also possible that the resonance was a modification of the lower order mode cause by the heavy layer of silver. (It was not possible to measure the effect of the internal dampers on this resonance since silver plating had migrated into the damper cavity.)

Overall, the plating experiment did not produce the desired results. Some plated blades increased in amplitude while others decreased. A better procedure would be to plate all the blades equally. Cost and time prohibited that experiment immediately. The experiment did emphasize, however, the usefulness of the laser-light probes in acquiring data from all blades for tests of any bladed disk.

E. EXPERIMENT 4 – EFFECT OF PLASTIC INSERTS

The final experiment conducted on the XTE-66 turbine rotor was to determine whether inserting thick plastic bushings into the space between the bottom of the grove in the rotor and the base of the turbine blade, made a difference in the variance in data acquired in successive sweeps between successive starts and stops. The idea was to reduce the variability of the blades reseating themselves in the fir-tree root assembly.

Pratt and Whitney had previously reported “good” repeatability in their experiments, using averages of only three sweeps. In the present study (experiment 2), sweeps between 5 stops were required to establish the effect of magnet offset (Figure 22 through Figure 26) because of a lack of consistency using averages of five sweeps in a single test. Plastic inserts used by P&W were not used initially in the present study due to possible overheating and melting from the eddy-current process. Also, a better representation of engine behavior might be seen in results taken without the use of plastic

inserts. However, inserts were omitted initially because a high-temperature rubber material that was substituted (seen in Figure 2) failed at high RPM. In the final XTE-66 experiment, plastic inserts similar to those used by P&W were inserted in order to examine their effect on repeatability.

In this experiment, with plastic inserts under the blades, one run was conducted at the magnet-offset position of 0.0 inches, i.e. reference position. The run included 5 tests, i.e. 5 starts and stops of the rotor, and each test contained 3 sweeps of the rotor RPM, down through the 12EO. The following table shows the data file names, which were based on the time of the sweep.

Table 9. Experiment 4 Data File Names

Run #203		Time (xxxx)		
Date_time		Sweep 1	Sweep 2	Sweep 3
020117_xxxx	Test 1	1125	1130	1136
	Test 2	1152	1158	1207
	Test 3	1217	1222	1228
	Test 4	1240	1245	1250
	Test 5	1302	1307	1311

A data file was created for each of light probe 1 (xxxx_1) and light probe 2 (xxxx_2). The standard deviation for the deflection of each blade was computed from the three sweeps, for each test. The results for the five tests are shown for probe 1 in Figure 37 and Figure 38 shows the results for just the final three tests. It appears from the results that the first two tests allowed the inserts to settle and mold into place, after that, the blades remained in their seats when the rotor was stopped.

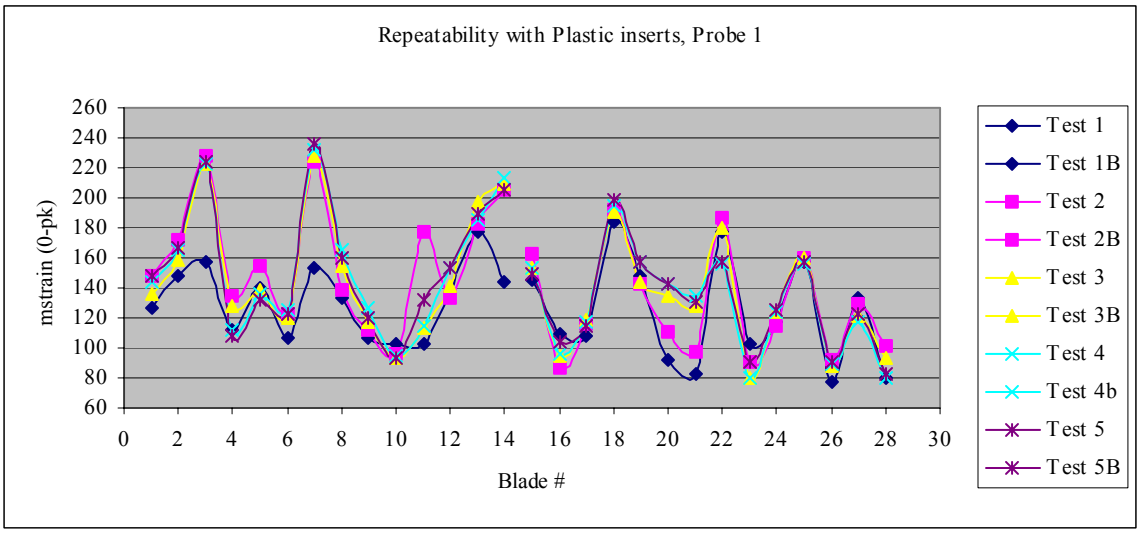

Figure 37 Blade Microstrain with Inserts (5 Tests)

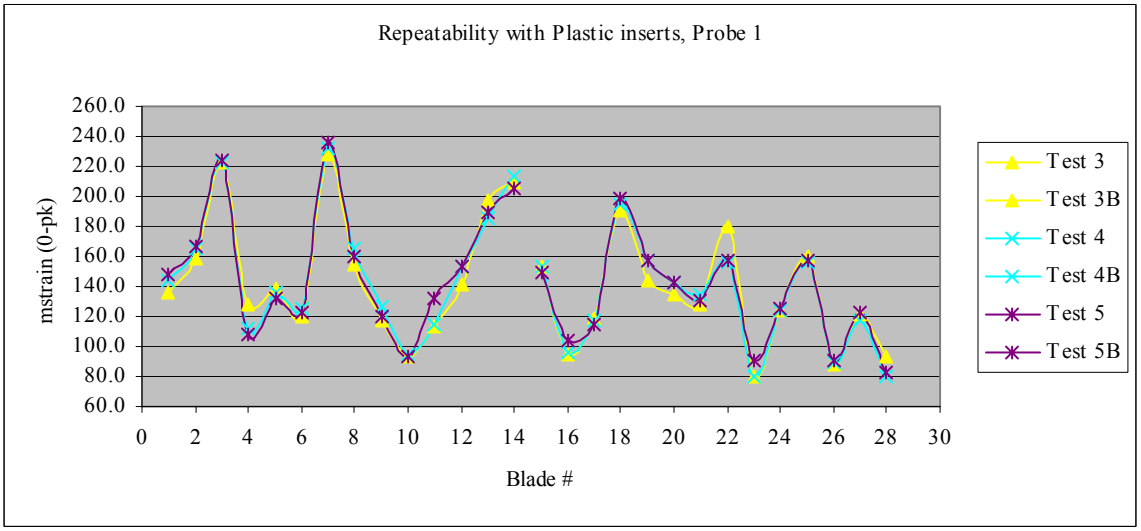

Figure 38 Blade Microstrain with Inserts (Last 3 Tests)

The standard deviations for the multiple sweeps are shown in Table 10. It can be seen that the average was only 9.5% for probe 1 and 10.8% for probe 2 using the standard deviations for the last three tests.

Table 10. Standard Deviation (Average of All Blades and 3 Sweeps)

Run #203 17 January 2002			
date_time		Probe 1 Standard Dev.	Probe 2 Standard Dev.
020117_xxxx	Test 1	17.83%	21.56%
	Test 2	10.93%	12.34%
	Test 3	9.84%	11.04%
	Test 4	9.09%	11.53%
	Test 5	9.63%	9.90%

The reference tests that were conducted without the plastic inserts occurred on 16 November 2001. With the same spin-pit setup, 12EO and 0.0" magnet position, 5 tests (start/stop) were conducted with one sweep each, and one test with 3 sweeps (continuous). The results are shown in Table 11.

Table 11. Results of Reference Tests (No Inserts)

Run #197 16 November 2001			
		Probe 1 Standard Dev.	Probe 2 Standard Dev.
Start/stop	Average of Tests 1,2,3,4,5	13.94%	13.11%
Continuous	Test 6 (3 sweeps)	11.03%	9.06%

It is seen that the start/stop tests showed a higher standard deviation and that the continuous sweep results are consistent with the data from the plastic insert tests. This is consistent with the likelihood that allowing blades to unseat and reseat will introduce some variability in the resonant behavior. Detailed results are shown plotted in Appendix H.

VI. CONCLUSIONS AND RECOMMENDATIONS

A. CONCLUSIONS

Experiment 1 showed that the NSMS was capable of measuring small deflections and that the qualitative behavior was in concurrence with that of the strain gauges. Both the NSMS and the strain gauge results suggested that the dampers had little effect on the lowest bending mode. However, without larger excitation amplitudes, the damper effectiveness could not be properly assessed.

Experiment 2 showed the usefulness of NSMS in obtaining data from all blades in the system. The data from three strain gauges, by themselves, was unclear; but the deflections measured for all the blades clearly pointed to a behavior that was more realistic. The calibration of the probes to strain gauges was very successful; however, it was only applicable for the first bending mode. A more complete calibration using multiple strain gauges and NSMS probes would be needed in order to examine higher order modes.

Experiment 3 did not produce the results that were expected; however, useful data were obtained. Even though a particular blade had been silver plated, a higher magnitude of resonance was not necessarily obtained. System dynamics appeared to play a significant role in the results. Also it was hypothesized that each blade might be structurally slightly different and therefore would generate different magnitudes of strain. A statistical survey of all the blades in a bladed disk to obtain data on the weakest (most susceptible to resonance) to the strongest blade (most resistant to resonance) is required in order to quantify the 'life' of the blades.

Experiment 4 produced very definitive results. The repeatability of tests was clearly improved through the use of plastic inserts. After two initial stops and starts, the average of a series of three sweeps gave excellent repeatability. Without inserts, when the XTE-66 blades were allowed to unseat and reseat themselves on successive starts, the data were not very repeatable. This finding suggests that inserts should be used when

assessing damper effectiveness in spin tests, but also suggests that assessment measurements in an engine might require a number of stops and starts.

Overall, the four experiments showed the utility of the NSMS system. Collecting data for all blades was useful in analyzing trends. By strain gauging a few blades, it was possible to develop a strain to deflection relationship in the first bending mode, thereby allowing the measurement of all the blades. Data from all blades in a rotor can be statistically analyzed, so that a probable lifetime of blades subjected to occasional resonance can be determined.

B. RECOMMENDATIONS

Hood Technology has generated updated software that calculates the SDOF curve-fits for all the blades without the user having to cycle through each blade. This feature drastically reduces the workload involved in data processing. It is recommended that the program be used to re-reduce data in the present report, and any differences be resolved. With the data processing workload diminished, more attention should be focused on using more probes, measuring higher frequency modes and statistically sampling the deflections as the rotor blades are cycled through resonance. Future work should also include the finite element analysis of the blades being measured in order to place the probes in optimum positions to analyze targeted modes.

APPENDIX A : THEORY OF MEASUREMENT

[The figures and review of the measurement theory in the present section are from Ref. 5, Ch. 4, and are published with the permission of Hood Technology Corporation]

A. BLADE MODES, FREQUENCIES, AND ENGINE ORDERS

The Campbell diagram shown schematically in Figure 39, combines the rotor speed, the engine orders of excitation, and the system's modes of vibration (natural frequencies) on one chart in order to identify operational engine speeds that are high-risk with respect to structural resonant vibrations. Created during the design of an engine, this diagram enables a quick assessment of the type and possibility of experiencing resonant conditions at various operating engine RPMs from idle to maximum. The engine orders are defined as a synchronous type of excitation. For example, if the engine had 20 inlet guide vanes, the first rotor blades would experience a 20 EO excitation at about 7500 RPM. The mode would be the 1st torsion of the blade at a natural frequency of 6000 Hz. The modes are related to the natural frequencies of the blades and are a function of nodal diameters (harmonics). It is not uncommon to see 1st and 2nd order bending, torsion, and chord-wise bending on a Campbell diagram. Higher order bending modes may also be displayed.

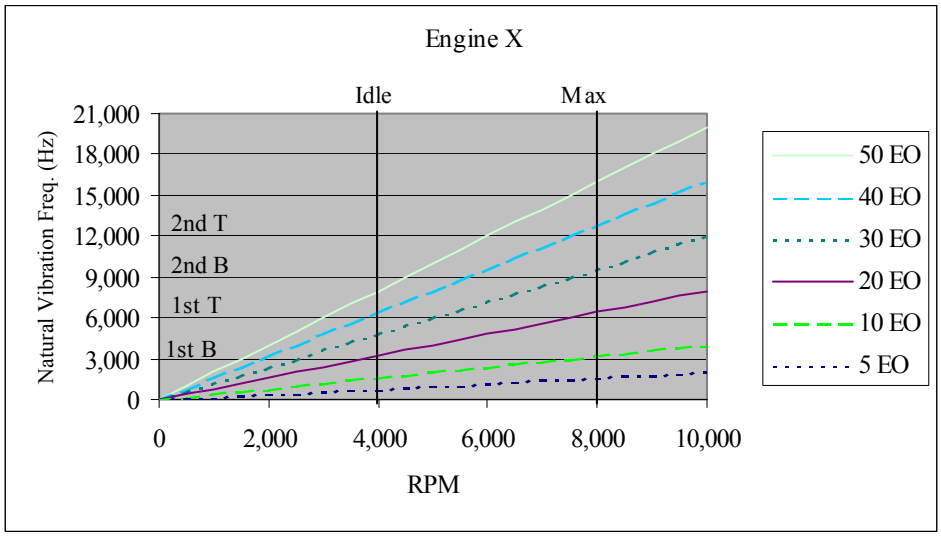

Figure 39 Campbell Diagram Example

B. CLASSIFICATION AND SENSORS

Potentially damaging blade vibration in rotating machinery can be caused by either synchronous or asynchronous resonance. A resonance occurs when a blade's natural frequency is reached and the vibrations (oscillations) reach large amplitudes from small inputs. Asynchronous resonance pertains to flutter, stalling or other aerodynamic instabilities, not associated with a consistent input. Synchronous resonance is excited at multiples of the rotational speed of the rotor, i.e. from interference of stator or inlet guide vanes; hence the resonance is in synch with the rotor. [Ref. 2] The present experiment is focused on synchronous resonance.

There are several ways to measure the synchronous resonance using NSMS. The four ways discussed by Hood Technologies incorporates time of arrival (TOA) information to calculate blade vibrations for every blade on the rotor. The single sensor fit incorporates one sensor per rotor and uses a direct measurement method through a curve fit. The curve fit procedure is simple and requires minimal equipment and simple computations. However, single sensor measurements of blade apparent deformation will also contain RPM dependent signals not associated with the resonance. The removal of these signals, 'detrending', is required to give accurate deflection and frequency measurements, which is an additional step in the single sensor method. The present experiment dealt entirely with the single sensor approach for the synchronous vibration.

The two-sensor approach incorporates a differential method of calculation between two closely placed sensors. The advantage for this approach is automatic detrending, however, the method requires more than one sensor. The multiple sensor approach uses at least 3 sensors per rotor. A least-squares fit can be performed to identify the vibration parameters. The main advantage of the three-probe method is that the amplitude of the vibration can be estimated while the engine is dwelling at a certain power setting. This gives an instantaneous estimate of static position and vibration. The fourth method discussed by Hood is the four-sensor method. With the larger number of sensors one can more reliably decide on the harmonic or include several superimposed harmonic responses. The number of deployed sensors is the drawback of the method. In all four approaches, the number of sensors was always much smaller than the Nyquist

sampling limit. The sample frequency maximum being measured must not be greater than two times the highest signal frequency sampling rate. The Nyquist sampling limit must be at least 2 times higher than the highest frequency being sampled to avoid aliasing. Aliasing is the inaccurate reporting (frequency change) of a measured frequency due to the lack of sampling rate.

C. DEFLECTION MEASUREMENT USING TOA INFORMATION

Multiplying the blade speed by the time-of-arrival (TOA) for each of the blades (Nr) equates to an estimate of the arc length between each blade's reference position and the shaft reference point (zero point). The calculated time of arrival defines the position a blade should be in. A difference between the calculated and measured TOA is reported as a blade lag, either positive or negative. A non-deforming blade will always have the same TOA, assuming the static deformation to be constant. See Figure 40.

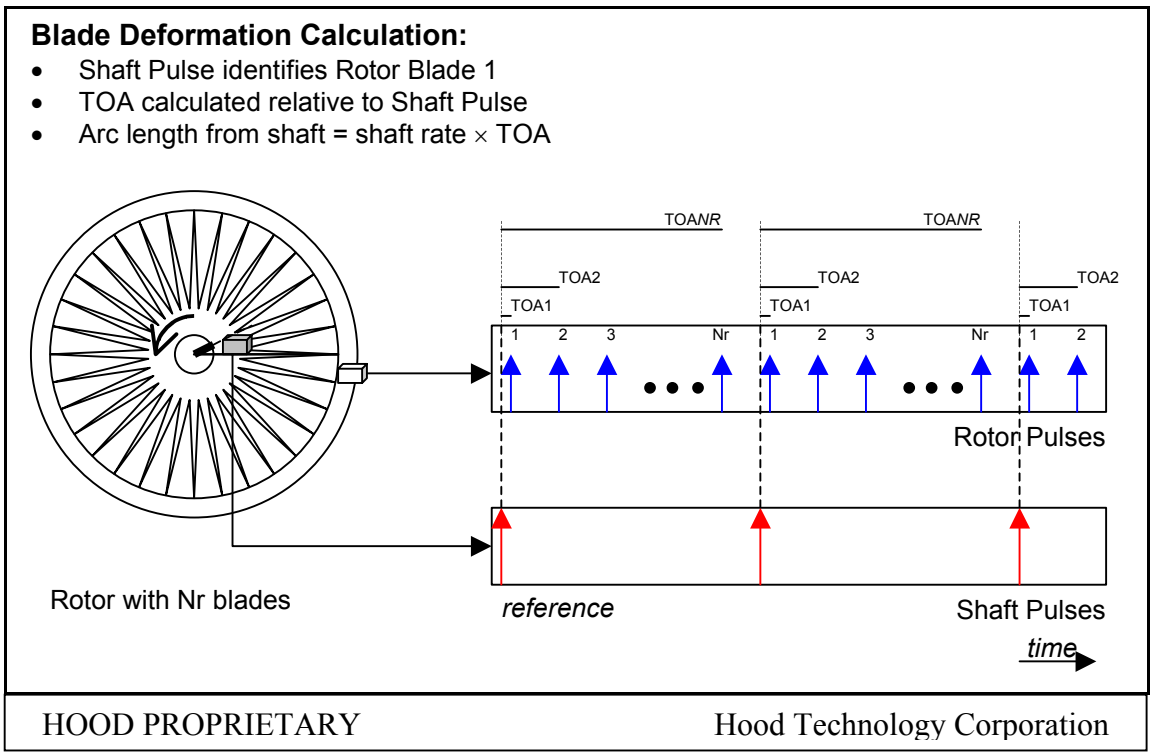

Figure 40 Illustration of Blade Time-of-Arrival

As stated before, synchronous vibration occurs at a frequency directly related to shaft rate. When the rotor is periodically excited at frequency ω the circumferential deformation due to vibration can be expressed as

$$\delta(t) = A(\omega)\sin\left(\omega t + \phi(\omega)\right)$$

Where $\delta(t)$ = Deformation of the blade at time t.

$A(\omega)$ = Frequency dependent amplitude

$\phi(\omega)$ = Frequency dependent phase

The amplitude and phase frequency dependency are a function of the blade's structural dynamics. Again, assuming static deformation to be constant, the detector senses the blade for every revolution at time

$$t_k = \frac{2\pi k}{R} + dt_k$$

Where k = The revolution number

R = The shaft rate

dt_k = The time lag resulting from the blade's deformation

To the first order, the measured deformation is

$$\delta_k = A(\omega)\sin\left(\frac{2\pi k\omega}{R} + \phi(\omega)\right)$$

When the vibration frequency is a multiple of the shaft rate, $\omega = NR$, it is synchronous. The sample deformation is then

$$\delta_k = A(NR)\sin\left(\frac{2\pi kNR}{R} + \phi(NR)\right) = A(NR)\sin(NR)$$

N = Integer multiple of the shaft rate, R

Therefore, if R is constant, then δ_k should remain constant. If NR goes through a blade resonance as the shaft rate varies, the phase $\phi(NR)$ changes by $180°$, which allows the resonance to unravel itself in front of the detector as $A(NR)$ goes through a maximum. See Figure 41.

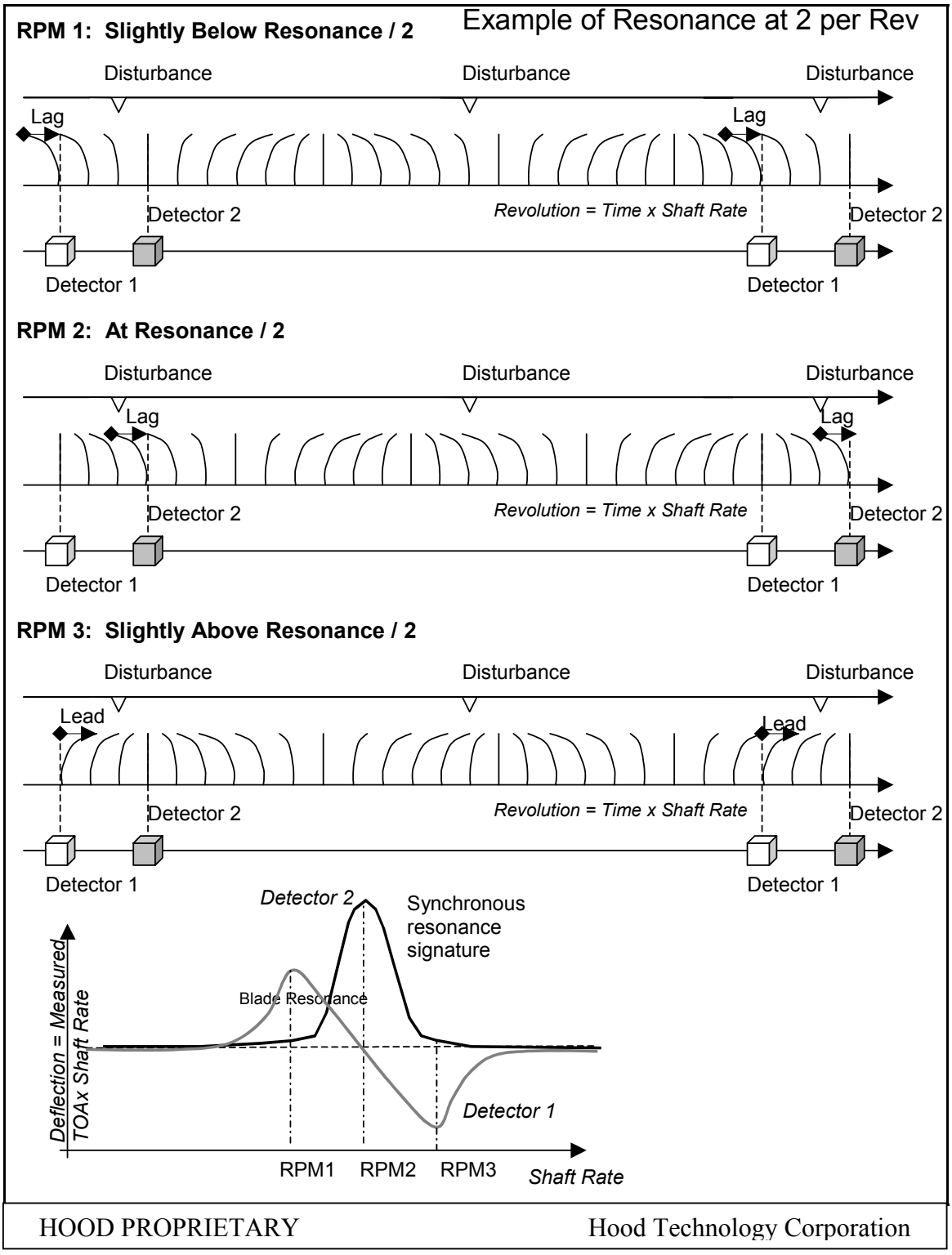

Figure 41 Synchronous Blade Resonance as Seen by Two Detectors

Asynchronous vibration occurs at a frequency not associated to the shaft rate, therefore, the ratio rate $r = \frac{\omega}{R}$ is not an integer and the sample deformation is:

$$\delta_k = A(\omega)\sin\left(2\pi r k + \phi(\omega)\right)$$

The asynchronous vibration is sampled at a fixed shaft rate as seen in Figure 42Since the angle $\theta = 2\pi r$ is not an integer multiple of 2π, the observation δ_k is likely to coincide with a peak $+A(\omega)$ and an anti-peak $-A(\omega)$ over time. An estimate of the peak-to-peak asynchronous vibration amplitude can be made at a given shaft rate by comparing the maximum lead and maximum lag observed over a number of revolutions. Processing detrends the TOA data and separates the blade resonance from the shaft vibration.

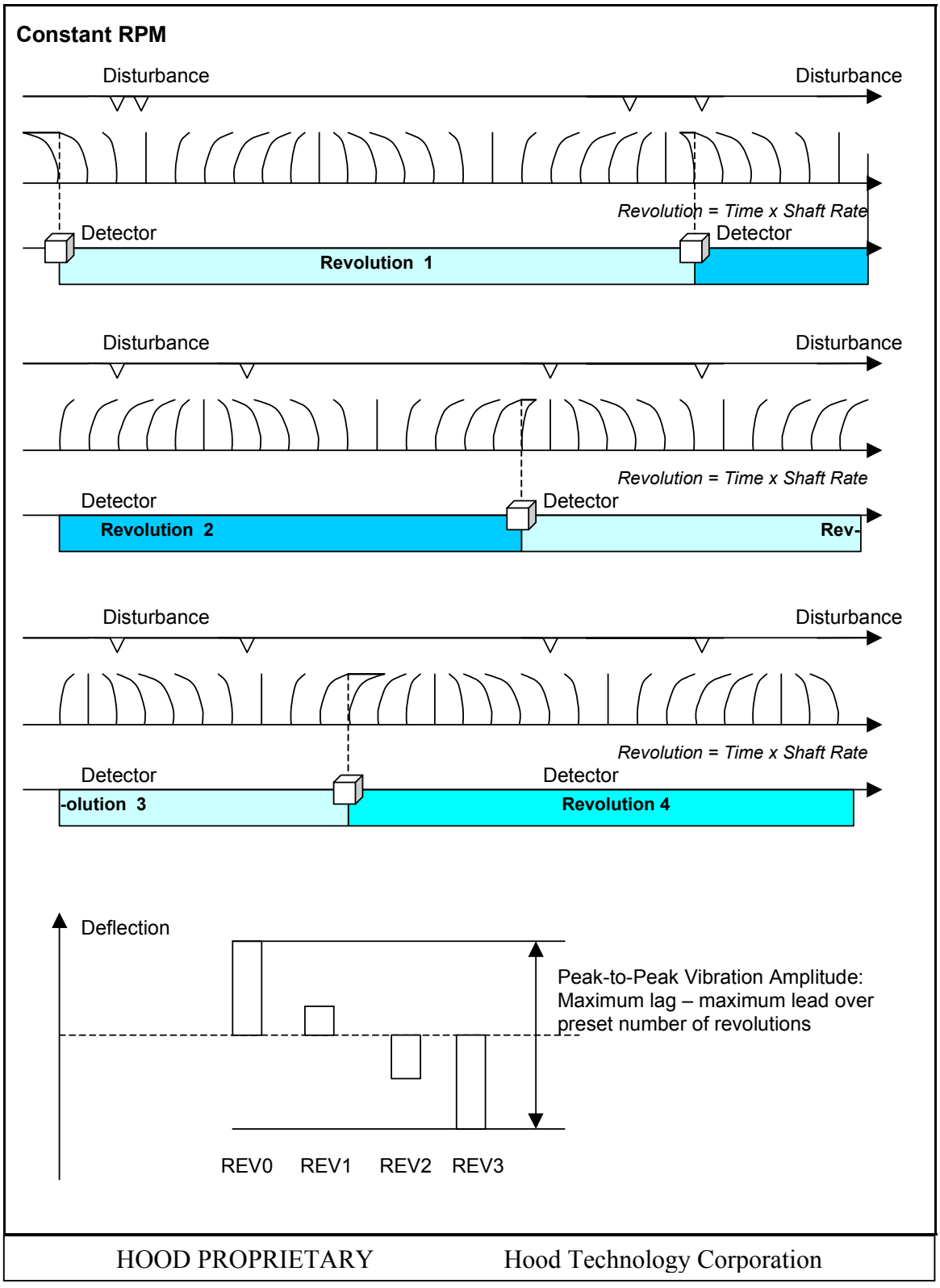

Figure 42 Asynchronous Blade Resonance as Seen by a Detector

D. GEOMETRIC CONSIDERATIONS FOR AMPLITUDE ESTIMATES

The frequency and mode shape characterize a structural resonance. The 1st torsion mode shape, for a typical blade, is shown in Figure 43. Two types of sensors are also depicted. The point sensor (PS) is a capacitive sensor, which is triggered by a very local area of the blade's tip. The line sensor (LS) uses a light line interrupted by the leading edge blade tip. See Figure 43

Assuming the major deformation occurs perpendicular to the blade's surface, this change of the normal vector (M) is categorized by

$$\Delta(M) = a\phi(M)\begin{bmatrix} -\sin\Theta_B \\ \cos\Theta_B \end{bmatrix}$$

Where a = The vibration amplitude at the moment of detection

$$a = A\sin\phi$$

ϕ = The vibration phase at detection time

Deformation is distributed in a chord-wise direction according to the mode shape ϕ, which is a scalar function since the direction of the deformation is already assumed. This assumed deformation direction holds for tip modes of bending, however, it does not hold for root bending. Therefore, mode shape cannot accurately be measured with the single line sensor probe, as is the problem with strain gauges. However, mode shapes are always calculated during the design process hence the requirement of mode determination is not seen as a factor in line sensor measurement method.

The point sensor detects blade deformation as seen in Figure 44At the position $\{X_{PS} \quad Y_{PS}\}$, point M, the measured deformation is

$$\delta_{PS} = a\cos\Theta_B\phi(X_{PS} + a\sin\Theta_B) \approx a\cos\Theta_B\phi(X_{PS})$$

The line sensor detects blade deformation at the position $\{X_{LS} \quad Y_{LS}\}$, point T, with the measured deformation being

$$\delta_{LS} = a\frac{\cos(\Theta_B - \Theta_{LS})}{\cos\Theta_{LS}}\phi(X_{LS})$$

The ratio of sensitivities between a line sensor and a point sensor located at the tip is

$$\frac{\cos(\Theta_B - \Theta_{LS})}{\cos\Theta_{LS}\cos\Theta_B}$$

If the angle of the blade, Θ_B=60 degrees and the angle of the line sensor is 45 degrees, the sensitivity ratio will be about 2.7. The main reason why the line sensor is better than the point sensor is that the point sensor is more susceptible to geometry deformation because it can only measure deflection at a point. The line sensor will measure along the length of the light line, thus removing geometrical changes. However, for both the line and point sensors, if the sensor is placed at a nodal point of bending (the axis about which the bending occurs, i.e. for higher order bending modes), it may not register any deflection at that point on the blade.

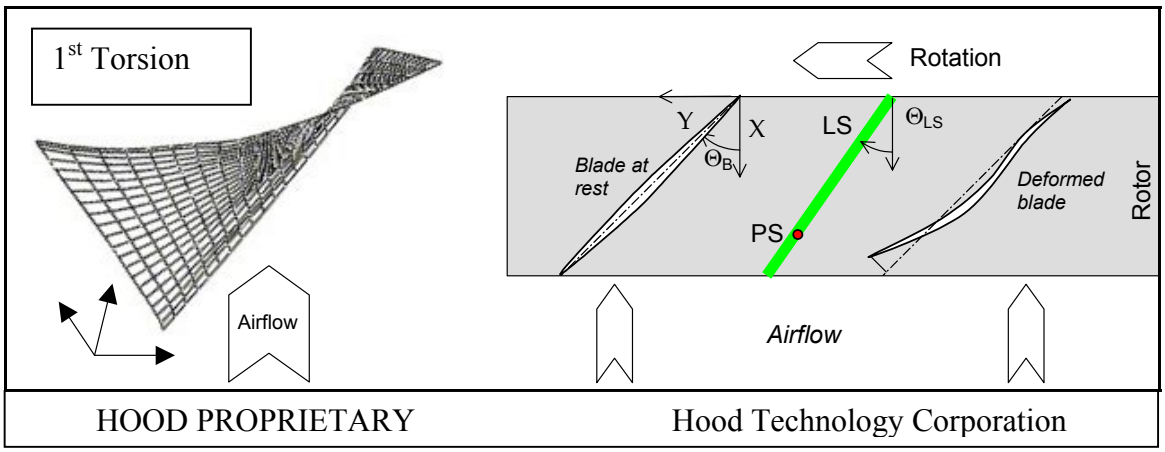

Figure 43 Geometric Consideration: Mode Shape, Point Sensor, Line Sensor

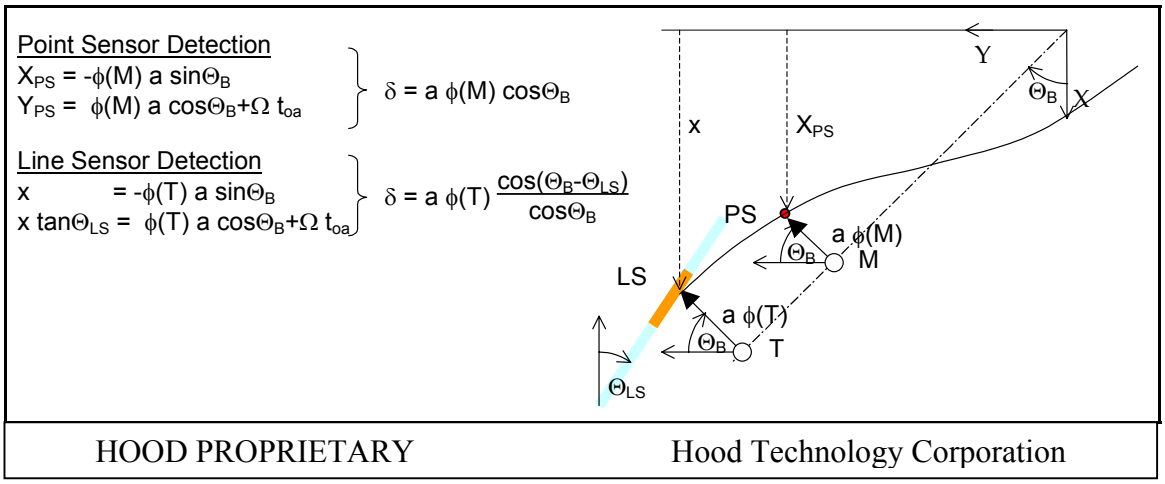

Figure 44 Geometry for Specific Detectors

E. THE CURVE FIT AND SINGLE DEGREE OF FREEDOM

It was assumed that each rotor blade was excited by a synchronous periodic excitation at $\omega = NR$, where ω is the excitation frequency, N is the integer multiple of the shaft rate, and R is the shaft rate. It is further assumed that each blade has the following transfer function from excitation to tip displacement (static position removed):

$$G(s) = \frac{\frac{Ks\Omega}{Q}}{s^2 + \frac{s\Omega}{Q} + \Omega^2}$$

where K = the maximum gain (unspecified unit)

Ω = The blade's resonance

s = The complex Laplace variable

Q = The quality factor (the measure of dampening)

The blade's response time is expressed as

$$\varphi(t) = \Re e\left\{G(jNR)\, e^{jNRt} U\right\}$$

where $\varphi(t)$ = The tip vibration

$\Re e$ = the real part of the equation in brackets

G = The Laplace transform defined above

$j^2 = -1$

N = Integer multiple of the shaft rate, R

U = The disturbance amplitude

At every revolution, the blade detector samples the motion at

$$t = \frac{\theta_o + 2\pi k}{R}$$

where θ_o = The detector aimuth relative to a vibration peak

k = the integer number of revolutions

R = The shaft rate

Therefore, the amplitude recorded by the sensor is

$$\varphi_{sensor} = \Re e\left\{G\left(jNR\right)e^{jN\theta_o}U\right\}$$

Now, define the normalized shaft rate:

$$r \cong R\frac{1}{\Omega / N}$$

Define the response amplitude:

$$A \cong KU$$

The sensor output can now be written as

$$\varphi_{sensor} = \left[\frac{r^2/Q^2}{\left(1-r^2\right)^2 + r^2/Q^2}\right]A\cos N\theta_o - \left[\frac{\left(1-r^2\right)r/Q}{\left(1-r^2\right)^2 + r^2/Q^2}\right]A\sin N\theta_o$$

Further define:

$$f(r,Q)=\left[\frac{r^2/Q^2}{\left(1-r^2\right)^2+r^2/Q^2}\right]$$

$$g(r,Q)=\left[\frac{\left(1-r^2\right)r/Q}{\left(1-r^2\right)^2+r^2/Q^2}\right]$$

The sensor output can now be written

$$\varphi_{sensor}=f(r,Q)A\cos N\theta_o-g(r,Q)A\sin N\theta_o$$

The effect of Q, quality factor is seen in Figure 45. The lower Q has a less sharp peak than the higher magnitude of Q. A sharp peak is desired in finding the resonance. The single degree of freedom (SDOF) curve fit is modeled in Figure 46. Notice at the 0 degree phase angle, the peak of the resonance is at the center, whereas at a phase angle of 90 degrees, the magnitude is divided between the upper and lower portion of the normalized axis.

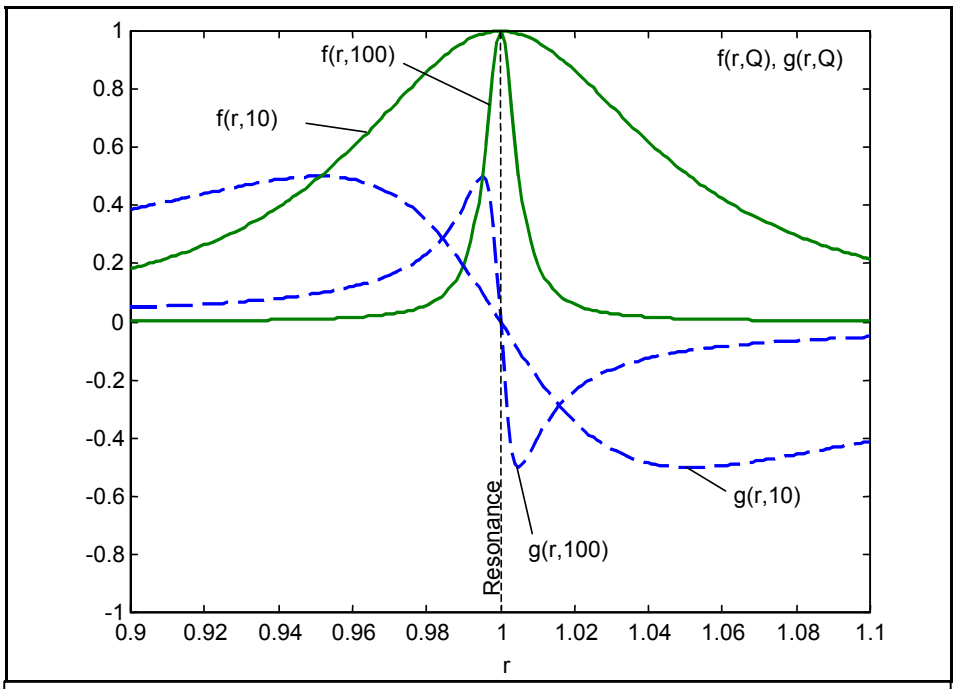

HOOD PROPRIETARY Hood Technology Corporation

Figure 45 Different Values of Q for Normalized RPM

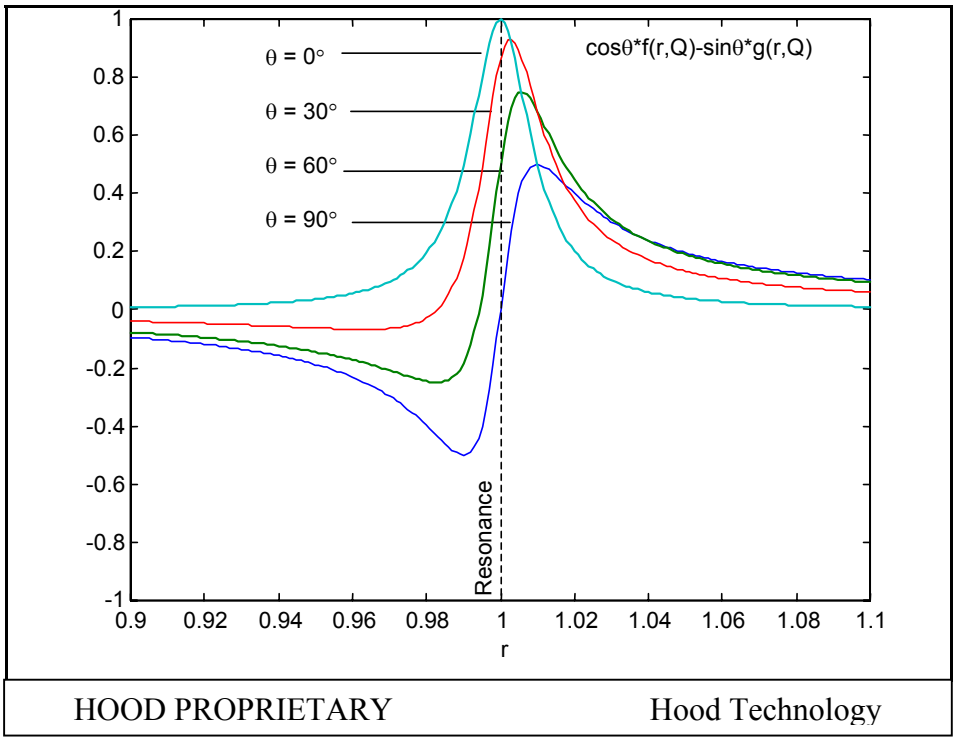

Figure 46 Sensor Output as a Function of Shaft Rate and Sensor Location to Node

Q is also useful for developing a sweep rate. A fast sweep rate of the rotor through the resonance will result in a poor sampling of the vibrations. However, a slower sweep rate through the resonance vibration will have enough data points to register a good sample. A good rule of thumb for sweep rate (ΔRPM) is the following:

$$\frac{\Delta RPM}{RPM} = \frac{1}{Q}$$

F. DETRENDING

The TOA data contains all the apparent deformation, synchronous as well as asynchronous. The asynchronous data has the shaft axial motion which cause blade pitch and the blade static deformation due to aerodynamic and centrifugal loading. The detrending of the asynchronous data is executed by averaging all the blades to provide a

good estimate of the static position shifts, while also smoothing out the synchronous resonance signatures contained in the TOA signals:

$$\varphi_i = \Theta_i - \frac{1}{Nr-1}\sum_{j \neq i} \Theta_j$$

where φ_i = The synchronous vibration

Θ_i = The blade arrival angle measured from the shaft reference for blade i

Nr = The number of blades

The blade arrival angles (Θ_i) include the blade static position, the blade static deformation due to loads, and variations induced by axial shaft motion.

THIS PAGE INTENTIONALLY LEFT BLANK

APPENDIX B : NSMS OPERATIONAL PROCEDURE

Turn on the power to the light probe system at least 5 minutes before a test in order for the probes to warm up and also to set up the computer, HP Infinium, and BVSI Board.

1. Turn the power strip on and ensure the switch at the back of the probe case is turned on.
2. Allow the probes to warm up for 5 minutes in the standby mode. (Red lights will be on). Turn the probe switches on (transmitter and receiver) when the pit is started to ensure signals are being received. Green lights will be on. See Figure 47.

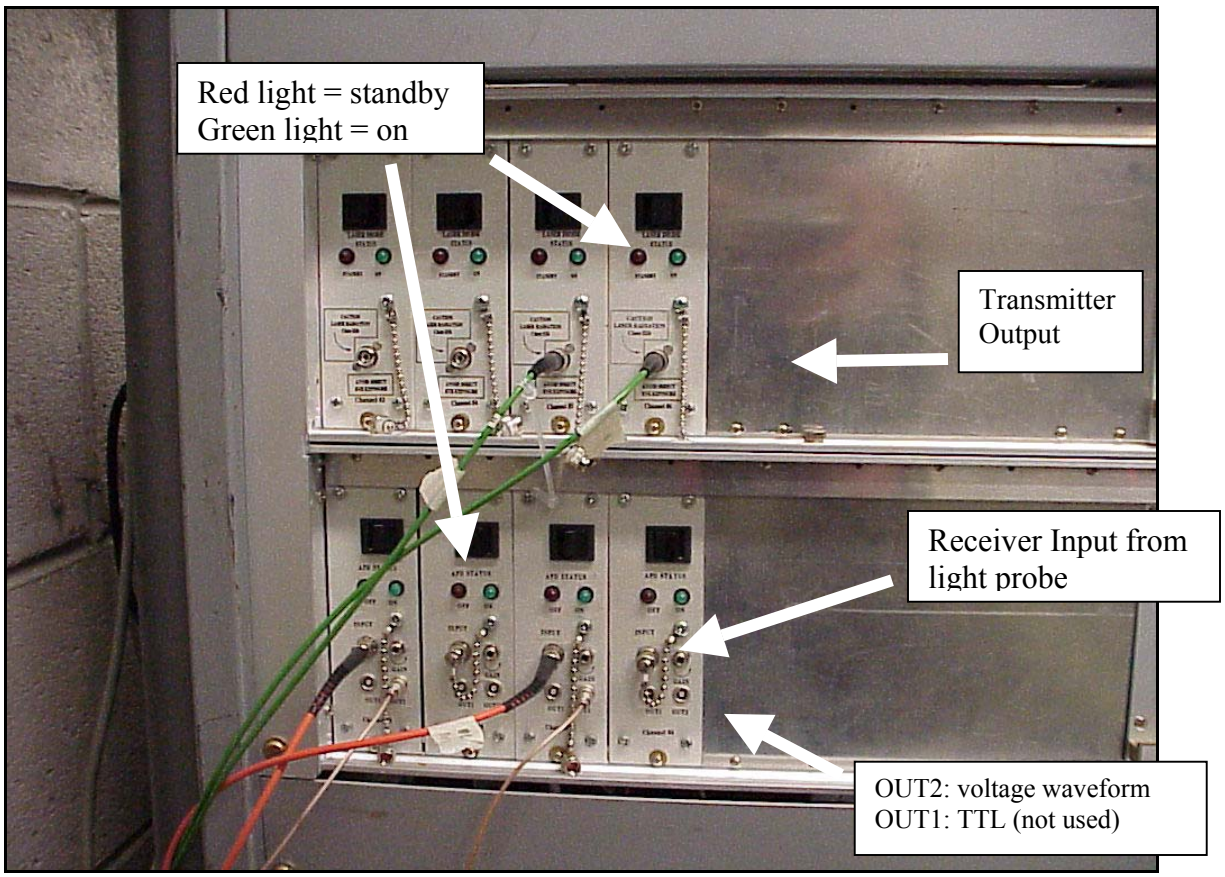

Figure 47 Laser Transmitter/Receiver Case

Turn on the HP Infinium. The Infinium (Figure 48) needs to be set up as follows:

3. Select "Vertical" Soft key #1, probe 1

4. Select “Vertical” Soft key #2, probe 2
5. Select “Vertical” Soft key #4, the one per rev (1/rev). The trigger for the scope will be set using this pulse and the “Trigger” option on the scope from the 1/rev.
6. All “Vertical” positions are set at “DC” and “1MΩ”
7. “Trigger” setup will be “edge”, “4”, use the up-slope, “trig’d” and “DC”. The level knob will control where the trigger is set on line #4. The trigger should be adjusted to 50% higher than the horizontal “zero” line (see Figure 49)
8. The “vertical” should be set at 2V/div and the “Horizontal” scale should be set at 500μs/div

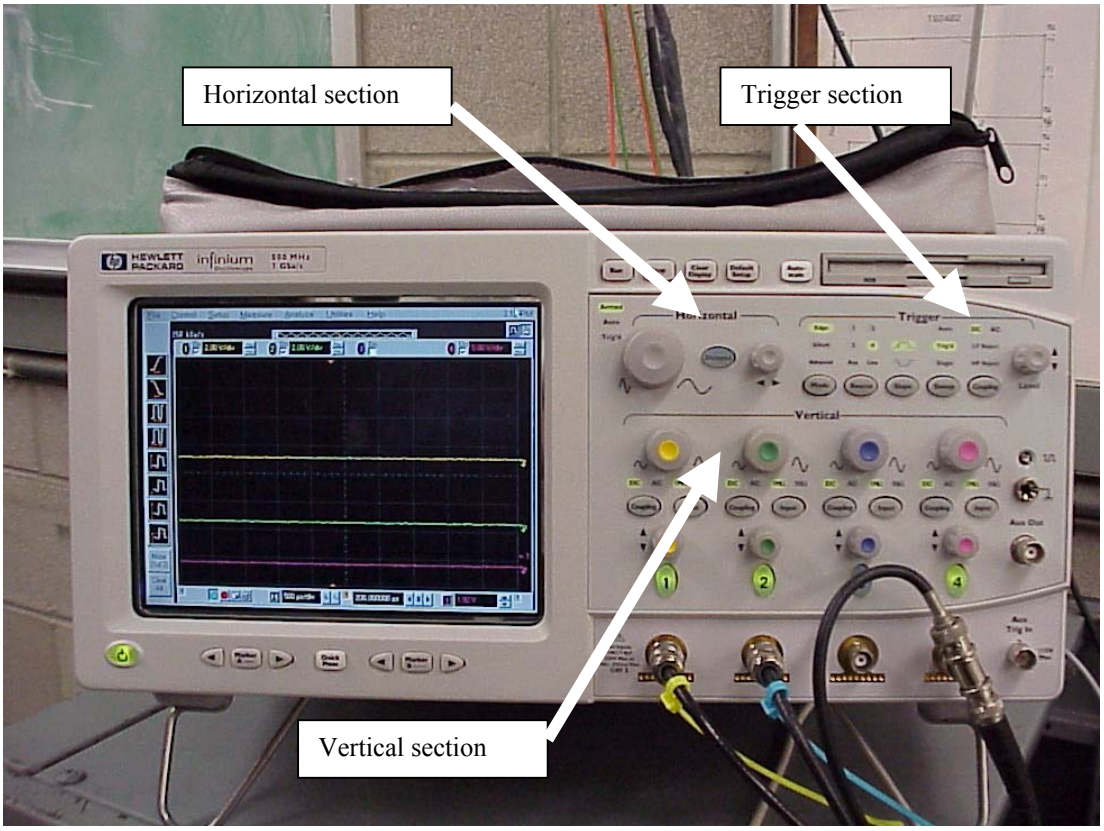

Figure 48 HP Infinium Display Set up

Figure 49 Infinium Display with 1/Rev Trigger Level Shown

Once the pit gets up to speed the display should look as shown in Figure 50.

Figure 50 HP Infinium Final Display

Set up the BVSI Board (Figure 51).

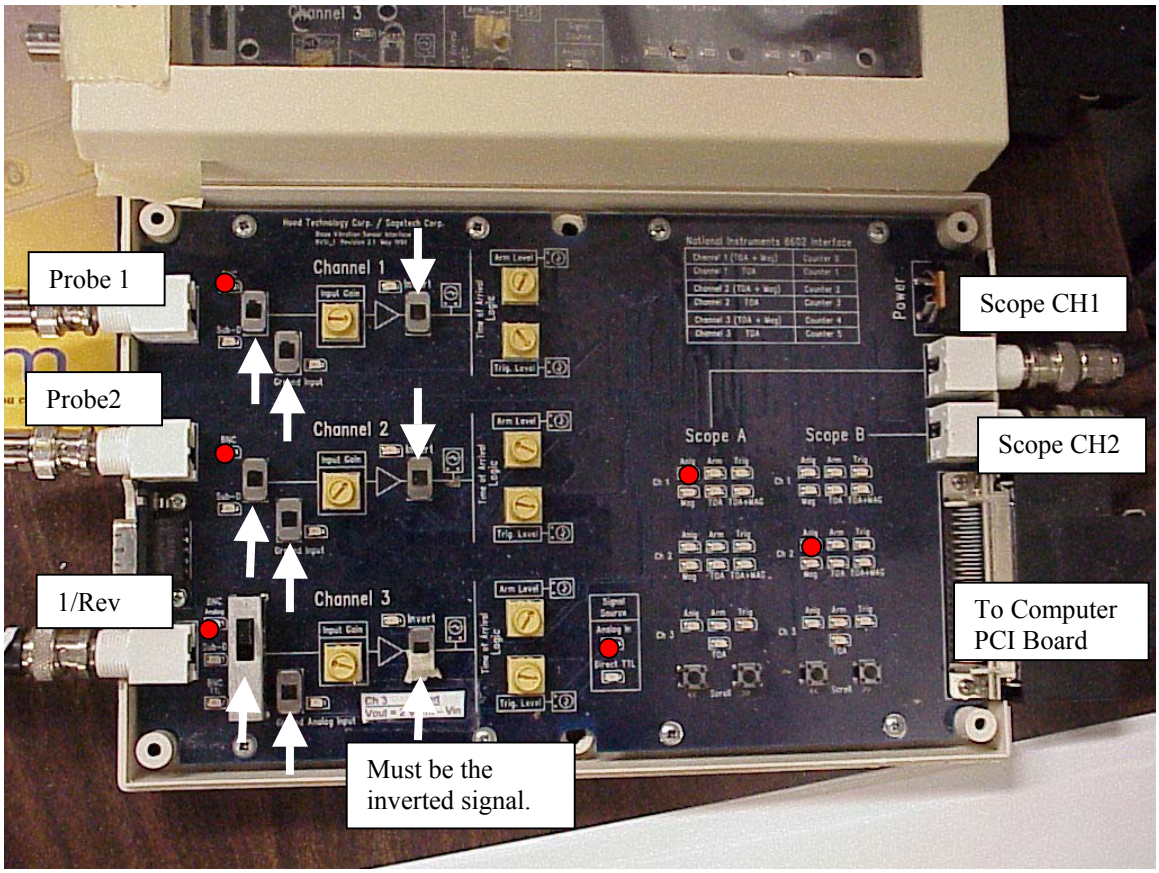

Figure 51 Digitizer Set up

The arm and trigger levels should be set according to the signal received from the probes. Use the scroll buttons and scroll Scope A and B onto the same probe (ie CH1 or CH2) and adjust the arm and trigger levels, Figure 52. The Infinium vertical adjust position for #1 and #2 should be at the same level (i.e. put them on the zero line) to get an accurate placement for arm and trigger level, Figure 53.

9. Configure the arm and trigger for both probes 1 and 2 (i.e. CH1 and CH2).

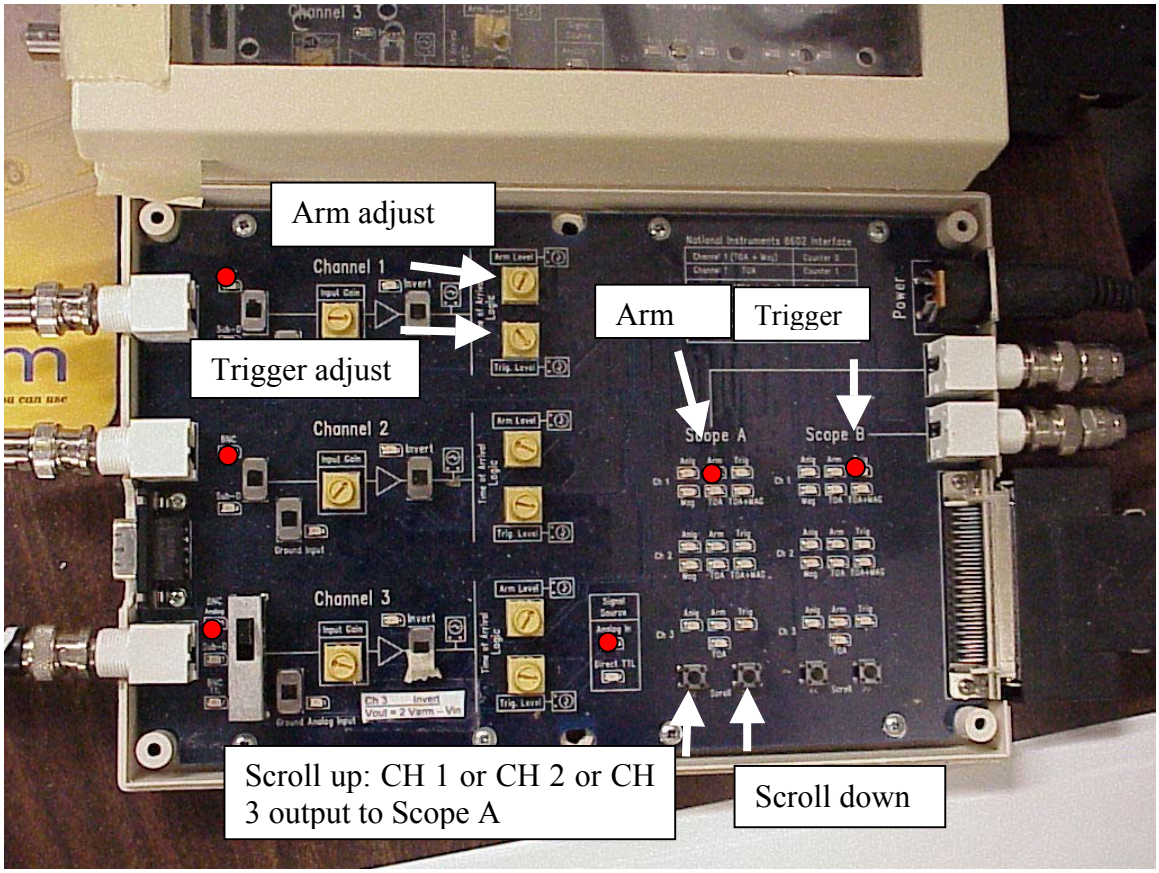

Figure 52 BVSI Arm/Trigger Manipulation

Figure 53 Arm Level to Probe Output

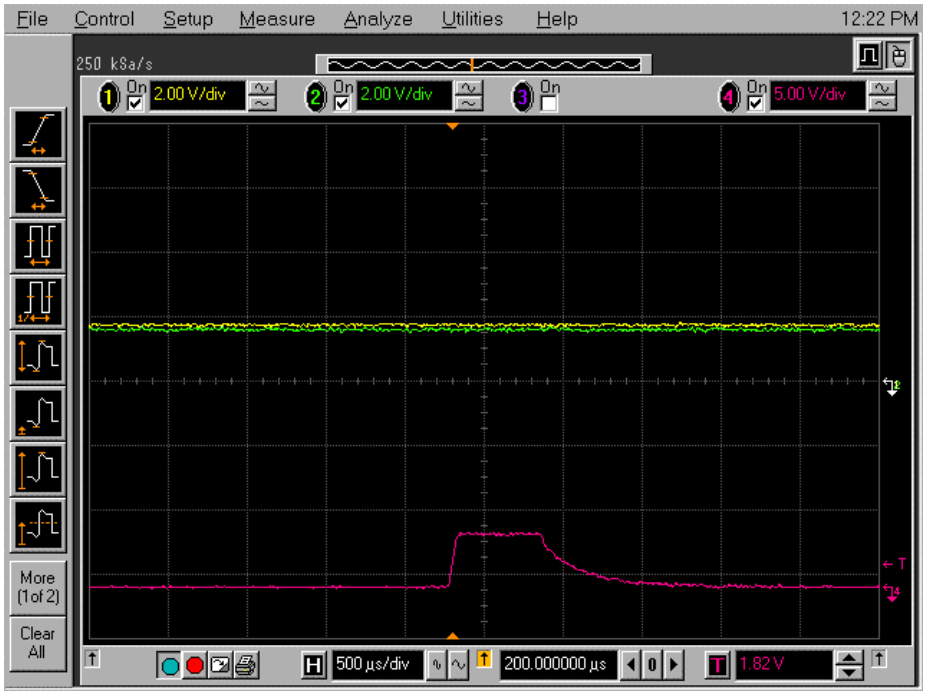

Figure 54 Arm and Trigger Levels

The 1/Rev signal can be checked by scrolling down to channel 3 “Anlg”, “Arm “, and “Trig” and ensuring the Arm is set on the curve down slope of the 1/Rev in order that the “Trig” can be set at the sharp up slope of the 1/Rev. The 1/Rev is checked by scrolling to “TOA” and see the exact time of arrival (see Figure 55).

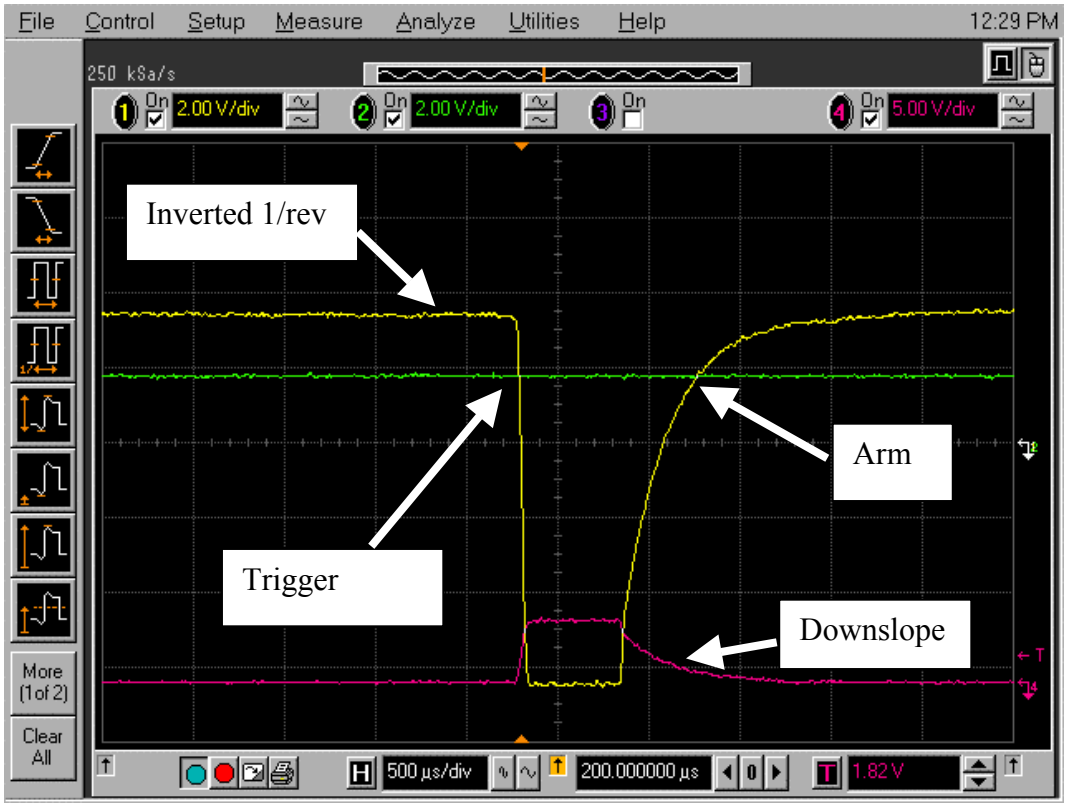

Figure 55 BVSI 1/rev Correct Placement for Inverse Switch

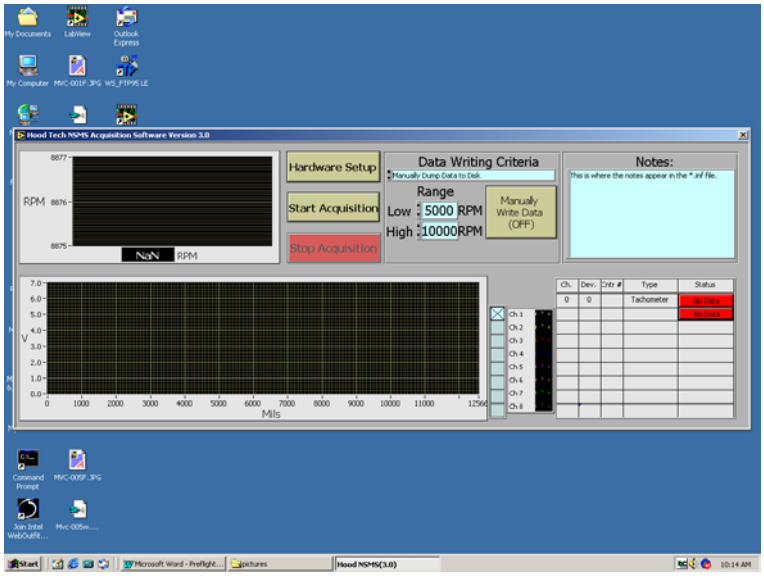

Figure 56 Data Acquisition Main

10. Double click shortcut to Hood NSMS 3.0 (Figure 56)
11. Single click **Hardware Setup** for the XTE-66 parameters: [dia=22.5, # blades = 28]. Input the appropriate parameters (shown in Figure 57) and then select **RETURN**.

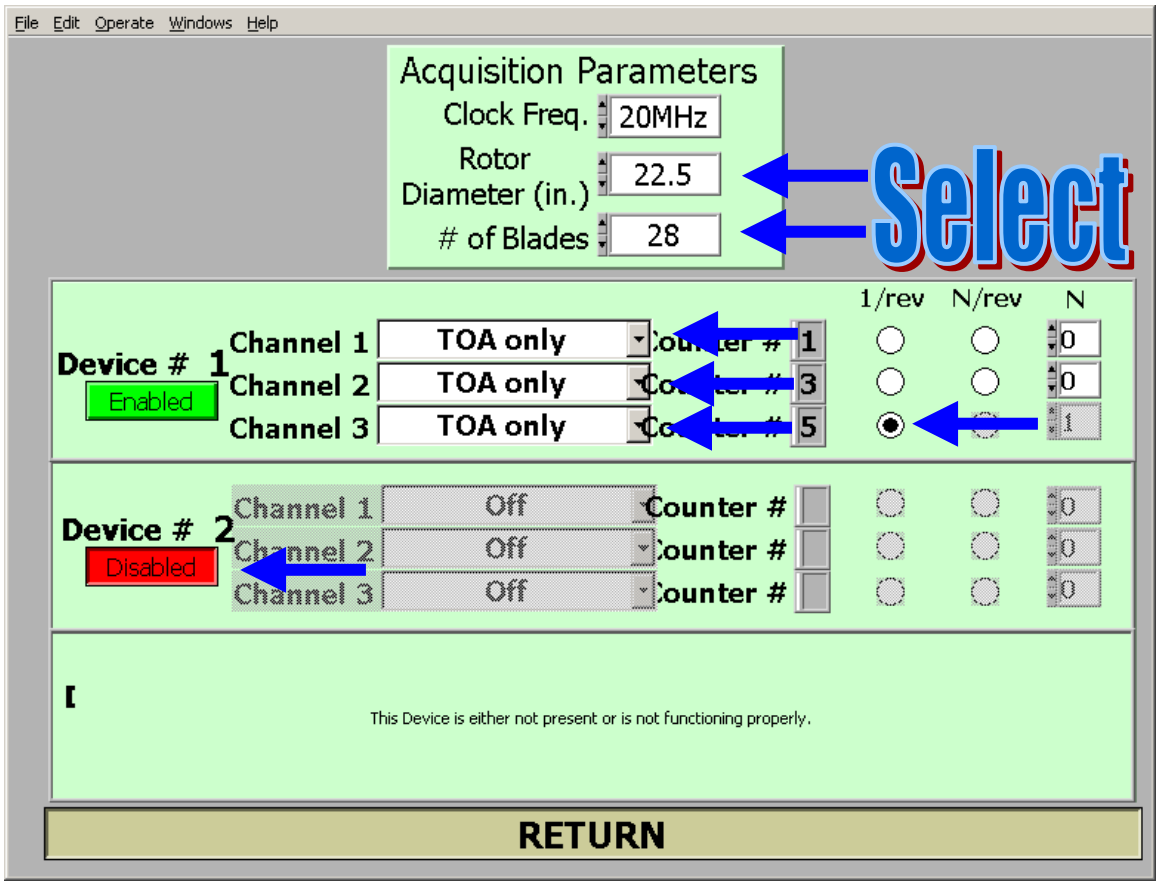

Figure 57 Data Acquisition Hardware Setup

The NSMS system is now ready to take data.

12. Press **Start Acquisition** in order for the computer to display the BVSI output. (Figure 58)
13. To record the data, **Manually Write Data** must be selected. After you have recorded the amount data you want, deselect **Manually Write Data** and a "save as" window will appear.
14. Save the data in the D:/Hood NSMS 3.0 folder with all the previously recorded data. Save by "year/month/day_time" format (i.e. 020120_1125). A probe 1 (*.1)and probe 2 file (*.2) will be recorded in addition to a time stamp file *.0 and a setup file *.inf. . The *.inf, *.0, *.1, and *.2 were the extensions of the four files, created with a single user defined file name. The *.inf file contained the hardware setup information.

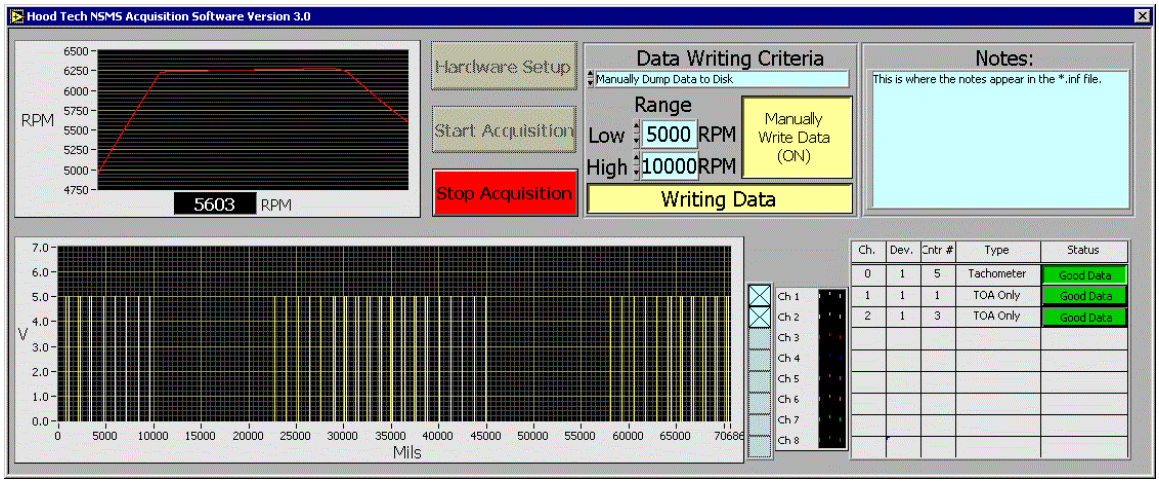

Figure 58 Operating Acquisition NSMS Software

Open the Hood Tech NSMS DATAVIEWER (Figure 59)

15. The file just recorded can be viewed by opening the DATAVIEWER and selecting the file from the D:/Hood NSMS 3.0/*.1 or *.2

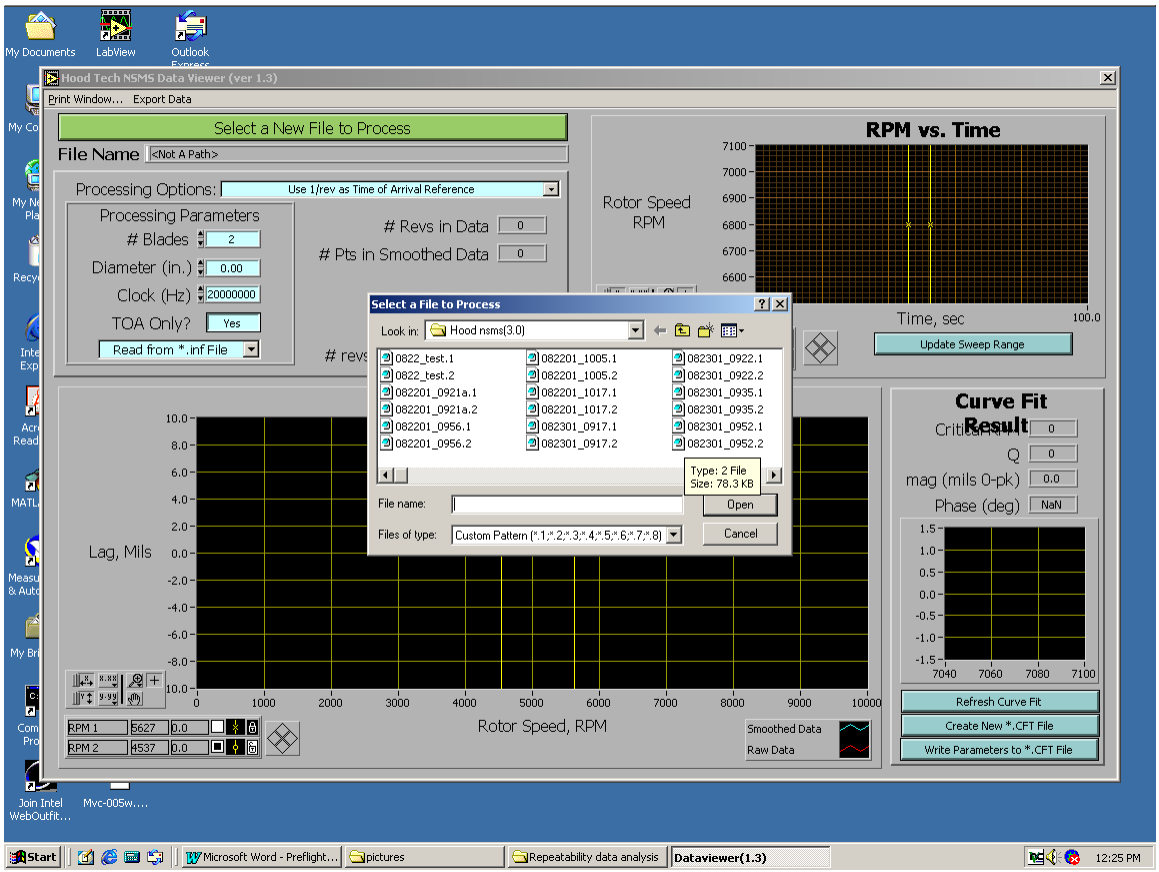

Figure 59 Data Viewer Main Page

16. Select Transformation of Inter-blade Angle for Time of Arrival. (Figure 60)

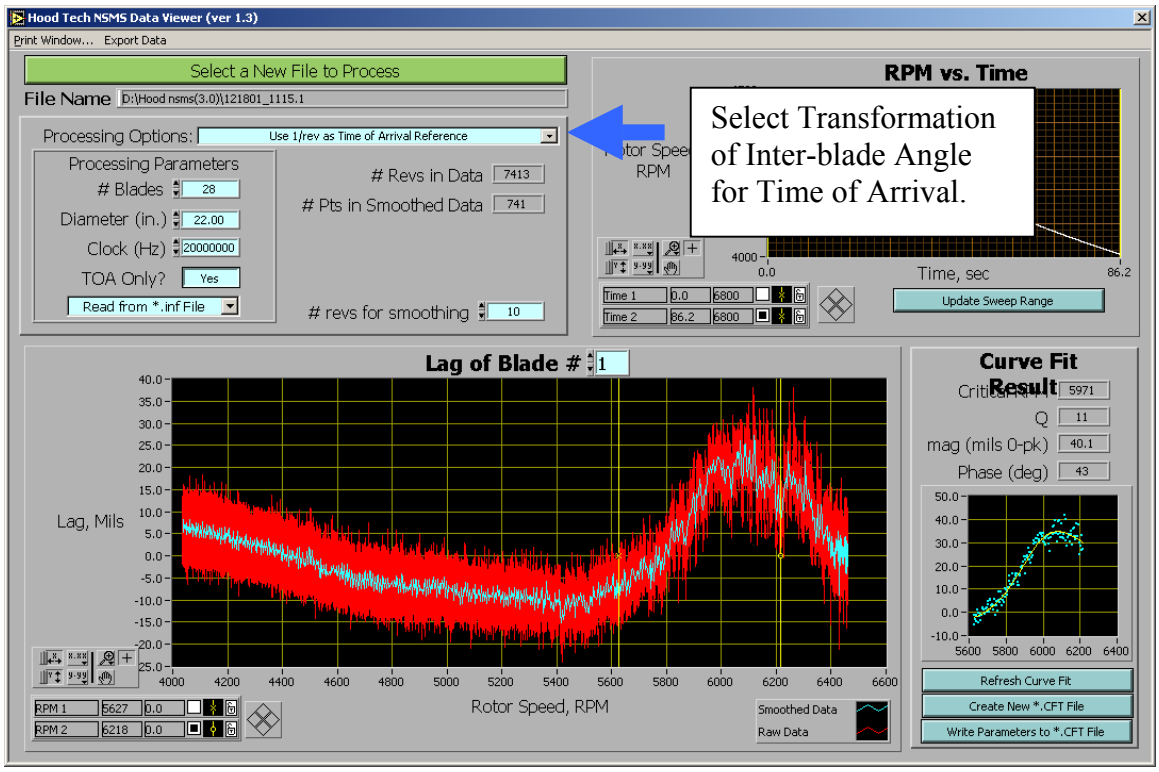

Figure 60 Processed Data Using 1/rev as TOA Reference

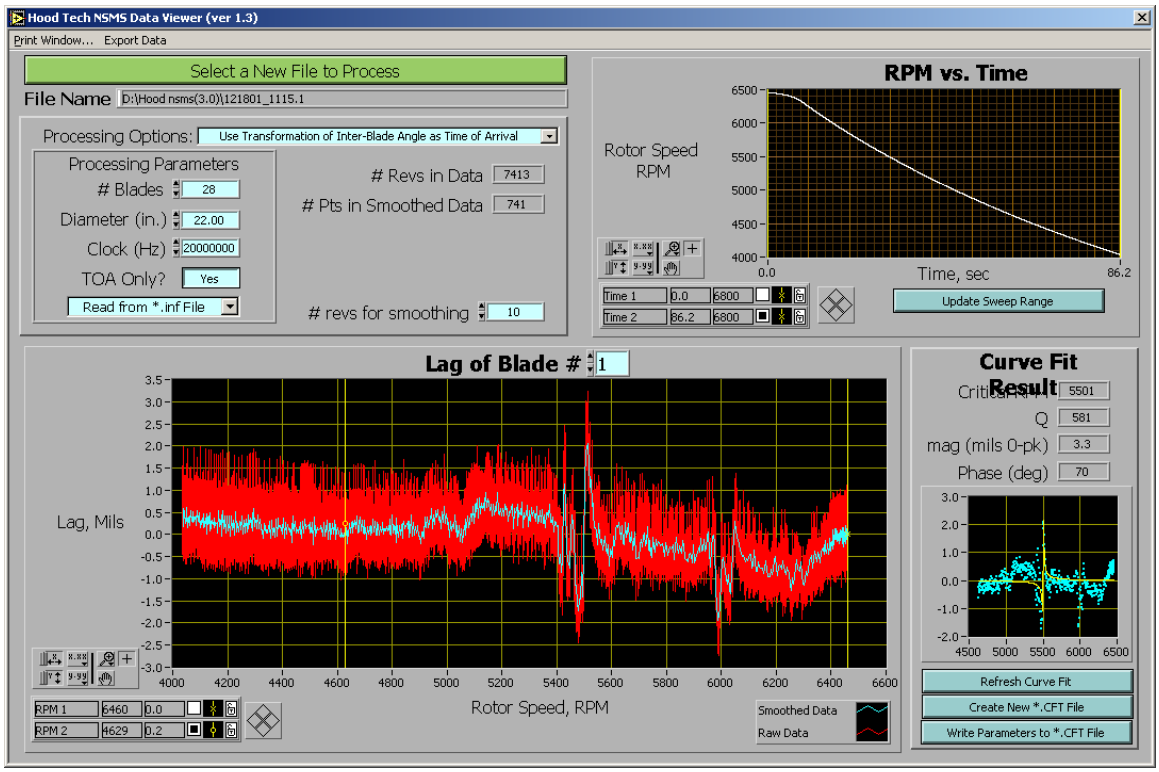

Figure 61 Processed Data Using Transformation of Inter-Blade Angle

The Processing Parameters are read from the *.inf file and do not need to be changed. The # revs for smoothing takes out some noise. 10 is a good starting point for smoothing. The RPM vs time window can be used to narrow the range the Lag of Blade window sees. The Lag of Blade # can be scrolled up or down through the number of blades. (Figure 61)

The Curve Fit Result is a single degree of freedom curve fit and is a function of where the verticle yellow lines are place in the Lag vs. RPM window. Usually the range can remain constant and remain set at certain max and min RPM's. However, sometimes the resonance causes the curve fit to hiccup and therefore the range must be changed. **Each time the range is changed, the Refresh Curve Fit option must me used**.

17. Select Create New *.cft file in order to output 5 parameters:
    1. Blade number
    2. CriticaL RPM
    3. Q
    4. Mag (mils 0-pk)
    5. Phase (deg)
18. Select "Write Parameters to File" for each blade's curve fit and the data will be appended.

Input the file to the processing system of choice; Excel, MATLAB, etc. and begin averaging.

THIS PAGE INTENTIONALLY LEFT BLANK

APPENDIX C : PROCESSED DATA

A. EXPERIMENT 1: AJE AND EFFECT OF DAMPERS

Run Number	Date	Type	Damping	Test Number	Sweep Number	Processed File Name
184	091301	8EO	No	1	1	091301_1038_1.cft
			No	1	2	091301_1044_1.cft
			No	1	3	091301_1100_1.cft
			No	1	4	091301_1126_1.cft
185	091801	8EO	Yes	1	1	091801_0906_1.cft
			Yes	1	2	091801_0926_1.cft
			Yes	1	3	091801_0939_1.cft
			Yes	1	4	091801_1001_1.cft
			Yes	1	5	091801_1005_1.cft
			Yes	1	6	091801_1018_1.cft
			Yes	1	7	091801_1032_1.cft
186	091901	8EO	No	1	1	091901_1009_1.cft
			No	1	2	091901_1021_1.cft
			No	1	3	091901_1025_1.cft
			No	1	4	091901_1052_1.cft
			No	1	5	091901_1054_1.cft
			No	1	6	091901_1117_1.cft
			No	1	7	091901_1131_1.cft
187	092501	12EO	No	1	1	092501_1447_1.cft
			No	1	2	092501_1505_1.cft
			No	1	3	092501_1507_1.cft
			No	1	4	092501_1520_1.cft
			No	1	5	092501_1532_1.cft
			No	1	6	092501_1545_1.cft
			No	1	7	092501_1554_1.cft
188	092701	12EO	Yes	1	1	092701_1316_1.cft
			Yes	1	2	092701_1327_1.cft
			Yes	1	3	092701_1348_1.cft
			Yes	1	4	092701_1354_1.cft
			Yes	1	5	092701_1407_1.cft
			Yes	1	6	092701_1423_1.cft
			Yes	1	7	092701_1436_1.cft
			Yes	1	8	092701_1452_1.cft
189	100401	12EO MOD	Yes	1	1	100401_1112_2.cft
			Yes	1	2	100401_1119a_2.cft
			Yes	1	3	100401_1134_2.cft
			Yes	1	4	100401_1150_2.cft
			Yes	1	5	100401_1211_2.cft
			Yes	1	6	100401_1224_2.cft

190	100501	12EO MOD	No	1	1	100501_1024a_2.cft
			No	1	2	100501_1030_2.cft
			No	1	3	100501_1046_2.cft
			No	1	4	100501_1102_2.cft
			No	1	5	100501_1138_2.cft
191	101101	12EO MOD	No	1	1	101201_1421a_2.cft
			No	1	2	101201_1509_2.cft
			No	1	3	101201_1523a_2.cft

B. EXPERIMENT 2: ECE AND NSMS CALIBRATION TO STRAIN GAUGES

Run Number	Date	Type	Test Number	Sweep Number	Processed File Name	
193	110501	12EO	1	1	110501_1058a_1.cft	110501_1058a_2.cft
			1	2	110501_1125_1.cft	110501_1125_2.cft
194	110701	12EO	1	1	110701_1029_1.cft	110701_1029_2.cft
			2	1	110701_1040_1.cft	110701_1040_2.cft
			3	1	110701_1137_1.cft	110701_1137_2.cft
			4	1	110701_1204_1.cft	110701_1204_2.cft
195	110901	12EO	1	1	110901_1205_1.cft	110901_1205_2.cft
			2	1	110901_1239_1.cft	110901_1239_2.cft
			3	1	110901_1247_1.cft	110901_1247_2.cft
			4	1	110901_1255_1.cft	110901_1255_2.cft
			5	1	110901_1304_1.cft	110901_1304_2.cft
196	111401	12EO	1	1	111401_1113_1.cft	111401_1113_2.cft
			2	1	111401_1144_1.cft	111401_1144_2.cft
			3	1	111401_1155_1.cft	111401_1155_2.cft
			4	1	111401_1203_1.cft	111401_1203_2.cft
			5	1	111401_1213_1.cft	111401_1213_2.cft
197	111601	12EO	1	1	111601_0935_1	111601_0935_2
			2	1	111601_0949_1	111601_0949_2
			3	1	111601_0958_1	111601_0958_2
			unused	unused	111601_1004_1	111601_1004_2
			unused	unused	111601_1015_1	111601_1015_2
			unused	unused	111601_1022_1	111601_1022_2
			4	1	111601_1035_1	111601_1035_2
			5	1	111601_1041_1	111601_1041_2
			no data	no data	111601_1051_1	111601_1051_2
			6	1	111601_1102_1	111601_1102_2
			6	2	111601_1107_1	111601_1107_2
			6	3	111601_1112_1	111601_1112_2
198	112001	12EO	1	1	112001_0856_1	112001_0856_2
			2	1	112001_0926_1	112001_0926_2
			3	1	112001_0933_1	112001_0933_2

C. EXPERIMENT 3: EFFECT OF SILVER PLATING

Run Number	Date	Type	Test Number	Sweep Number	Processed File Name	
201	121801	12EO	1	1	121801_1115_1	121801_1115_2
			2	1	121801_1125_1	121801_1125_2
			3	1	121801_1135_1	121801_1135_2
			4	1	121801_1145_1	121801_1145_2
			5	1	121801_1155_1	121801_1155_2
202	121801	12EO	1	1	121801_1345_1	121801_1345_2
			2	1	121801_1355_1	121801_1355_2
			3	1	121801_1415_1	121801_1415_2
			4	1	121801_1435_1	121801_1435_2

D. EXPERIMENT 4: EFFECT OF PLASTIC INSERTS

Run Number	Date	Type	Test Number	Sweep Number	Processed File Name	
203	011702		1	1	020117_1125_1	020117_1125_2
OR #1 for 2002			1	2	020117_1130_1	020117_1130_2
			1	3	020117_1136_1	020117_1136_2
			2	1	020117_1152_1	020117_1152_2
			2	2	020117_1158_1	020117_1158_2
			2	3	020117_1207_1	020117_1207_2
			3	1	020117_1217_1	020117_1217_2
			3	2	020117_1222_1	020117_1222_2
			3	3	020117_1228_1	020117_1228_2
			4	1	020117_1240_1	020117_1240_2
			4	2	020117_1245_1	020117_1245_2
			4	3	020117_1250_1	020117_1250_2
			5	1	020117_1302_1	020117_1302_2
			5	2	020117_1307_1	020117_1307_2
			5	3	020117_1311_1	020117_1311_2

THIS PAGE INTENTIONALLY LEFT BLANK

APPENDIX D : AJE DATA AT 8EO, 10EO, AND 12EO

A. AIR JET TEST RESULTS FOR EVERY BLADE AT 8EO AND 10EO.

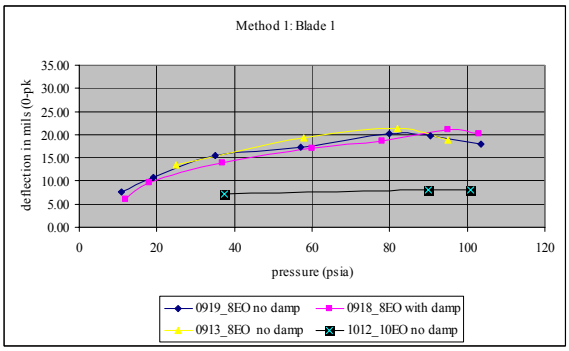

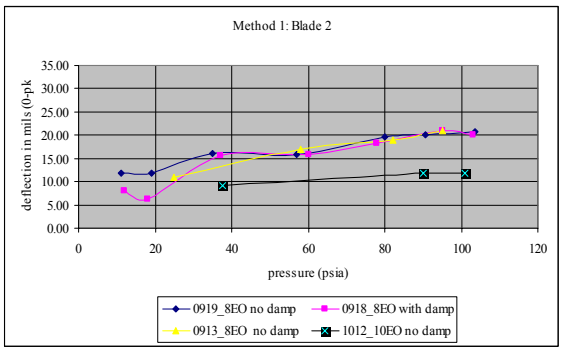

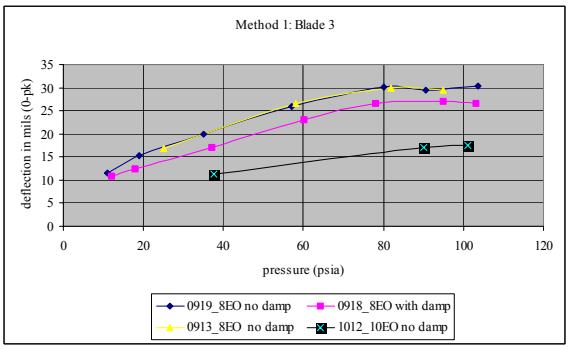

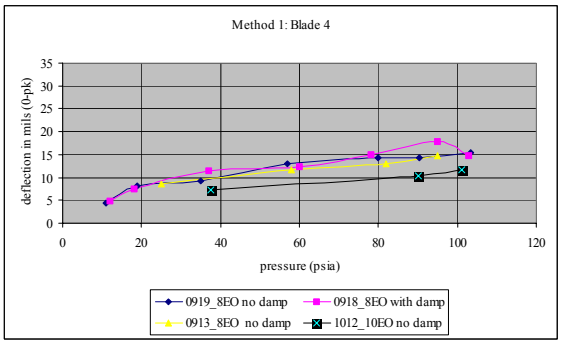

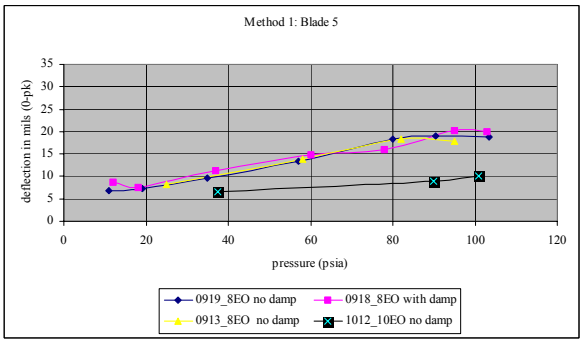

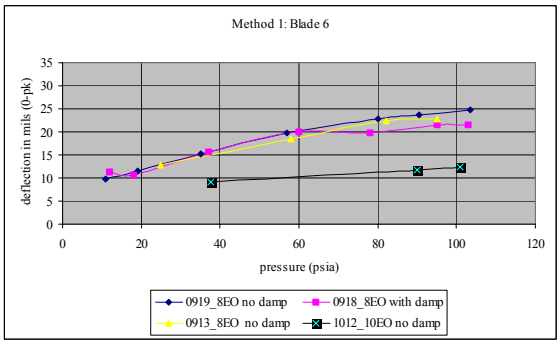

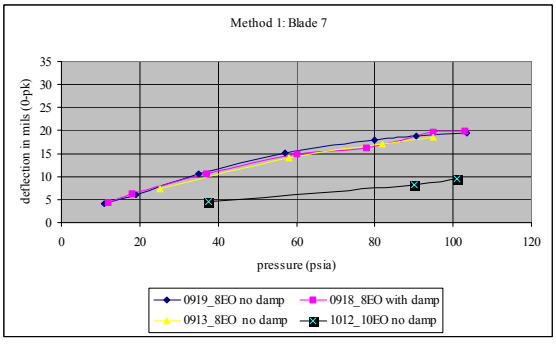

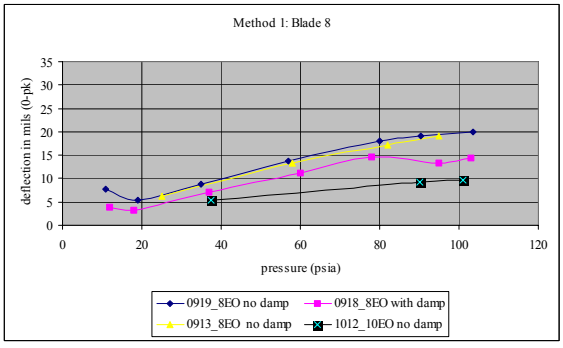

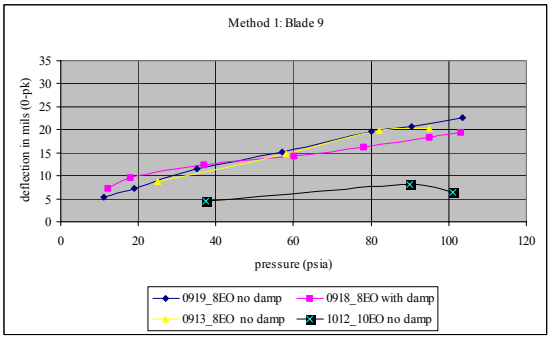
Method 1: Blade 9
deflection in mils (0-pk)
pressure (psia)
0919_8EO no damp
0918_8EO with damp
0913_8EO no damp
1012_10EO no damp

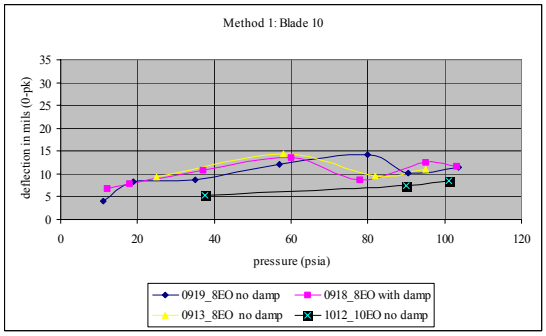
Method 1: Blade 10
deflection in mils (0-pk)
pressure (psia)
0919_8EO no damp
0918_8EO with damp
0913_8EO no damp
1012_10EO no damp

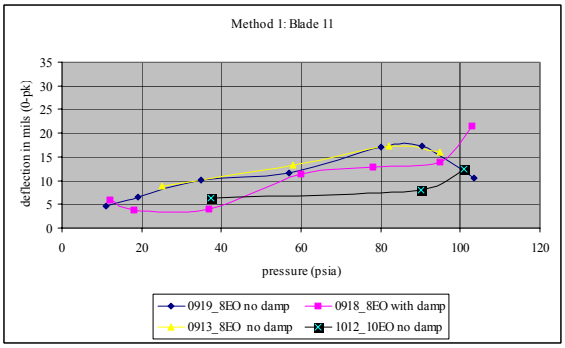
Method 1: Blade 11
deflection in mils (0-pk)
pressure (psia)
0919_8EO no damp
0918_8EO with damp
0913_8EO no damp
1012_10EO no damp

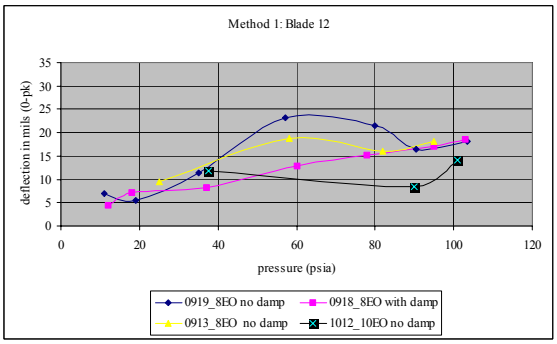
Method 1: Blade 12
deflection in mils (0-pk)
pressure (psia)
0919_8EO no damp
0918_8EO with damp
0913_8EO no damp
1012_10EO no damp

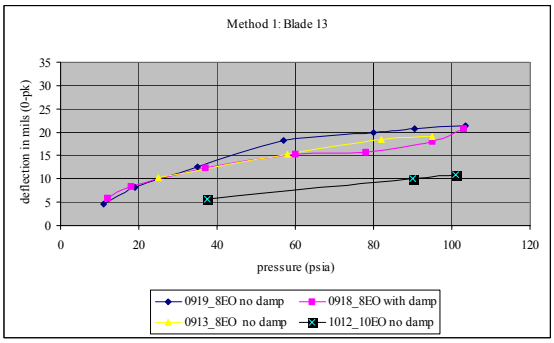
Method 1: Blade 13
deflection in mils (0-pk)
pressure (psia)
0919_8EO no damp
0918_8EO with damp
0913_8EO no damp
1012_10EO no damp

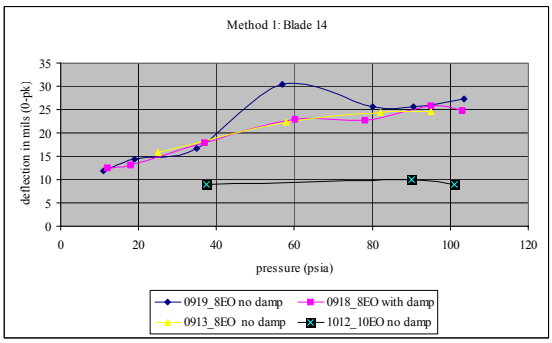
Method 1: Blade 14
deflection in mils (0-pk)
pressure (psia)
0919_8EO no damp
0918_8EO with damp
0913_8EO no damp
1012_10EO no damp

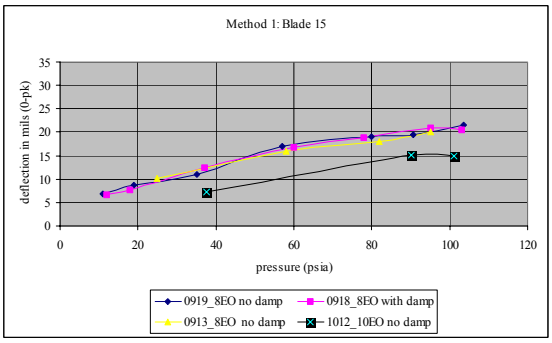
Method 1: Blade 15
deflection in mils (0-pk)
pressure (psia)
0919_8EO no damp
0918_8EO with damp
0913_8EO no damp
1012_10EO no damp

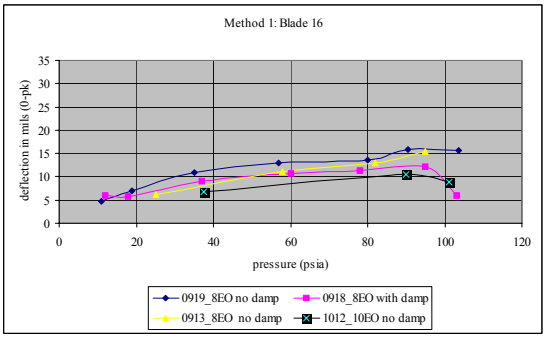
Method 1: Blade 16
deflection in mils (0-pk)
pressure (psia)
0919_8EO no damp
0918_8EO with damp
0913_8EO no damp
1012_10EO no damp

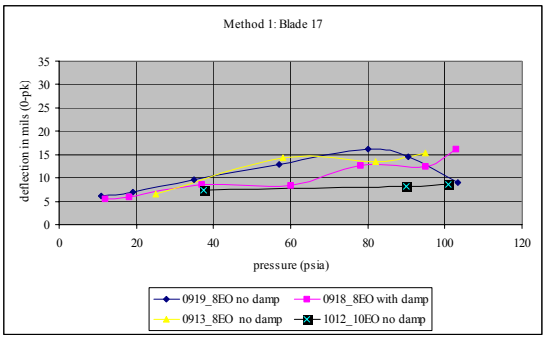
Method 1: Blade 17
deflection in mils (0-pk)
pressure (psia)
0919_8EO no damp
0918_8EO with damp
0913_8EO no damp
1012_10EO no damp

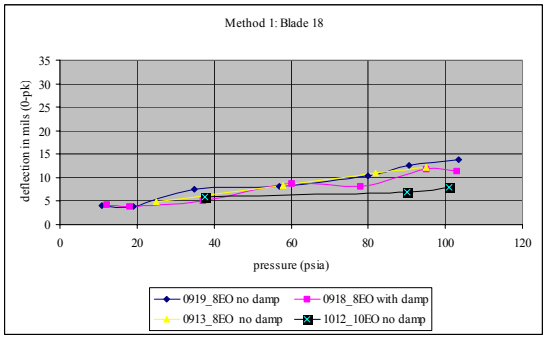
Method 1: Blade 18
deflection in mils (0-pk)
pressure (psia)
0919_8EO no damp
0918_8EO with damp
0913_8EO no damp
1012_10EO no damp

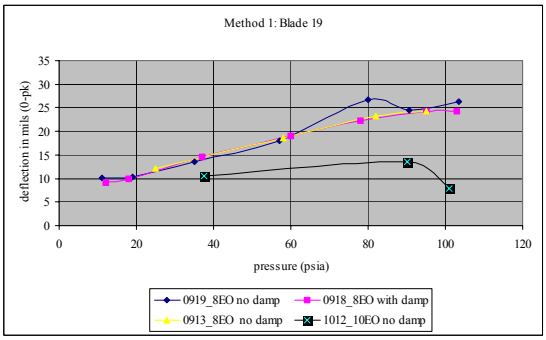
Method 1: Blade 19
deflection in mils (0-pk)
pressure (psia)
0919_8EO no damp
0918_8EO with damp
0913_8EO no damp
1012_10EO no damp

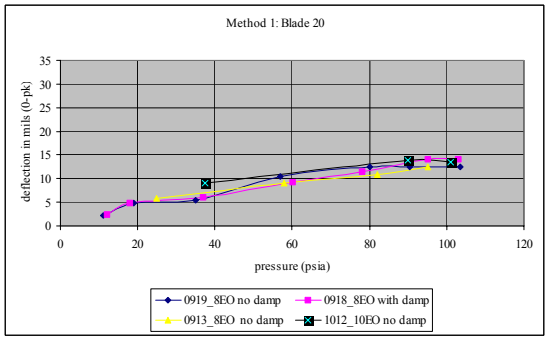
Method 1: Blade 20
deflection in mils (0-pk)
pressure (psia)
0919_8EO no damp
0918_8EO with damp
0913_8EO no damp
1012_10EO no damp

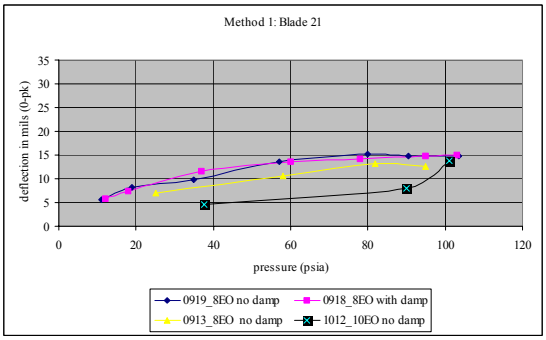
Method 1: Blade 21
deflection in mils (0-pk)
pressure (psia)
0919_8EO no damp
0918_8EO with damp
0913_8EO no damp
1012_10EO no damp

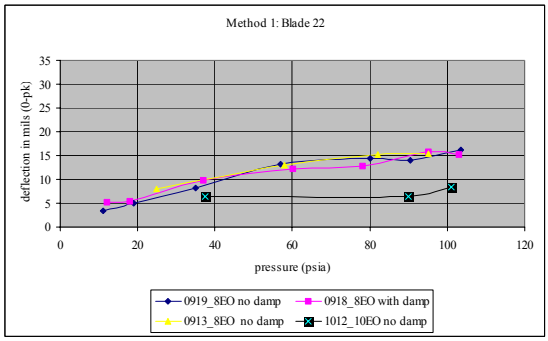
Method 1: Blade 22
deflection in mils (0-pk)
pressure (psia)
0919_8EO no damp
0918_8EO with damp
0913_8EO no damp
1012_10EO no damp

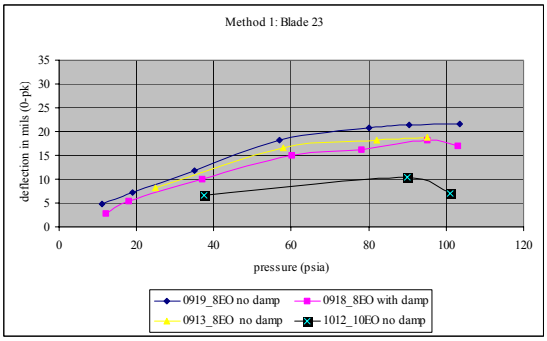
Method 1: Blade 23
deflection in mils (0-pk)
pressure (psia)
0919_8EO no damp
0918_8EO with damp
0913_8EO no damp
1012_10EO no damp

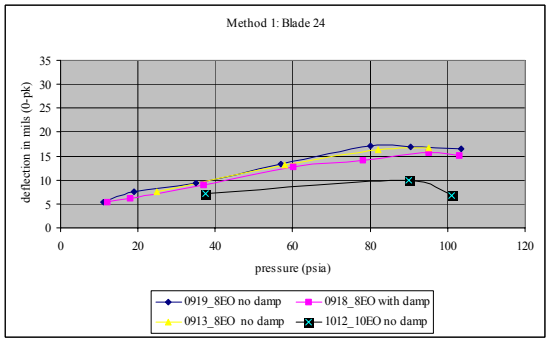
Method 1: Blade 24
deflection in mils (0-pk)
pressure (psia)
0919_8EO no damp
0918_8EO with damp
0913_8EO no damp
1012_10EO no damp

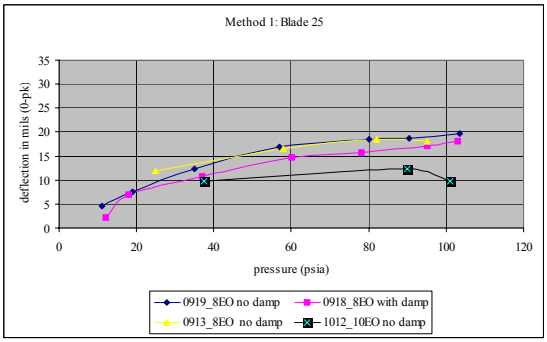

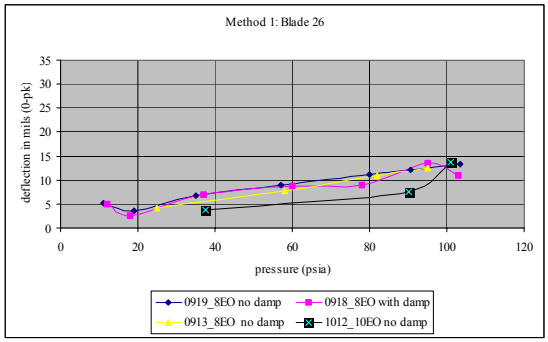

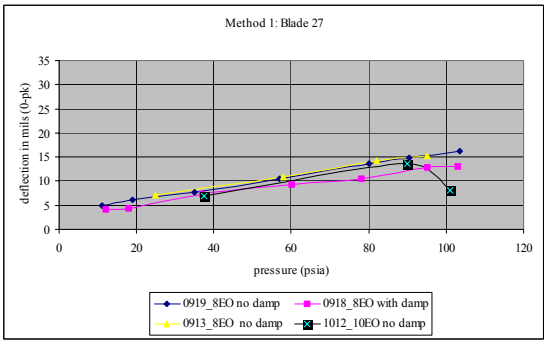

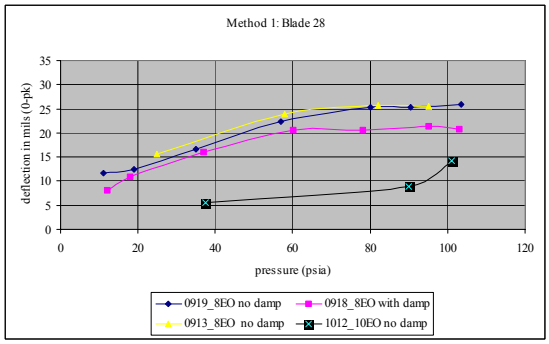

B. AIR JET TEST RESULTS FOR EVERY BLADE AT 12EO.

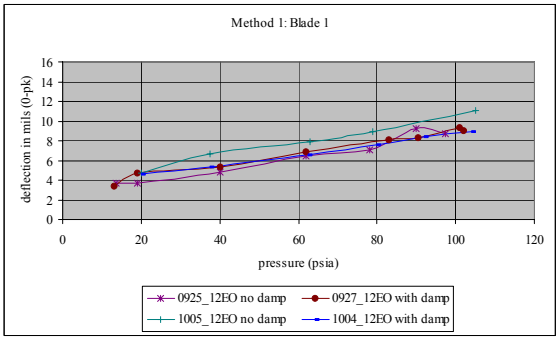

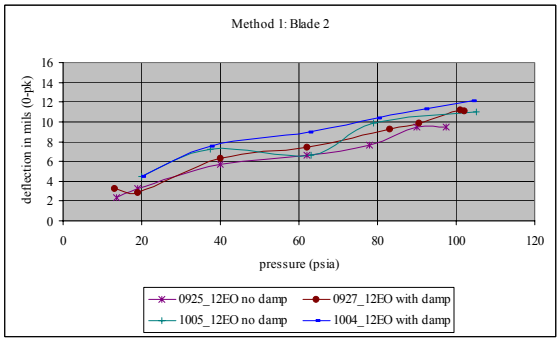

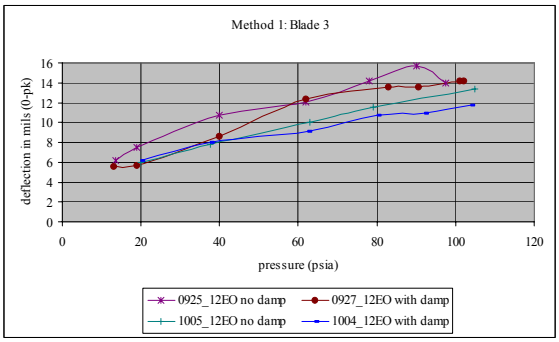

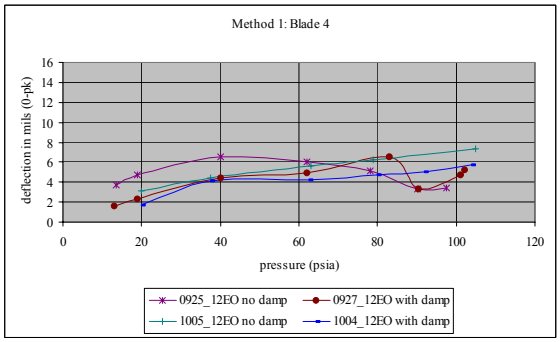

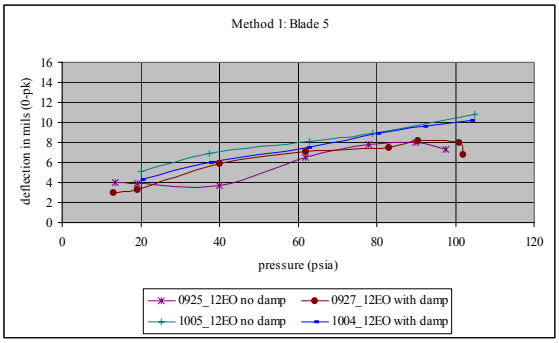
Method 1: Blade 5
deflection in mils (0-pk)
pressure (psia)
0925_12EO no damp
0927_12EO with damp
1005_12EO no damp
1004_12EO with damp

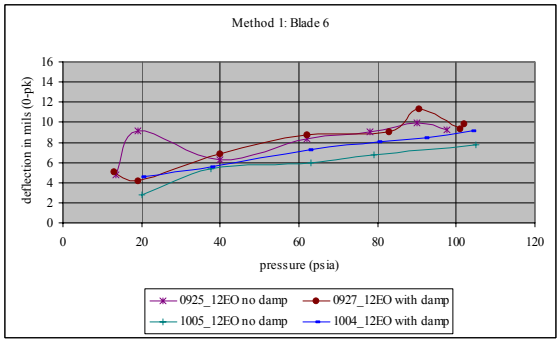
Method 1: Blade 6
deflection in mils (0-pk)
pressure (psia)
0925_12EO no damp
0927_12EO with damp
1005_12EO no damp
1004_12EO with damp

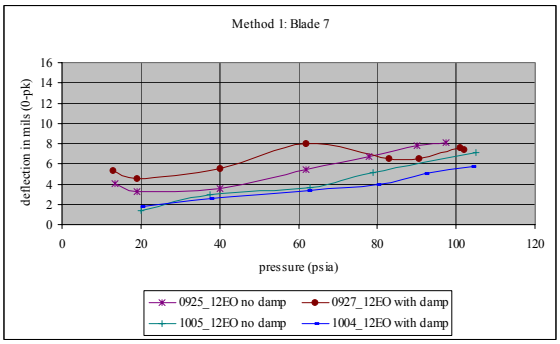
Method 1: Blade 7
deflection in mils (0-pk)
pressure (psia)
0925_12EO no damp
0927_12EO with damp
1005_12EO no damp
1004_12EO with damp

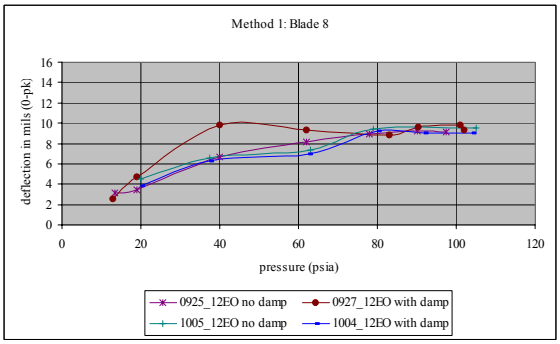
Method 1: Blade 8
deflection in mils (0-pk)
pressure (psia)
0925_12EO no damp
0927_12EO with damp
1005_12EO no damp
1004_12EO with damp

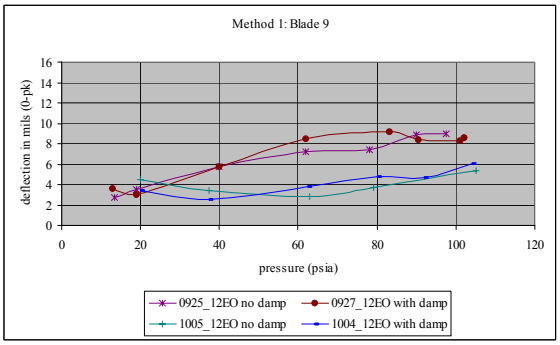
Method 1: Blade 9
deflection in mils (0-pk)
pressure (psia)
0925_12EO no damp
0927_12EO with damp
1005_12EO no damp
1004_12EO with damp

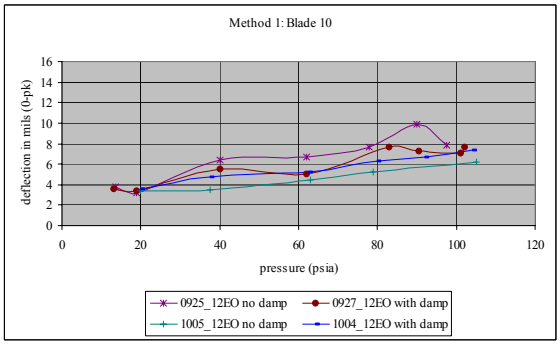
Method 1: Blade 10
deflection in mils (0-pk)
pressure (psia)
0925_12EO no damp
0927_12EO with damp
1005_12EO no damp
1004_12EO with damp

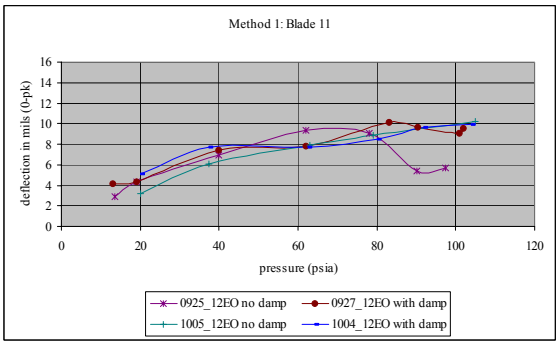
Method 1: Blade 11
deflection in mils (0-pk)
pressure (psia)
0925_12EO no damp
0927_12EO with damp
1005_12EO no damp
1004_12EO with damp

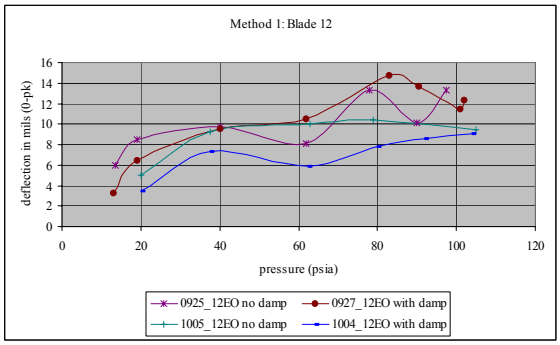
Method 1: Blade 12
deflection in mils (0-pk)
pressure (psia)
0925_12EO no damp
0927_12EO with damp
1005_12EO no damp
1004_12EO with damp

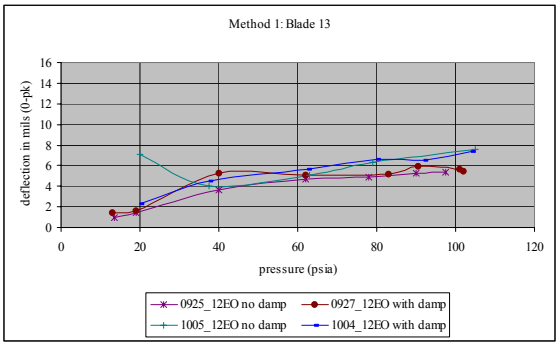
Method 1: Blade 13
deflection in mils (0-pk)
pressure (psia)
0925_12EO no damp
0927_12EO with damp
1005_12EO no damp
1004_12EO with damp

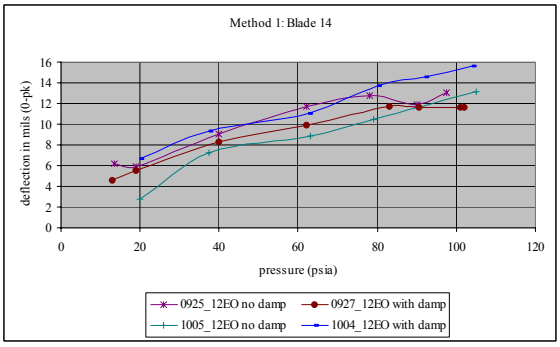
Method 1: Blade 14
deflection in mils (0-pk)
pressure (psia)
0925_12EO no damp
0927_12EO with damp
1005_12EO no damp
1004_12EO with damp

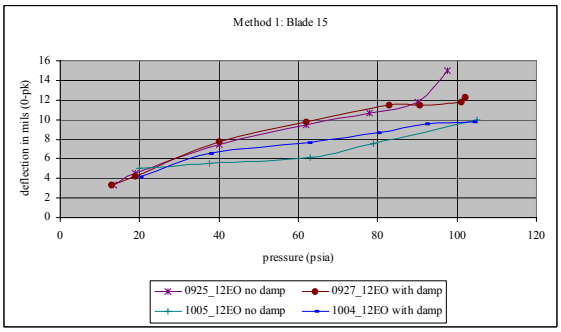
Method 1: Blade 15
deflection in mils (0-pk)
pressure (psia)
0925_12EO no damp
0927_12EO with damp
1005_12EO no damp
1004_12EO with damp

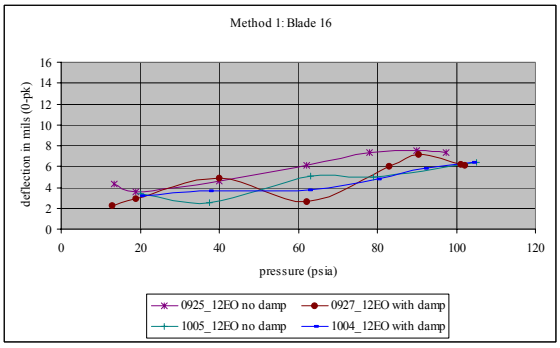
Method 1: Blade 16
deflection in mils (0-pk)
pressure (psia)
0925_12EO no damp
0927_12EO with damp
1005_12EO no damp
1004_12EO with damp

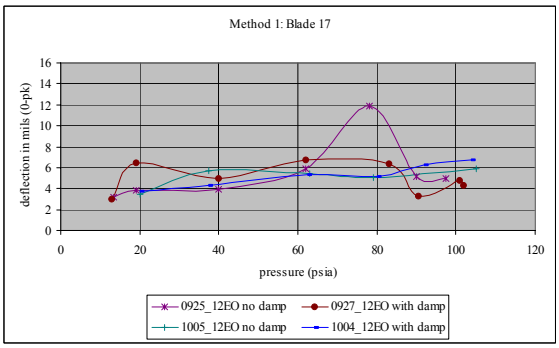
Method 1: Blade 17
deflection in mils (0-pk)
pressure (psia)
0925_12EO no damp
0927_12EO with damp
1005_12EO no damp
1004_12EO with damp

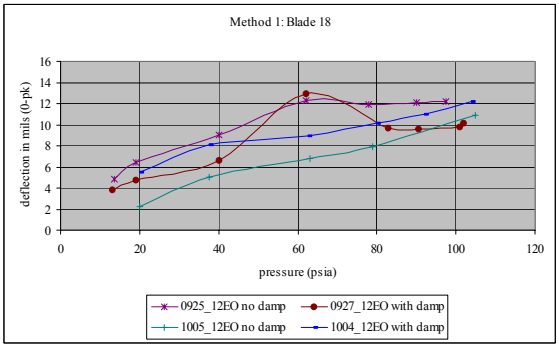
Method 1: Blade 18
deflection in mils (0-pk)
pressure (psia)
0925_12EO no damp
0927_12EO with damp
1005_12EO no damp
1004_12EO with damp

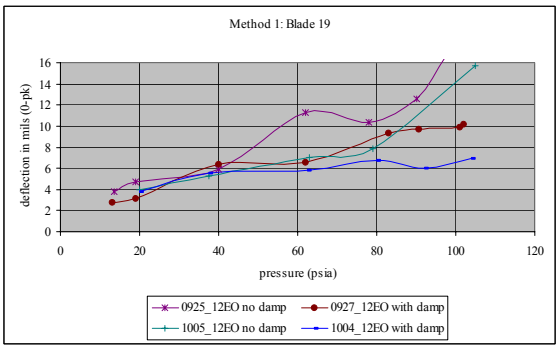
Method 1: Blade 19
deflection in mils (0-pk)
pressure (psia)
0925_12EO no damp
0927_12EO with damp
1005_12EO no damp
1004_12EO with damp

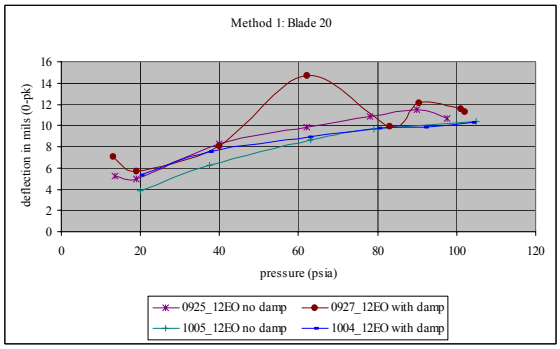
Method 1: Blade 20
deflection in mils (0-pk)
pressure (psia)
0925_12EO no damp
0927_12EO with damp
1005_12EO no damp
1004_12EO with damp

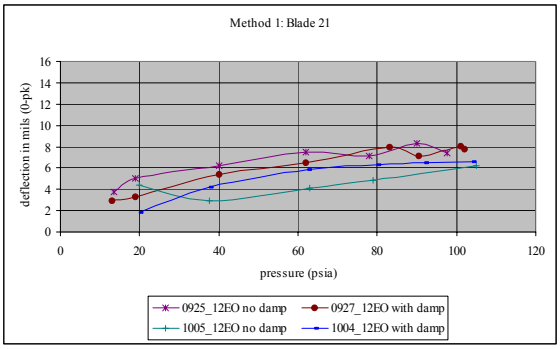
Method 1: Blade 21
deflection in mils (0-pk)
pressure (psia)
0925_12EO no damp
0927_12EO with damp
1005_12EO no damp
1004_12EO with damp

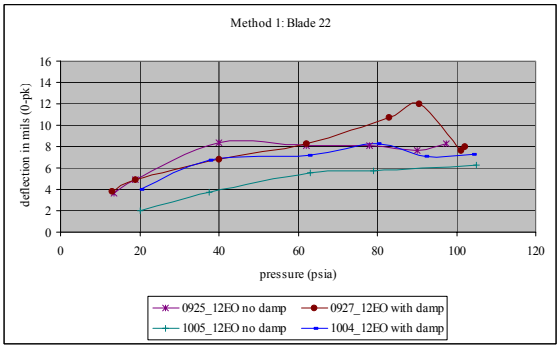
Method 1: Blade 22
deflection in mils (0-pk)
pressure (psia)
0925_12EO no damp
0927_12EO with damp
1005_12EO no damp
1004_12EO with damp

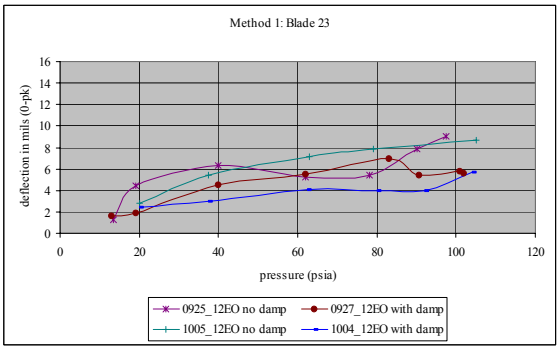
Method 1: Blade 23
deflection in mils (0-pk)
pressure (psia)
0925_12EO no damp
0927_12EO with damp
1005_12EO no damp
1004_12EO with damp

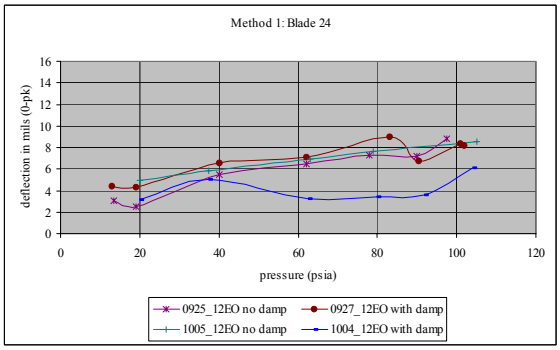
Method 1: Blade 24
deflection in mils (0-pk)
pressure (psia)
0925_12EO no damp
0927_12EO with damp
1005_12EO no damp
1004_12EO with damp

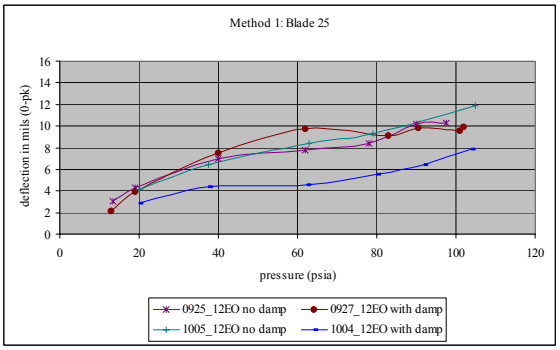
Method 1: Blade 25
deflection in mils (0-pk)
pressure (psia)
0925_12EO no damp
0927_12EO with damp
1005_12EO no damp
1004_12EO with damp

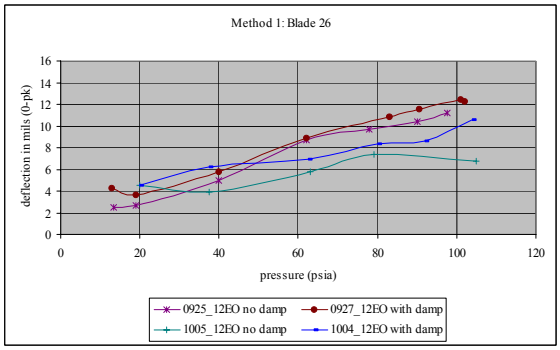
Method 1: Blade 26
deflection in mils (0-pk)
pressure (psia)
0925_12EO no damp
0927_12EO with damp
1005_12EO no damp
1004_12EO with damp

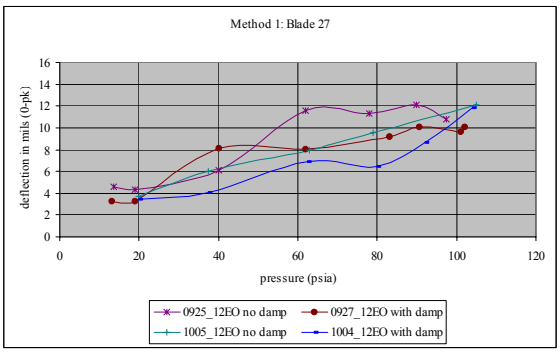
Method 1: Blade 27
deflection in mils (0-pk)
pressure (psia)
0925_12EO no damp
0927_12EO with damp
1005_12EO no damp
1004_12EO with damp

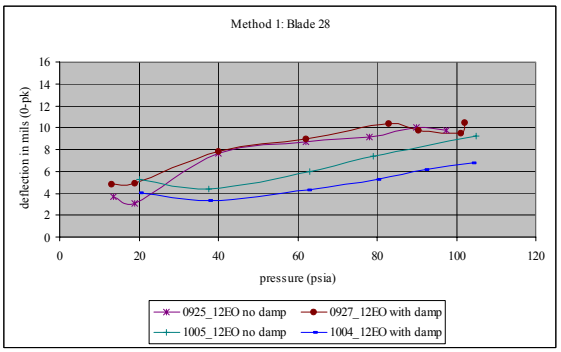
Method 1: Blade 28
deflection in mils (0-pk)
pressure (psia)
0925_12EO no damp
0927_12EO with damp
1005_12EO no damp
1004_12EO with damp

THIS PAGE INTENTIONALLY LEFT BLANK

APPENDIX E : STRAIN GAUGE VS. NSMS CORRELATION

Correlation of root strain gauges to Probes 1 and 2's corresponding blade number's

A. STRAIN 11 = PROBE 1 BLADE25 = PROBE 2 BLADE 20

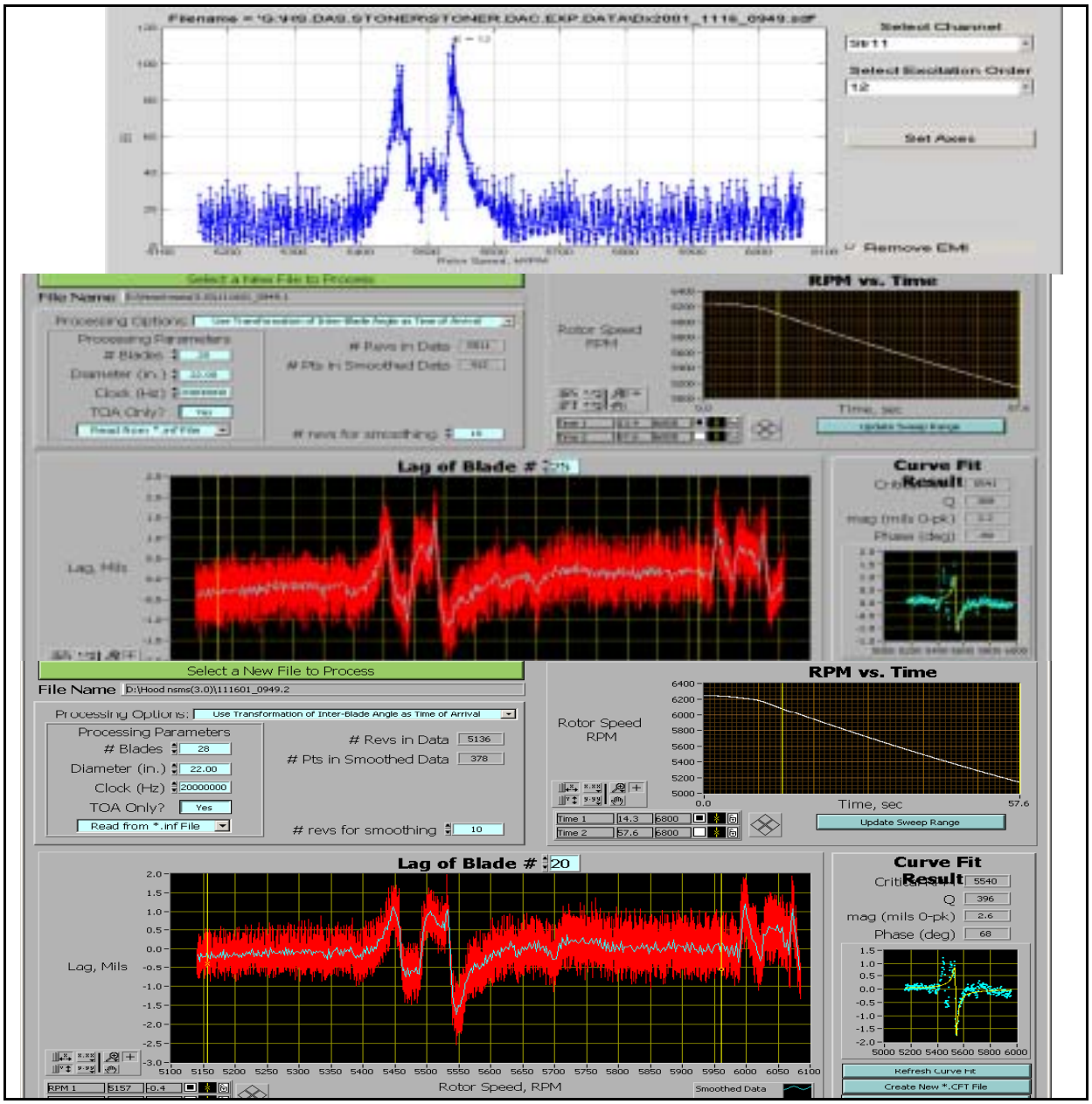

Figure 62 Strain 11 Compared to Probes 1 and 2:

B. STRAIN 13 = PROBE 1 BLADE 28 = PROBE 2 BLADE 23

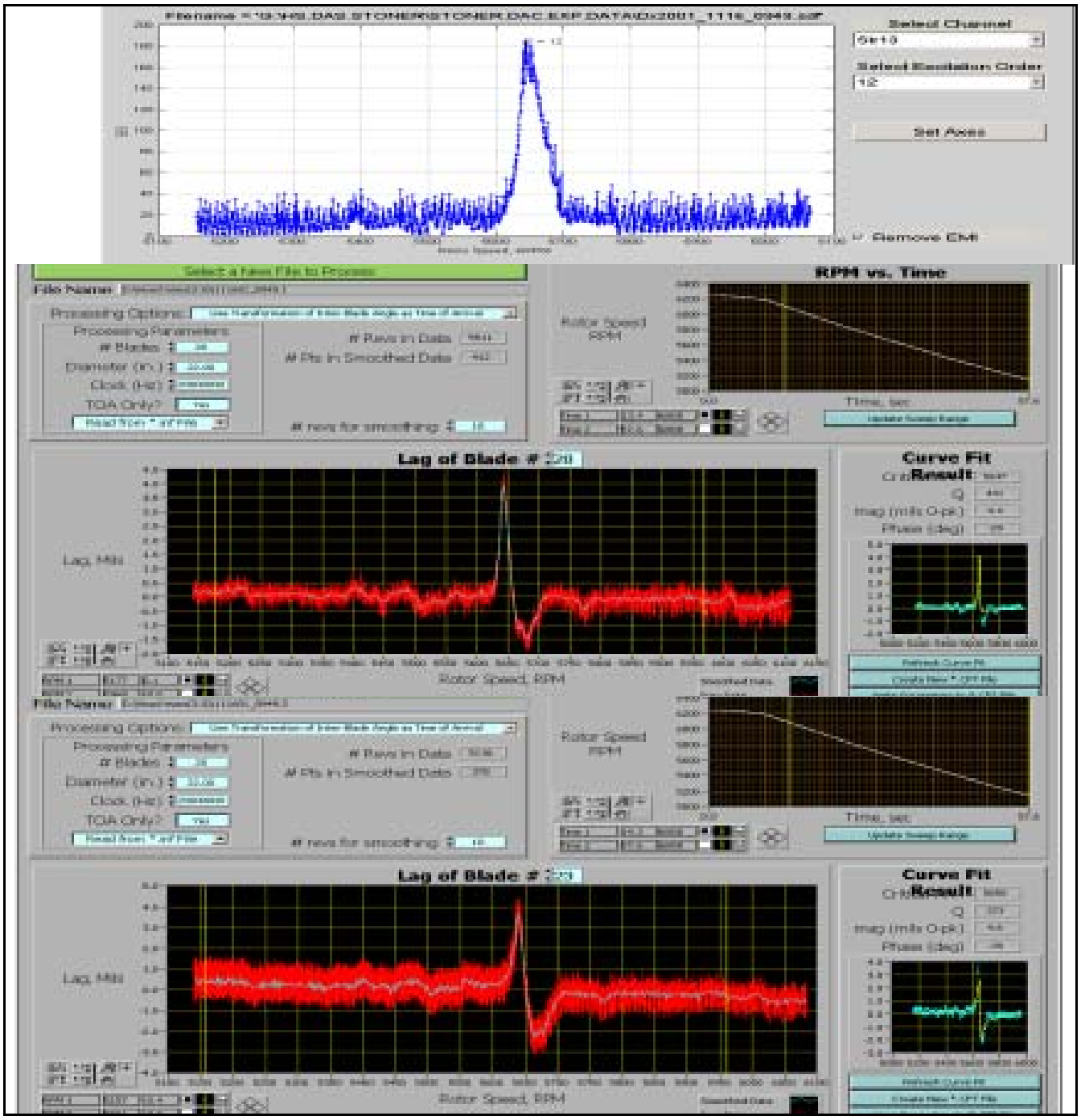

Figure 63 Strain 13 Compared to Probes 1 and 2:

C. STRAIN 14 = PROBE 1 BLADE 15 = PROBE 2 BLADE 10

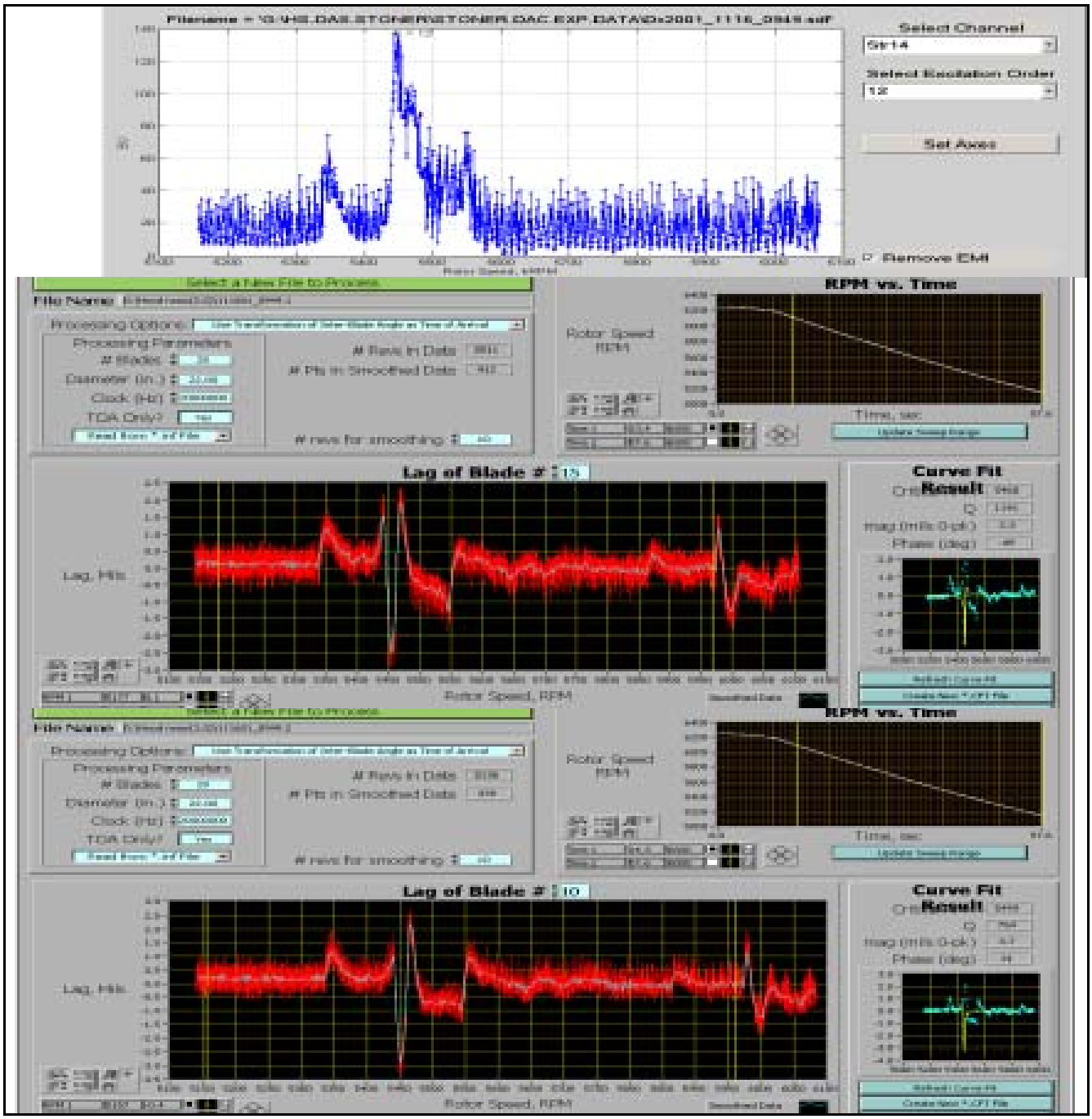

Figure 64 Strain 14 Compared to Probes 1 and 2:

THIS PAGE INTENTIONALLY LEFT BLANK

APPENDIX F : CORRELATION DATA OF STRAIN GAUGES TO PROBES

A. STRAIN GAUGE 11 TO NSMS

12EO Repeatability Strain Gauge Data

Run	File Name	Strain 11 Peak mstrain	Freq	probe1 blade25 deflection (mils)	Freq	probe2 blade20 deflection (mils)	Freq
195	1109_1205	83.00	5555.00	1.71	5555.76	1.73	5555.91
-5/8	1109_1239	78.00	5540.00	1.31	5549.00	2.04	5460.16
-0.625	1109_1247	73.00	5540.00	1.67	5540.00	1.84	5539.70
	1109_1255	84.00	5535.00	1.73	5537.43	1.79	5537.27
	1109_1304	83.00	5535.00	1.79	5533.89	1.85	5533.47
	averages	80.20	5541.00	1.64	5543.22	1.85	5525.30
	stdev	4.66	8.22	0.19	8.97	0.12	37.41
196	1114_1113	74.00	5555.00	1.32	5553.73	1.26	5551.29
+1 1/4	1114_1144	108.00	5550.00	1.89	5547.98	2.03	5545.72
1.25	1114_1155	96.00	5545.00	1.80	5539.76	2.08	5539.38
	1114_1203	105.00	5535.00	1.94	5535.54	2.24	5534.93
	1114_1213	90.00	5540.00	1.67	5535.20	1.97	5534.02
	averages	94.60	5545.00	1.72	5542.44	1.92	5541.07
	stdev	13.56	7.91	0.25	8.15	0.38	7.35
197	1116_0935	109.00	5550.00	2.14	5635.54	2.10	5548.00
reference	1116_0949	115.00	5540.00	1.42	5633.59	2.53	5539.78
/stop-start	1116_0958	119.00	5530.00	1.59	5630.66	2.41	5534.40
0	1116_1035	111.00	5518.00	1.77	5621.59	2.51	5521.29
	1116_1041	110.00	5525.00	1.74	5622.33	2.64	5520.21
	averages	112.80	5532.60	1.73	5628.74	2.44	5532.74
	stdev	4.15	12.60	0.27	6.44	0.21	11.97
197	1116_1051	122.00	5525.00				
reference	1116_1102	108.00	5528.00	2.22	5523.90	2.47	5522.50
continuous	1116_1107	109.00	5516.00	2.12	5520.36	2.43	5519.42
	1116_1112	100.00	5513.00	2.10	5516.61	2.37	5515.38
	averages	109.75	5520.50	2.15	5520.29	2.42	5519.10
	stdev	9.11	7.14	0.06	3.65	0.05	3.57
198	1120_0856	125.00	5550.00	3.43	5451.50	2.90	5459.06
1/4	1120_0916	107.00	5545.00				
0.25	1120_0926	122.00	5540.00	2.75	5532.13	3.00	5532.38
	1120_0933	134.00	5530.00	2.78	5528.02	3.14	5527.96
	1120_0941	145.00	5528.00				
	averages	126.60	5538.60	2.99	5503.88	3.01	5506.47
	stdev	14.15	9.48	0.38	45.41	0.12	41.12
		Strain 11 Peak mstrain	Freq	probe1 blade25 deflection (mils)	Freq	probe2 blade20 deflection (mils)	Freq

B. STRAIN GAUGE 13 TO NSMS

12EO Repeatability Strain Gauge Data

Run	File Name	Strain 13 Peak mstrain	Freq	probe1 blade28 deflection (mils)	Freq	probe2 blade23 deflection (mils)	Freq
195	1109_1205	111.00	5670.00	2.38	5666.62	2.58	5665.33
-5/8	1109_1239	120.00	5660.00	2.48	5660.87	2.79	5660.16
-0.625	1109_1247	143.00	5648.00	2.93	5652.14	3.32	5651.58
	1109_1255	119.00	5650.00	2.84	5650.46	3.17	5648.91
	1109_1304	128.00	5650.00	2.77	5647.23	3.17	5646.58
	averages	124.20	5655.60	2.68	5655.46	3.01	5654.51
	stdev	12.11	9.32	0.24	8.02	0.31	7.94
196	1114_1113	143.00	5640.00	2.65	5635.15	2.12	5646.35
+1 1/4	1114_1144	168.00	5655.00	3.31	5654.07	3.54	5654.39
1.25	1114_1155	158.00	5645.00	3.12	5645.75	3.38	5646.45
	1114_1203	167.00	5645.00	3.39	5642.42	3.80	5642.60
	1114_1213	158.00	5635.00	3.36	5638.93	3.74	5639.97
	averages	158.80	5644.00	3.16	5643.26	3.31	5645.95
	stdev	10.03	7.42	0.31	7.22	0.69	5.45
197	1116_0935	167.00	5650.00	3.67	5639.46	3.42	5643.10
reference	1116_0949	184.00	5650.00	4.44	5646.51	4.60	5650.25
/stop-start	1116_0958	196.00	5635.00	4.24	5642.92	4.58	5645.54
0	1116_1035	200.00	5630.00	4.47	5631.93	4.41	5636.33
	1116_1041	196.00	5630.00	4.31	5629.09	4.40	5632.58
	averages	188.60	5639.00	4.23	5637.98	4.28	5641.56
	stdev	13.48	10.25	0.33	7.33	0.49	7.10
197	1116_1051	175.00	5630.00				
reference	1116_1102	190.00	5628.00	4.15	5632.44	4.20	5634.88
continuous	1116_1107	179.00	5630.00	4.08	5628.23	4.21	5630.08
	1116_1112	196.00	5626.00	3.86	5624.40	3.96	5627.29
	averages	185.00	5628.50	4.03	5628.36	4.12	5630.75
	stdev	9.70	1.91	0.15	4.02	0.14	3.84
198	1120_0856	91.00	5630.00	1.78	5607.41	1.93	5614.23
1/4	1120_0916	101.00	5620.00				
0.25	1120_0926	108.00	5620.00	2.31	5605.81	2.32	5611.18
	1120_0933	104.00	5615.00	2.08	5610.09	2.31	5613.53
	1120_0941	117.00	5610.00				
	averages	104.20	5619.00	2.06	5607.77	2.19	5612.98
	stdev	9.52	7.42	0.27	2.16	0.22	1.60
		Strain 13 Peak mstrain	Freq	probe1 blade28 deflection (mils)	Freq	probe2 blade23 deflection (mils)	Freq

C. STRAIN GAUGE 14 TO NSMS

12EO Repeatability Strain Gauge Data

Run	File Name	Strain 14 Peak mstrain	Freq	probe1 blade15 deflection (mils)	Freq	probe2 blade10 deflection (mils)	Freq
195	1109_1205	130.00	5462.00	2.29	5470.47	2.49	5468.63
-5/8	1109_1239	71.00	5460.00	0.89	5463.74	0.95	5463.38
-0.625	1109_1247	116.00	5450.00	2.50	5451.75	2.68	5451.44
	1109_1255	136.00	5446.00	2.85	5450.37	3.09	5450.06
	1109_1304	138.00	5450.00	2.47	5447.13	2.69	5446.76
	averages	118.20	5453.60	2.20	5456.69	2.38	5456.05
	stdev	27.75	6.99	0.76	9.94	0.83	9.43
196	1114_1113	119.00	5475.00	2.19	5472.53	2.39	5471.39
+1 1/4	1114_1144	123.00	5455.00	2.58	5456.81	2.83	5456.12
1.25	1114_1155	129.00	5445.00	2.42	5450.83	2.70	5450.12
	1114_1203	133.00	5440.00	2.30	5448.48	2.44	5447.69
	1114_1213	94.00	5435.00	1.31	5466.35	1.41	5465.92
	averages	119.60	5450.00	2.16	5459.00	2.35	5458.25
	stdev	15.29	15.81	0.50	10.24	0.56	10.17
197	1116_0935	98.00	5455.00	0.95	5455.46	1.71	5459.64
reference	1116_0949	138.00	5445.00	3.19	5450.91	3.59	5449.16
/stop-start	1116_0958	138.00	5435.00	3.10	5441.66	3.31	5441.38
0	1116_1035	159.00	5425.00	3.03	5431.89	3.44	5433.45
	1116_1041	145.00	5428.00	3.32	5430.79	3.44	5431.40
	averages	135.60	5437.60	2.72	5442.14	3.09	5443.00
	stdev	22.70	12.40	1.00	11.05	0.78	11.65
197	1116_1051	182.00	5430.00				
reference	1116_1102	195.00	5422.00	3.36	5423.25	4.03	5424.79
continuous	1116_1107	189.00	5420.00	3.46	5436.58	4.10	5432.08
	1116_1112	183.00	5421.00	3.28	5436.23	3.90	5431.11
	averages	187.25	5423.25	3.37	5432.02	4.01	5429.33
	stdev	6.02	4.57	0.09	7.60	0.10	3.96
198	1120_0856	120.00	5452.00	1.53	5494.43	1.44	5496.34
1/4	1120_0916	184.00	5445.00				
0.25	1120_0926	144.00	5435.00	2.78	5440.22	2.99	5440.12
	1120_0933	118.00	5430.00	2.78	5440.22	2.66	5437.76
	1120_0941	131.00	5430.00				
	averages	139.40	5438.40	2.37	5458.29	2.37	5458.07
	stdev	27.00	9.76	0.72	31.30	0.82	33.16
		Strain 14 Peak mstrain	Freq	probe1 blade15 deflection (mils)	Freq	probe2 blade10 deflection (mils)	Freq

D. FINAL PLOTS RELATING STRAIN GAUGES TO PROBES 1 AND 2.

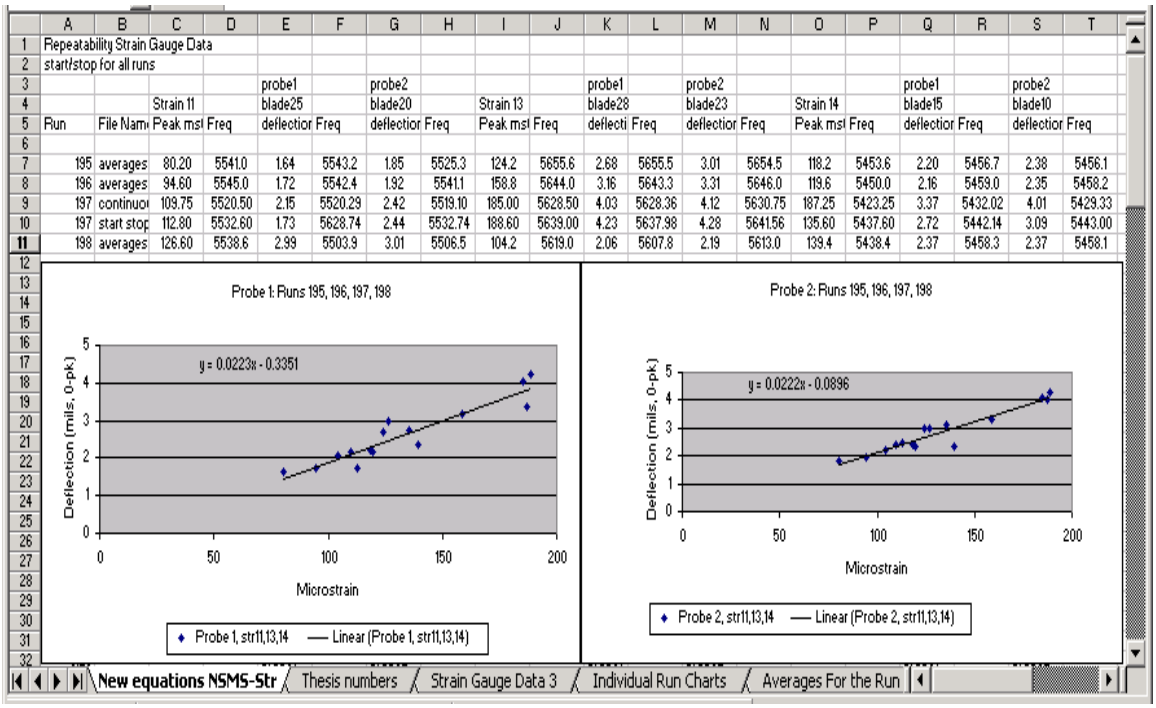

	A	B	C	D	E	F	G	H	I	J	K	L	M	N	O	P	Q	R	S	T
1	Repeatability Strain Gauge Data																			
2	start/stop for all runs																			
3					probe1		probe2				probe1		probe2				probe1		probe2	
4			Strain 11		blade25		blade20		Strain 13		blade28		blade23		Strain 14		blade15		blade10	
5	Run	File Nam	Peak mst	Freq	deflection	Freq	deflection	Freq	Peak mst	Freq	deflecti	Freq	deflection	Freq	Peak mst	Freq	deflection	Freq	deflection	Freq
6																				
7	195	averages	80.20	5541.0	1.64	5543.2	1.85	5525.3	124.2	5655.6	2.68	5655.5	3.01	5654.5	118.2	5453.6	2.20	5456.7	2.38	5456.1
8	196	averages	94.60	5545.0	1.72	5542.4	1.92	5541.1	158.8	5644.0	3.16	5643.3	3.31	5646.0	119.6	5450.0	2.16	5459.0	2.35	5458.2
9	197	continuo	109.75	5520.50	2.15	5520.29	2.42	5519.10	185.00	5628.50	4.03	5628.36	4.12	5630.75	187.25	5423.25	3.37	5432.02	4.01	5429.33
10	197	start stop	112.80	5532.60	1.73	5628.74	2.44	5532.74	188.60	5639.00	4.23	5637.98	4.28	5641.56	135.60	5437.60	2.72	5442.14	3.09	5443.00
11	198	averages	126.60	5538.6	2.99	5503.9	3.01	5506.5	104.2	5619.0	2.06	5607.8	2.19	5613.0	139.4	5438.4	2.37	5458.3	2.37	5458.1

APPENDIX G : EXPERIMENT 3 DATA

A. NON-PLATED: PROBE 1(WHITE), PROBE 2 (GRAY)

deflection
probe 1
y = 0.0223x - 0.3351
deflection =0.0223(microstrain)-0.3351

probe 2
y = 0.0222x - 0.0896
deflection=0.0222(mircrostrain)-0.0896

November

		0.0 non-plated			0.0 non-plated			avreagebtwi	0.25 non-plated			0.25 non-plated		
	blade #	probe 1	deflection (0-pk)	microstrain	probe 2	deflection (0-pk)	microstrain	pr1&pr2	probe 1	deflection (0-pk)	microstrain	probe 2	deflection (0-pk)	microstrain
	182	9	2.53	129	4	2.57	120	7%	9	2.87	144	4	2.75	128
	125	10	3.45	170	5	3.78	174	3%	10	3.83	187	5	4.24	195
	188	11	3.94	192	6	3.84	177	8%	11	4.18	202	6	4.28	197
	190	12	2.64	133	7	2.48	116	13%	12	2.63	133	7	2.61	122
	208	13	2.19	113	8	2.74	127	13%	13	2.49	127	8	2.63	123
	127	14	2.92	146	9	2.72	126	13%	14	3.01	150	9	3.00	139
str 14	**143**	**15**	**2.72**	137	**10**	**3.09**	143	5%	**15**	**2.37**	121	**10**	**2.37**	111
	195	**16**	**3.40**	168	**11**	**3.45**	159	5%	**16**	**3.87**	189	**11**	**3.92**	181
	243	17	1.73	93	12	2.04	96	3%	17	3.66	179	12	4.15	191
	123	18	1.86	98	13	1.88	89	10%	18	1.85	98	13	1.60	76
	121	19	3.70	181	14	3.57	165	9%	19	4.01	195	14	2.59	121
	181	20	4.31	208	15	4.33	199	5%	20	4.72	227	15	4.74	218
	166	**21**	**2.81**	141	**16**	**3.06**	142	1%	**21**	**2.85**	143	**16**	**3.33**	154
	74	22	3.42	168	17	3.69	170	1%	22	4.10	199	17	4.15	191
	154	23	2.99	149	18	3.18	147	1%	23	3.01	150	18	3.48	161
	173	24	2.90	145	19	2.49	116	20%	24	2.68	135	19	2.55	119
str 11	157	25	2.02	106	20	2.59	121	14%	25	2.99	149	20	3.01	140
	78	26	3.46	170	21	3.64	168	1%	26	3.63	178	21	3.97	183
	163	27	1.72	92	22	1.82	86	7%	27	1.88	99	22	2.17	102
str 13	137	28	4.23	205	23	4.28	197	4%	28	2.06	107	23	2.19	103
	209	**1**	**1.70**	91	**24**	**1.84**	87	5%	**1**	**2.66**	134	**24**	**2.96**	137
	135	**2**	**3.17**	157	**25**	**3.56**	165	5%	**2**	**3.32**	164	**25**	**3.83**	177
	77	3	2.02	105	26	2.55	119	13%	3	2.80	141	26	3.15	146
	142	4	3.07	153	27	2.93	136	11%	4	3.44	169	27	3.49	161
	183	5	1.47	81	28	1.57	75	8%	5	2.02	106	28	1.96	92
	141	6	2.01	105	1	1.93	91	13%	6	2.60	132	1	2.21	103
	178	**7**	**2.16**	112	**2**	**2.59**	121	8%	**7**	**2.10**	109	**2**	**2.32**	109
	120	8	2.99	149	3	3.43	158	6%	8	3.48	171	3	4.02	185
average			2.77	139.18		2.92	135.37	7%		3.04	151		3.13	145

B. PLATED: PROBE 1 (WHITE), PROBE 2 (GRAY)

December

n	0.0 Plated			0.0 Plated			0.25 Plated			0.25 Plated		
blade #	probe 1	deflection (0-pk)	microstrain	probe 2	deflection (0-pk)	microstrain	probe 1	deflection (0-pk)	microstrain	probe 2	deflection (0-pk)	microstrain
182	1	2.89	145	1	3.10	144	1	3.38	167	1	3.28	152
125	2	3.74	183	2	4.19	193	2	4.20	203	2	4.65	213
188	3	4.23	205	3	4.30	198	3	5.01	240	3	5.52	253
190	4	2.49	127	4	2.67	124	4	2.16	112	4	2.39	111
208	5	2.90	145	5	3.29	152	5	2.63	133	5	3.40	157
127	6	2.18	113	6	2.16	101	6	2.45	125	6	2.37	111
143	**7**	**4.23**	205	**7**	**4.14**	190	**7**	**4.55**	219	**7**	**5.26**	241
195	**8**	**3.05**	152	**8**	**3.23**	150	**8**	**2.80**	140	**8**	**3.21**	149
243	9	2.66	134	9	2.33	109	9	3.13	155	9	2.82	131
123	10	1.79	95	10	1.83	87	10	2.00	105	10	1.82	86
121	11	2.07	108	11	1.96	92	11	2.34	120	11	2.11	99
181	12	3.63	178	12	3.52	163	12	3.91	190	12	4.09	188
166	**13**	**3.40**	168	**13**	**3.77**	174	**13**	**3.05**	152	**13**	**3.67**	170
74	14	3.59	176	14	3.61	167	14	4.76	228	14	4.54	209
154	15	3.10	154	15	3.07	142	15	3.39	167	15	3.44	159
173	16	2.26	116	16	2.31	108	16	2.21	114	16	2.13	100
157	17	1.90	100	17	2.37	111	17	2.69	136	17	2.82	131
78	18	3.99	194	18	4.40	202	18	4.28	207	18	4.78	220
163	19	3.22	159	19	3.15	146	19	3.48	171	19	3.41	158
137	20	2.34	120	20	1.95	92	20	2.32	119	20	1.25	60
209	**21**	**2.64**	133	**21**	**2.38**	111	**21**	**2.32**	119	**21**	**2.92**	136
135	**22**	**3.36**	166	**22**	**3.43**	159	**22**	**3.69**	180	**22**	**3.81**	176
77	23	1.82	97	23	2.15	101	23	1.81	96	23	2.13	100
142	24	1.78	95	24	1.99	94	24	2.43	124	24	2.79	130
183	25	2.76	139	25	3.34	155	25	2.95	147	25	3.53	163
141	26	2.54	129	26	2.74	127	26	2.51	128	26	2.91	135
178	**27**	**3.31**	164	**27**	**3.53**	163	**27**	**3.67**	180	**27**	**4.37**	201
120	28	1.67	90	28	1.85	87	28	1.80	96	28	2.04	96
Averages		2.84	142		2.96	137		3.07	153		3.27	151

THIS PAGE INTENTIONALLY LEFT BLANK

APPENDIX H : EXPERIMENT 4 DATA

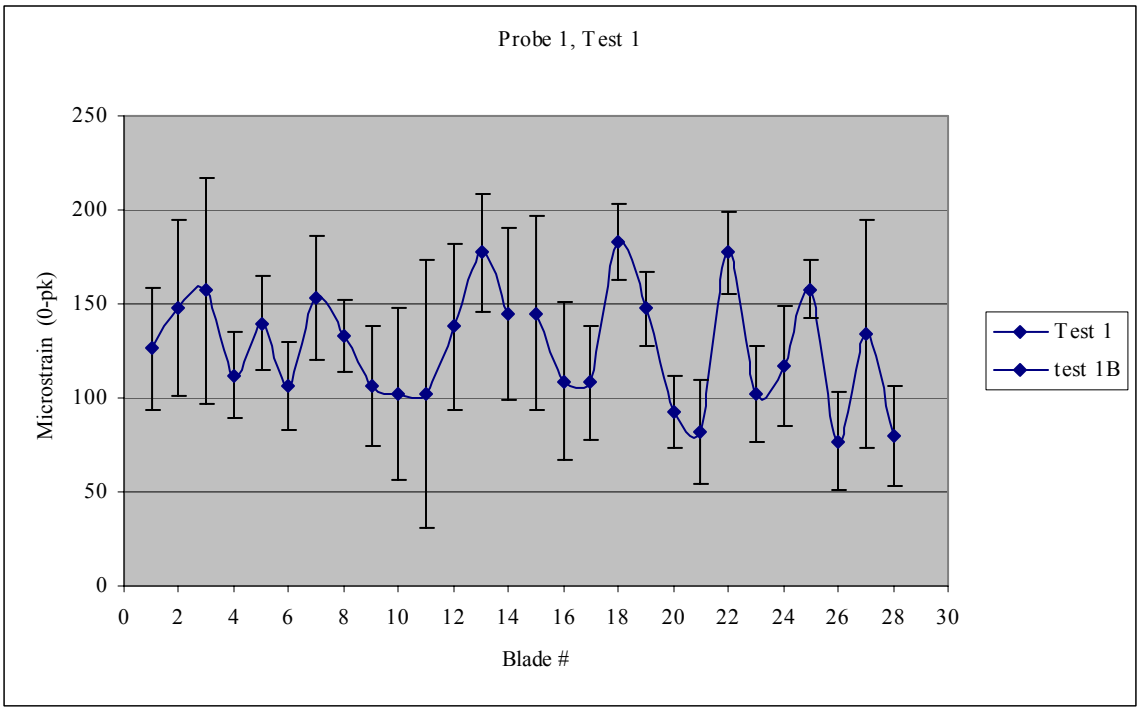

Figure 65 Average of 3 Sweeps in Test 1

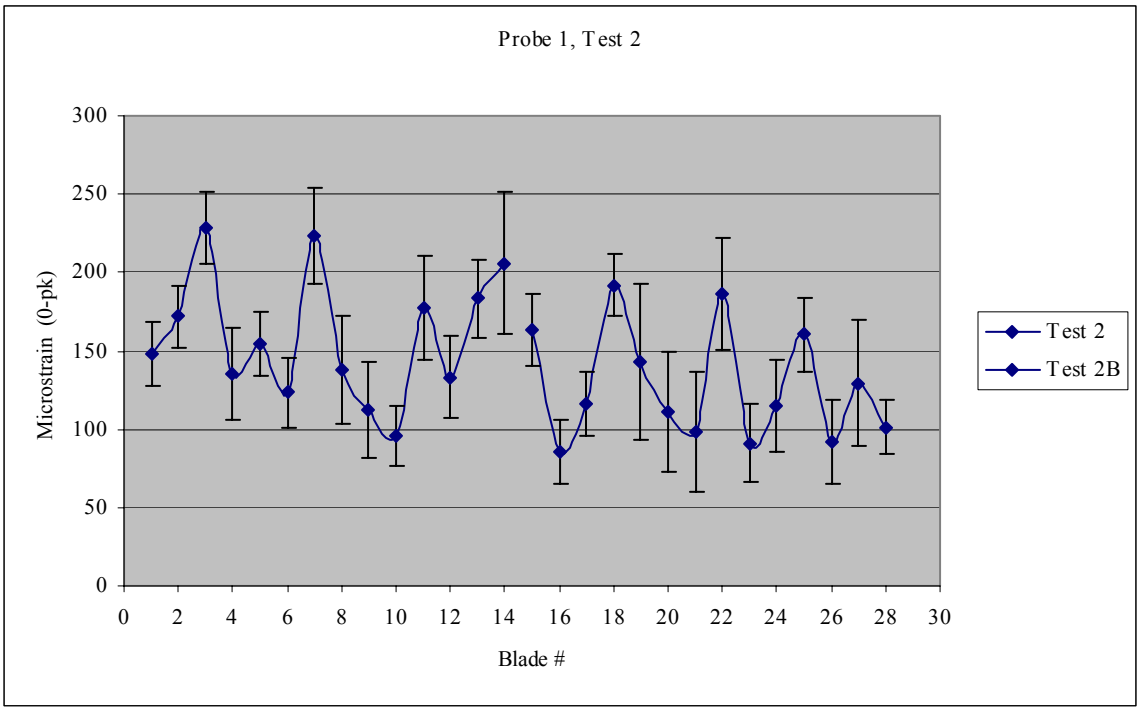

Figure 66 Average of 3 Sweeps in Test 2

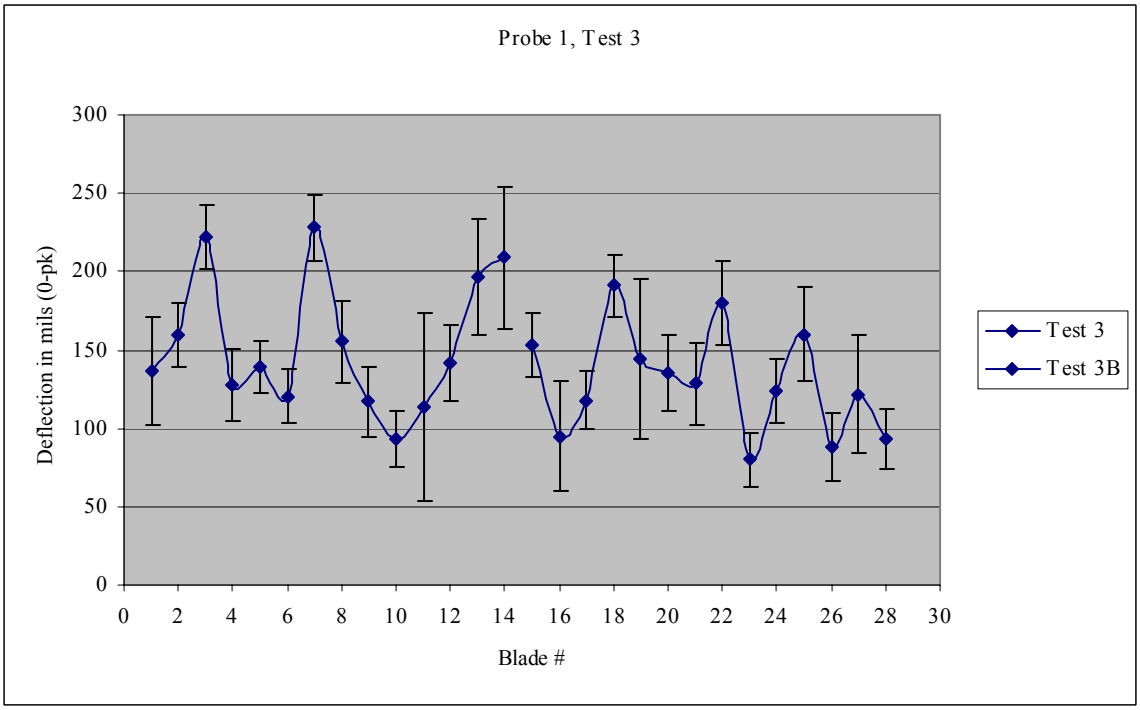

Figure 67 Average of 3 Sweeps in Test 3

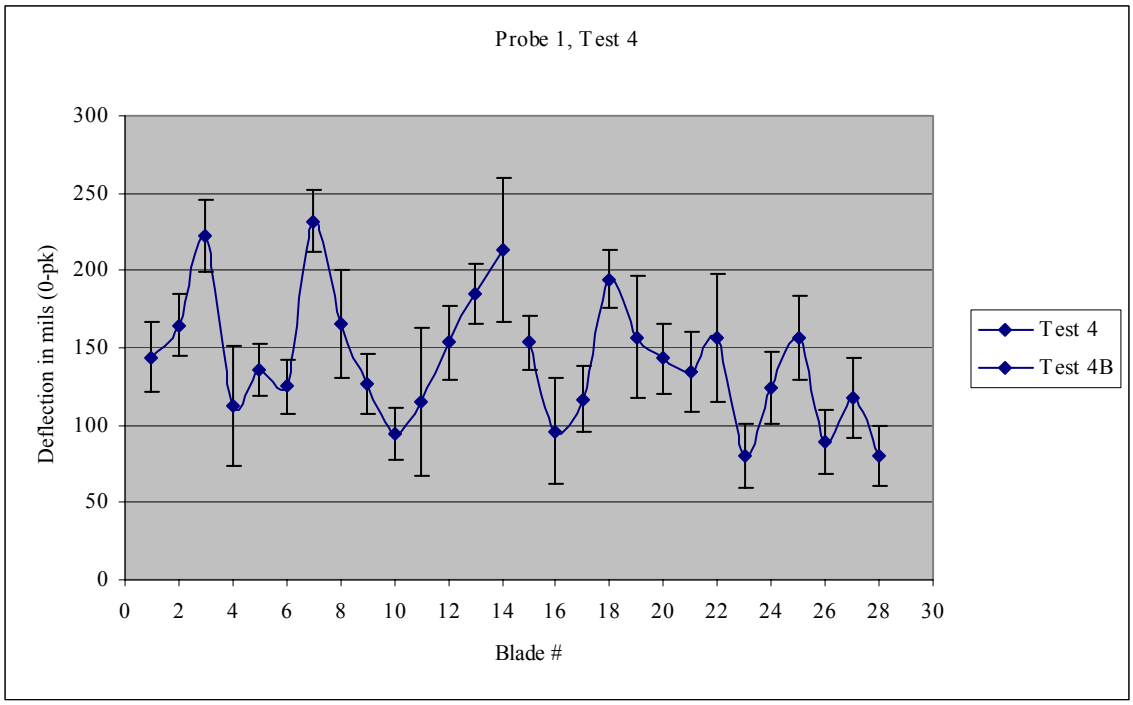

Figure 68 Average of 3 Sweeps in Test 4

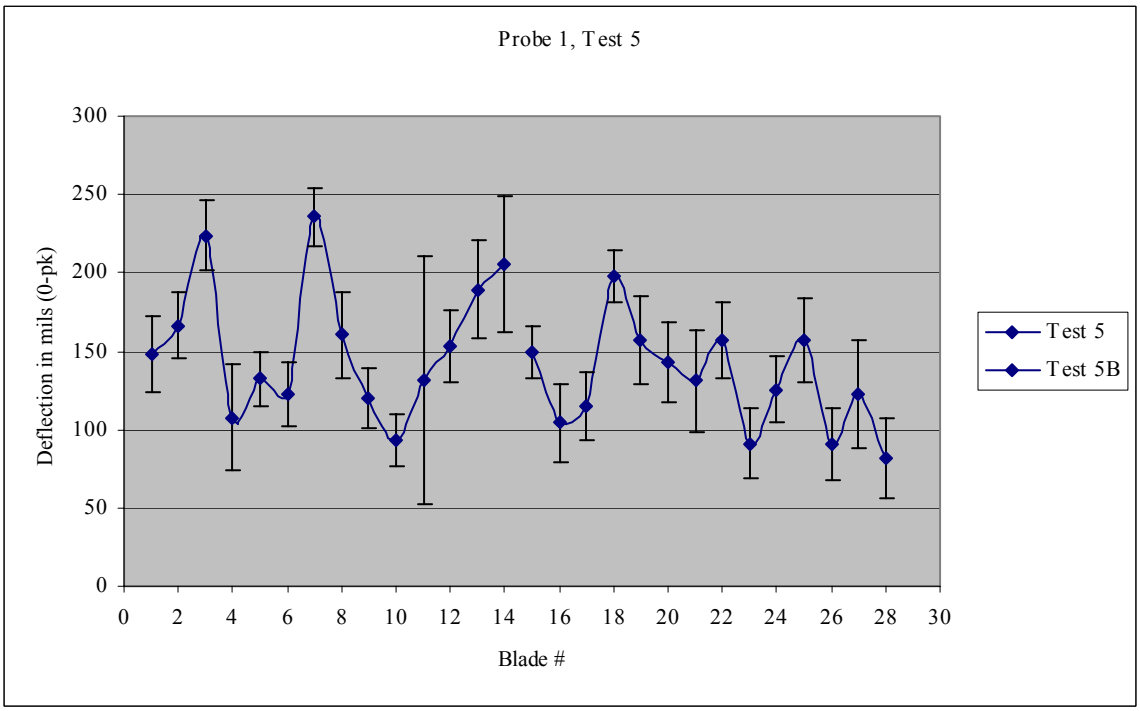

Figure 69 Average of 3 Sweeps in Test 5

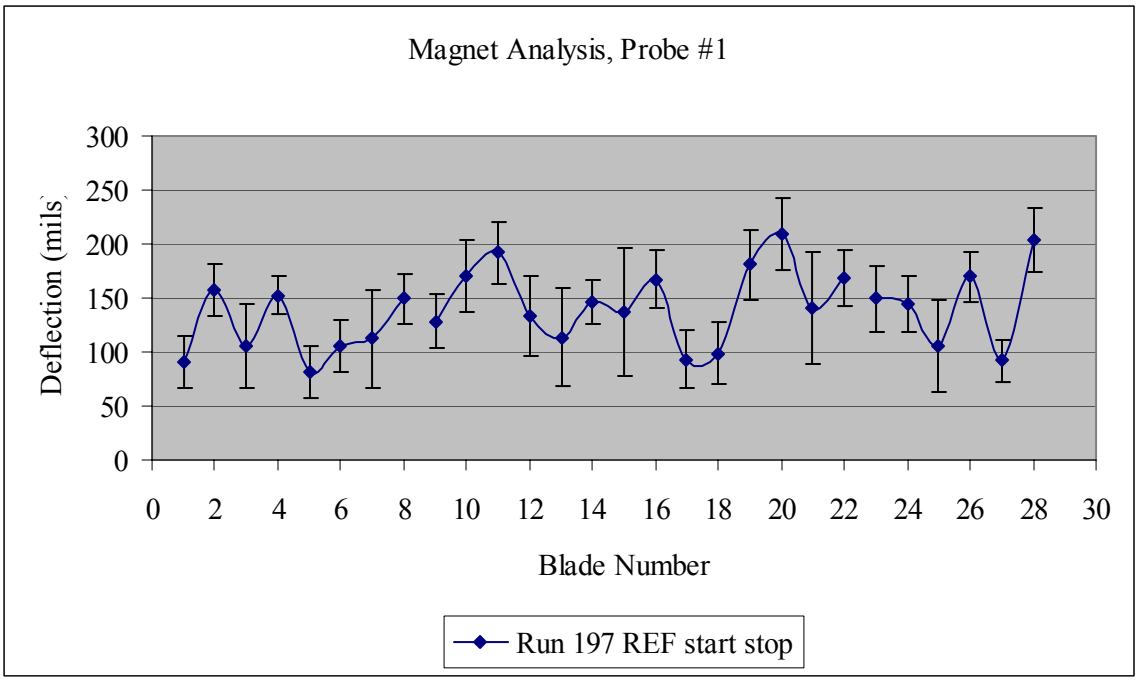

Figure 70 "Start/Stop" Standard Deviations for No Plastic inserts

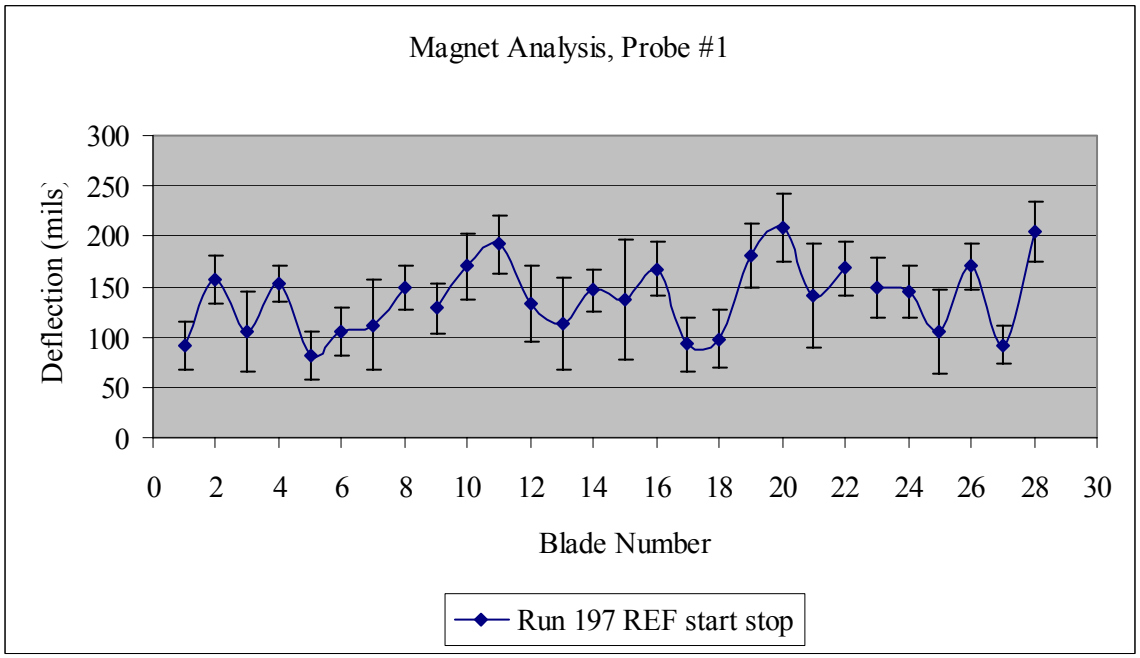

Figure 71 Continuous Standard Deviations for No Plastic Inserts

APPENDIX I PROBE AND BLADE NUMBER IDENTIFICATIONS

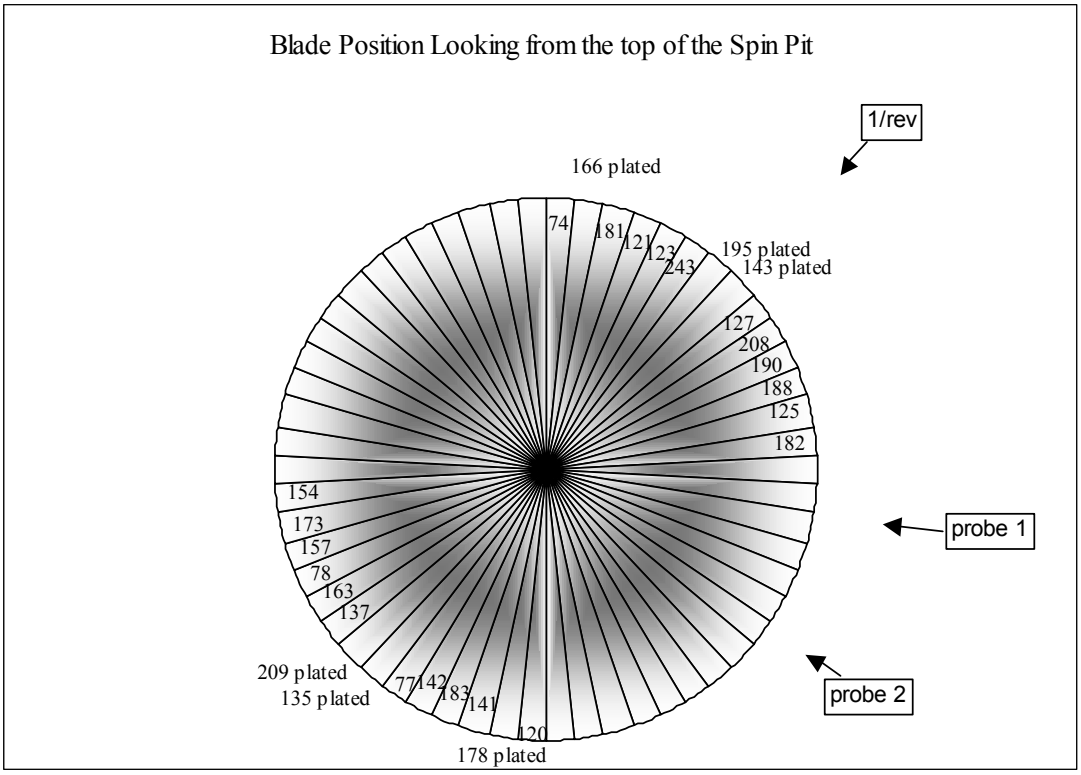

Figure 72 Names of Blades and Actual Position on Rotor

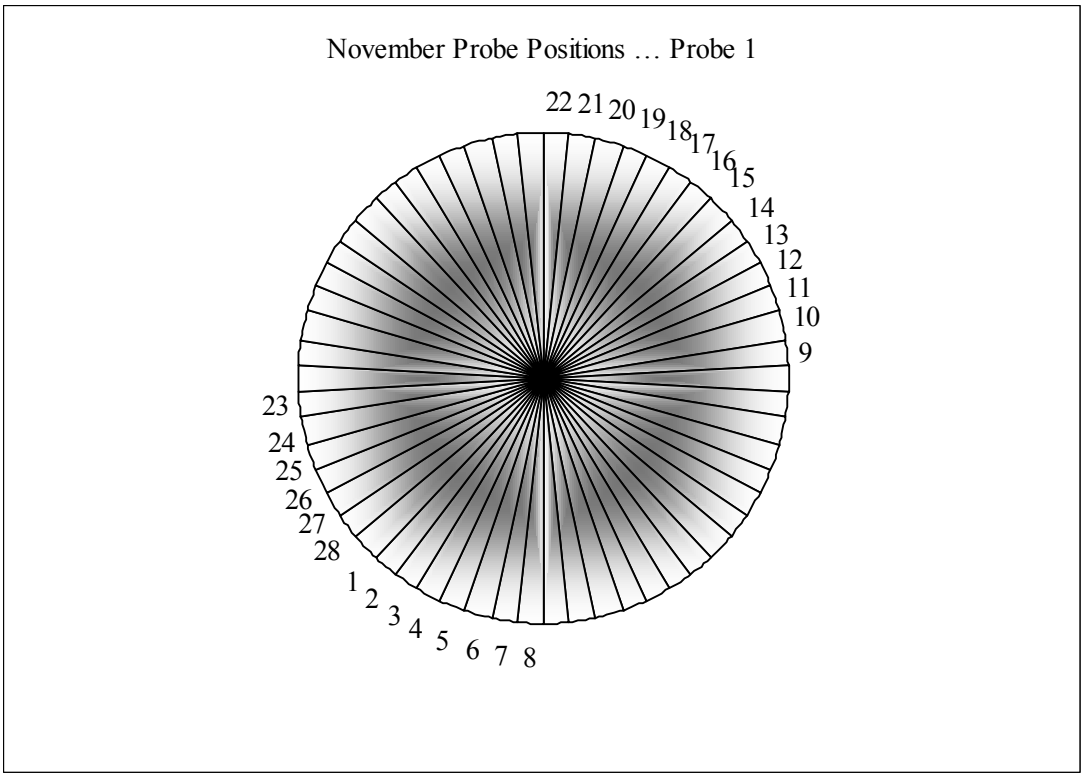

Figure 73 Probe 1 Assignments, November

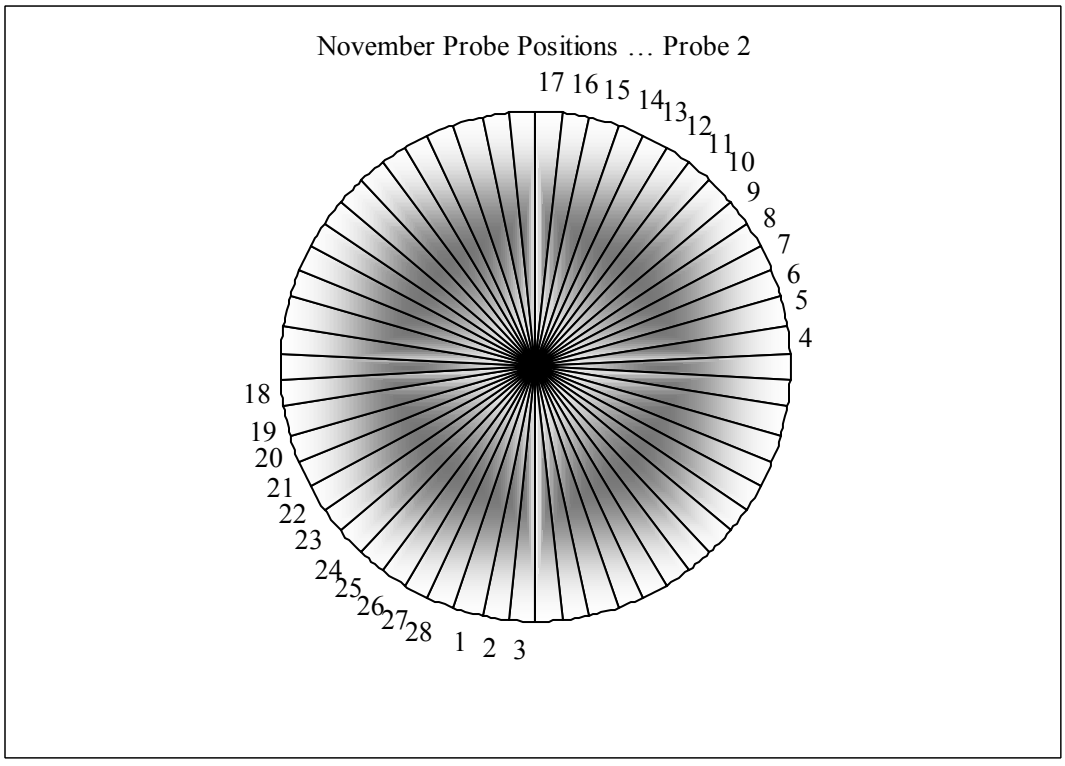

Figure 74 Probe 2 Assignment, November

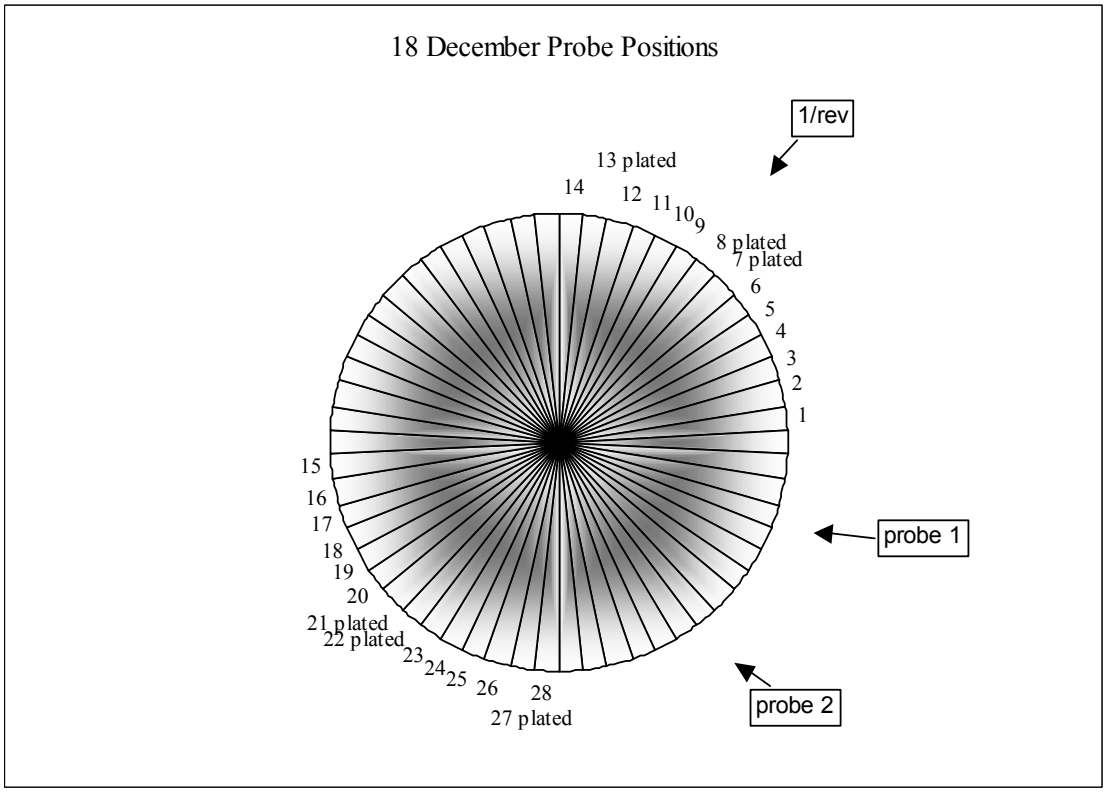

Figure 75 Probes 1 and 2 Blade Assignments, December

THIS PAGE INTENTIONALLY LEFT BLANK

LIST OF REFERENCES

1. Aerospace Industries and Test Measurement Divisions of ISA 45th International Instrumentation Symposium, May 2-6, 1999, Albuquerque, New Mexico; *Overview of Pratt & Whitney NSMS*, Robinson, Woodrow W.

2. Heath, S. and Imregun, M., "A Review of Analysis Techniques for Blade Tip Timing Measurements," Presented at The International Gas Turbine & Aeroengine Congress Exhibition, Orlando, FL, June 1997.

3. Shreeve, R.P., Seivwright, D.L. and Hobson, G.V., "Navy Rotor Spin Research Facility and Initial Program:, Paper presented at the 4th National Turbine Engine High-Cycle Fatigue Conference, Feb 9-11, 1999, Monterey, California.

4. Osburn, N. G. "Implementation of Two-Probe Tip-Timing Technique to Determine Compressor Blade Vibrations," June 2000.

5. Mercadal, M., von Flotow, A., Tappert, P., "Health Monitoring of Rotating Turbo Machinery Parts," Hood Technology Corporation, Hood River, OR, May, 1999.

6. Dhadwal, H. S., "Integrated Fiber Optic Laser Probe System For Monitoring Of Blade Tip Dynamics in Rotating Turbomachinery," July 1996, IFOLP-MANUAL.

7. Dhadwal, H. S. and Kurkov, A. P., "Dual Laser Probe Measurement of Blade Tip Clearance," The Journal of Turbomachinery, Vol. 121, PP. 481-485, July 1999.

8. Hood Technology Corporation's NSMS Acquisition Software Version 3.0 User's Manual, 1999.

9. Hood Technology Corporation's NSMS Data Viewer Software Version 1.3 User's Manual, 1999.

10. Mercadal, Mathieu, "Identification of Blade Resonances Using Direct or Differential Time of Arrival Data," Hood Technology Corporation, 1999.

11. Leitch, R. D., "Reliability Analysis for Engineers,"1995.

12. Duffy, K., Presentation at AF/Navy program review, Naval Postgraduate School November 29, 2001. (Unpublished)

THIS PAGE INTENTIONALLY LEFT BLANK

INITIAL DISTRIBUTION LIST

Defense Technical Information Center
Ft. Belvoir, Virginia

Dudley Knox Library
Naval Postgraduate School
Monterey, California

Chairman and Distinguished Professor Max F. Platzer, Code AA/PL
Department of Aeronautics and Astronautics
Naval Postgraduate School
Monterey, CA

Professor R. P. Shreeve, Code AA/Sf
Department of Aeronautics & Astronautics
Naval Postgraduate School
699 Dyer Road, Room 137
Monterey, CA

Professor Garth Hobson, Code AA/Hg
Department of Aeronautics and Astronautics
Naval Postgraduate School
Monterey, CA

Al Stoner Turbine Module Center
Project Engineer - Structural Analysis - HCF
1306 Avenue C
Pratt & Whitney
Arnold Engineering Development Center
Tullahoma, Tn
Stoner, Alan W.

Dr. Andy von-Flotow
Hood Technology Corporation
1750 Country Club Rd
Hood River, Oregon

Ray Pickering, NAVAIR
Naval Air Systems TEAM, 4.4.7.2
Aerospace Engineer
Patuxent River, MD

Ms. Kirsten P. Duffy
NASA Glenn Res CTR
Lewis Field
M/S 49-8 MACH DYN BR
21000 Brookpark Rd
Cleveland OH

Mr. Frank W. Leighley, Jr.
USAF AFRL/PRTC
Bldg. 18 Rm. D128
1950 Fifth St.
Wright-Patterson AFB, OH